PART I : THE CONSTRUCTION OF A MODE-LOCKED Nd^{3+}: GLASS LASER AND NON-LINEAR OPTICAL TECHNIQUES

PART II: APPLICATIONS OF PICOSECOND LASER PULSES IN CHEMISTRY: VIBRATIONAL RELAXATION TIMES IN LIQUID ALKANES AND ALKENES

Thesis

by

Saon Patumtevapibal

In Partial Fulfillment of the Requirements

for the Degree of Doctor of Philosophy

California Institute of Technology
Pasadena, California 91109

1975

(Submitted June 28, 1974)

"I REGARD NO MAN AS POOR
WHO HAS A GODLY MOTHER"

- Abraham Lincoln

This thesis is dedicated
to my mother.

Acknowledgements

First of all, I would like to thank my family and my best friend for their love and care, for waiting so patiently, and also for all the loving letters that have brightened my gloomiest days.

I wish to thank my adviser, Professor G. W. Robinson, for his help and encouragement, and for teaching me to have fun with science. I am also greatly indebted to Dr. Paul R. Monson who has started the picosecond spectroscopy work and taught me all the techniques in the laboratory. Part II of the thesis owes much to Dr. Kenneth J. Kaufmann, with his enthusiasm and humor, for useful and constructive discussions.

The laboratory works owe a great deal to Mr. W. Scheulke and the instrument shop, Mr. E. segal and the glass shop, and also the electronic shop, all with friendliness and willingness. I wish to thank Professor H. B. Gray and his group for the facility in using the Cary 14 and the cold-temperature dewar.

I thank C.I.T. for the GTA, GRA, research and library facilities, and the swimming pool. The scholarship from the Thai Government for both my undergraduate and graduate studies are gratefully acknowledged.

The late Professor Satang Mongkolsuk, Professor George Jura, and the late Dr. M. J. Jorgenson, have contributed much to my science education, and led me the way to chemical research. And to all my teachers, this thesis is also dedicated.

Last, but not least, I can only say that "I got by with little help

from my friends," With them, my Caltech years have been quite enjoyable. My very special thanks to Sister Gabriel Mary Hoare for providing my "second home" and many beautiful things. Her friendship has made my staying in the U. S. much more meaningful and less painful.

Abstract

PART I The construction and qualitative explanation of the pulsed, mode-locked laser are described: the generation of a train of picosecond 1.06μ pulses is achieved by properly aligning a saturable absorber in the Nd^{3+} : glass laser cavity. The pulsewidth, being on a picosecond time scale, has to be measured by a special two-photon method. In order to make the laser more chemically useful, second harmonic generation of the fundamental (1.06 μ) pulses is necessary. A phase-matched KDP crystal is employed in this process. Some non-linear optical techniques, such as stimulated Raman scattering and self-phased modulation, which generates continuum light from a monochromatic pulses, also enrich the usage of the laser. Azulene experiment is tried with our laser set-up.

PART II The dephasing times and vibrational lifetimes of C-H stretching vibrations are studied systematically in a series of liquid alkanes and alkenes, using the Raman effect. The results indicate that the vibrational energy loss takes place primarily through the methyl groups in these molecules. A preliminary result of the methylene C-H stretch vibrational lifetime is conducted in liquid CD_3-CH_2-CH_2-CD_3.

TABLE OF CONTENTS

		Page
Acknowledgement		iii
Abstract		v
PART I:	The Construction of a Mode-Locked Nd^{3+}:Glass Laser and Non-Linear Optical Techniques	
A.	Introduction	1
B.	The Laser	
Theory:	1. A General Description of a Solid State Laser	2
	2. Mode-Locking of the Laser	9
	3. Q-Switching Principles	12
	4. Saturable Absorption and Passive Mode-Locking	14
Experiment:	Picosecond Pulse Generation	20
C.	Two-Photon Method as a Pulse Width Measurement Experiment and Theory	35
D.	Second Harmonic Generation	
	Theory	43
	Experiment	48
E.	Two-Photon Method of Two Different Optical Frequencies	54
F.	Synchronization of Two Optical Paths	59
G.	Experiment on Radiationless Transitions of Azulene	65

Page

H. Generation of Continuum from 1.06 Laser Pulses 71

References 78

PART II: Applications of Picosecond Laser Pulses in Chemistry: Vibrational Relaxation Times in Liquid Alkanes and Alkenes.

A. Introduction 81

B. Historical Review of Vibrational Lifetime Works 83

C. Theory

Dephasing Time 84

Vibrational Relaxation Time 85

Stimulated Raman Scattering 85

Radiation Transfer Equations 93

D. Experiment

Materials 98

Dephasing Time Measurement 99

Vibrational Relaxation Time Measurement at Room Temperature 101

Vibrational Relaxation Time Measurement at Low Temperature 102

E. Results and Discussions 105

Temperature Effect 112

Page

References 115

PROPOSITIONS:

Proposition 1 118

Proposition 2 121

Proposition 3 124

Proposition 4 128

Proposition 5 138

A. Introduction

A typical solid state laser consists of an open optical resonator, which consists essentially of a pair of opposing flat or curved reflectors, and some laser gain medium within this resonator [1]. The arrangement of reflectors and the medium (a ruby or a Nd glass rod) constitute one form of Fabry-Perot interferometer. Standing light waves may be set up within the cavity at a series of discrete optical frequencies over which the gain of the laser medium exceeds the resonator losses. These frequencies are known as the Fabry-Perot modes, and the laser output consists of radiation at a number of closely spaced frequencies with variable durations (microsecond or less). The total output is dependent on many parameters, such as the amplitudes, frequencies, and relative phases of all of these oscillating modes. If there is nothing to fix these parameters, the random fluctuations and nonlinear effects in the laser medium will cause them to change with time and the output will vary in an uncontrollable way. If the oscillating modes are forced to maintain equal frequency spacings with a fixed phase relationship to each other, the output as a function of time will vary in a well-defined manner. The laser is then said to be "mode-locked" or "phase-locked" [2].

The technique of mode-locking the laser is done by employing a saturable dye inside the laser cavity to "Q-switch" the laser (i.e., to cause the laser to emit a short high power burst of energy). The properties of the dye must be such that the relaxation time is very short compared to the round trip time within the cavity length of the original laser pulse. By employing the right dye solution, one can

obtain the laser output consisting of a number of short, intense pulses of light, the duration of which is on the order of 10^{-12}sec, and the peak power is on the order of 10^{9}watts.

B. The Laser

Theory

1. A General Description of a Solid-State Laser

A laser oscillator consists of an active medium, having a complex refractive index as given by $n = n_o - ik$ (where n_o is the index of refraction of light in vacuum, and $k = \frac{2\pi}{\lambda}$), which is inserted between a pair of coaxial planes of spherical mirrors, separated by distance L, as shown in the diagram in Fig. 1.

The flash lamp, when triggered by a power supply, acts as an exciting source, inducing the population inversion in the upper energy state of the amplifying medium. There are in general two types of energy level structures: a three-level and a four-level type (shown in Fig. 2). Excitation is supplied to the solid by radiation of frequencies which produce absorption into the broad band [4] (consider the four-level type as an example). Most of the absorbed energy is transferred by fast, radiationless transitions into the intermediate sharp level [3]. The energy difference is given up to the crystal lattice as heat. The emission of radiation, associated with the spontaneous return from level 3 to 2 , is ordinary fluorescence. Such fluorescence will take place even at a low level of excitation. When the exciting radiation is sufficiently intense, it is possible to obtain

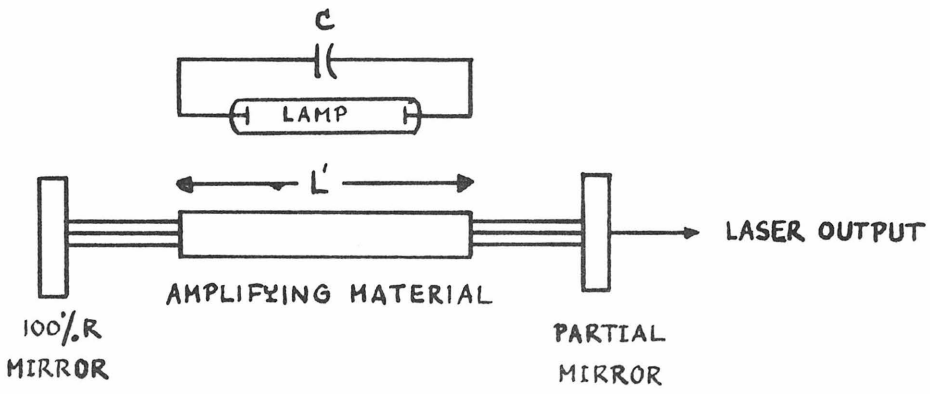

Figure 1. A Simple Laser Cavity

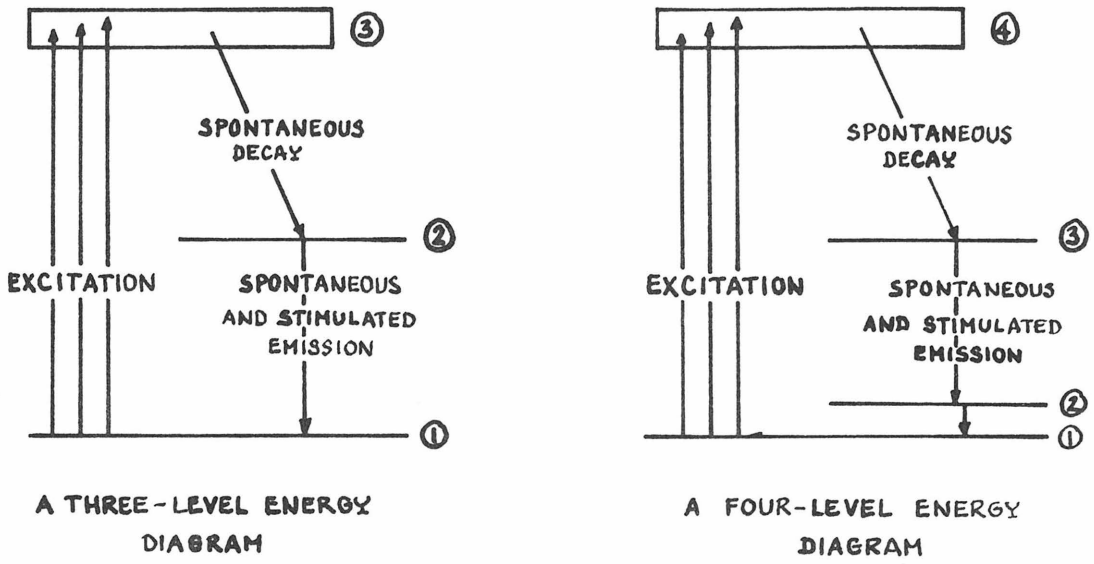

Figure 2. Simplified Energy Level Diagrams of Solid State Lasers

more atoms at level 3 than are left at ground state. The spontaneously emitted photons travelling through the crystal will stimulate additional radiation, and emission thus induced is superposed on the spontaneous emission. This emission is the laser action.

The laser light then travels back and forth inside the laser cavity (Fig. 1). In each passage, the loss factor of the intensity is γ per pass, due mainly to reflection losses, whereas the gain factor is $e^{\alpha L'}$

$$\gamma = -\frac{1}{2} \log r_1 r_2$$

α = gain per unit length

$$= k(\nu)_o n'$$

where r_1, r_2 are reflection coefficients of the mirrors,

$k(\nu)_o$ is the absorption in the unexcited laser material at frequency ν ,

n' is the relative population inversion

$$= \frac{1}{N_o} \left(\frac{g_1}{g_2} N_2 - N_1\right)$$

g_1, g_2 are the multiplicities of levels 1 and 2 (ground and excited states), respectively

N_1, N_2 are the populations of energy levels 1, 2

N_o is the total population.

If $\alpha L > \gamma$, the intensity of radiation of the proper frequency will build up rapidly until it becomes so large that the stimulated transitions will deplete the upper level and reduce the value of α .

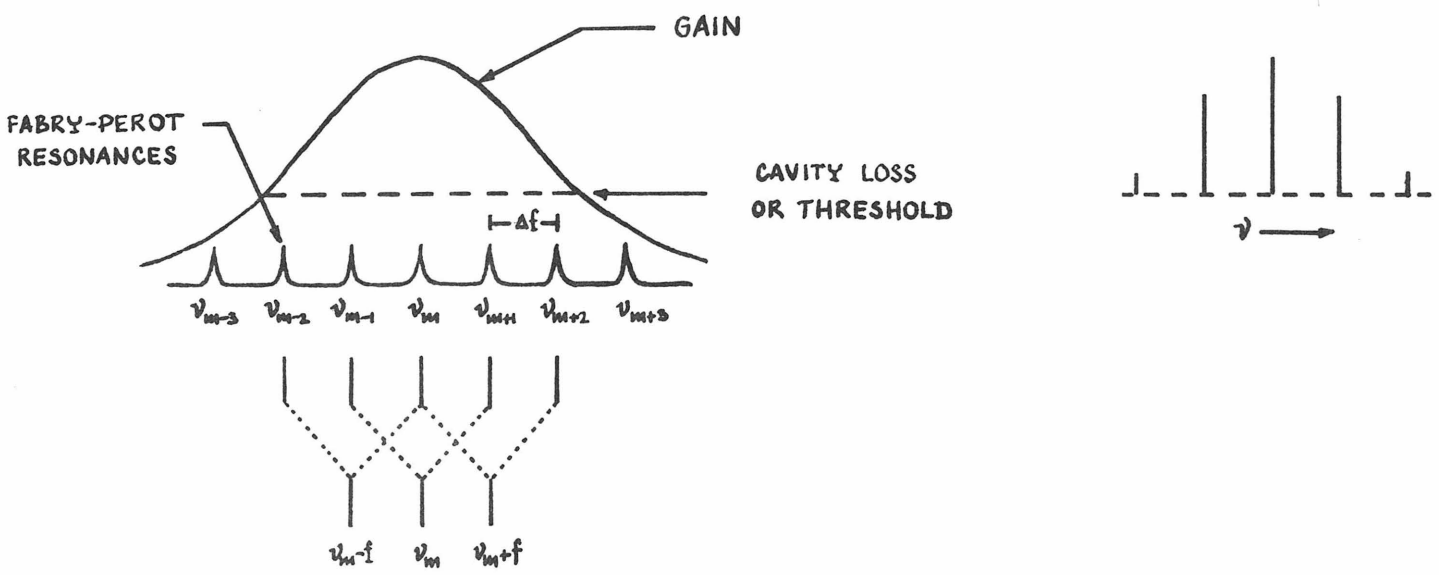
GAIN
FABRY-PEROT
RESONANCES
CAVITY LOSS
OR THRESHOLD
Δf
ν_{m-3} ν_{m-2} ν_{m-1} ν_m ν_{m+1} ν_{m+2} ν_{m+3}
$\nu_m - f$ ν_m $\nu_m + f$
ν

Figure 3

This is the dynamic situation that in most solid lasers gives rise to pulsations. On the other hand, if $\alpha L < \gamma$, the intensity of radiation does not build up; so the threshold of the laser oscillation is required

$$\alpha_m L = \gamma \tag{1}$$

The resonances of such a system are determined by the spectral linewidth of the laser transition and by a number of half wavelengths existing between the two mirrors which form a type of Fabry-Perot interferometer. The gain of a laser line profile superimposed on the resonances of a Fabry-Perot interferometer is shown in Fig. 3.

$$\nu_m = \frac{mc}{2Ln_o} \tag{2}$$

where ν_m is the interferometer resonant frequency

m is an integer representing the number of half wavelengths stored between the two reflectors

L is the resonator optical length or optical distance between the two mirrors

n_o is the index of refraction inside the cavity which is assumed constant.

In general, the optical paths between the mirrors is inhomogeneous (amplifying material and air); it is advantageous to introduce the optical distance

$$L'' = \int_0^L n(z)\, dz$$

integrated along the cavity length.

Then (2) becomes

$$\nu_m = \frac{mc}{2L'} \tag{3}$$

Since the threshold condition is met only in a restricted frequency range, laser oscillations will occur only for a few discrete frequencies ν_m which satisfies (3) and which lie in this restricted range.

The separation between modes is given by

$$f = \frac{c}{2L'} \tag{4}$$

so the round trip transit time is just,

$$\tau = \frac{1}{f} = \frac{2L'}{c} \tag{5}$$

Since the solid state laser resembles a long cylindrical cavity with conducting walls and parallel end surfaces, it is advantageous to introduce transverse electromagnetic modes to the laser wave inside the resonator. The longitudinal modes are those along the axis of the resonator, whereas the transverse modes refer to the one on the plane perpendicular to the axis. In the ordinary case the resonator output contains a number of longitudinal resonator modes (10^6 or more) [3]. An appropriate resonator must be designed for the laser to operate at a single longitudinal mode. For example, the laser resonator should be sufficiently short so that $c/2L'$ is greater than the bandwidth of the gain of the laser material. However, for each longitudinal mode number, there exists a set of transverse modes. For a curved mirror resonator with rectangular symmetry, the cross-sectional amplitude distribution is given closely by:

$$A(x,y) = A_{m,n}[H_m(\frac{\sqrt{2}\,x}{w})\ H_n(\frac{\sqrt{2}\,y}{w})]\exp(-(x^2+y^2)/w^2) \qquad (6)$$

where x,y are the transverse coordinates

$A_{m,n}$ is a constant whose value depends on the field strength of the mode

w is the radius of the fundamental mode (m=0,n=0) at 1/e maximum amplitude

$H_a(b)$ is the a^{th} order Hermite polynomial with argument b

m,n are called the transverse mode numbers, often referred to as TEM_{mn} .

Theoretically, the higher the TEM modes are, the more the energy of the light wave gets distributed into little modes away from the axis. Since the reflectors have finite dimension, some of the beam energy will not get intercepted and hence will be lost. Also, it turns out that for a good mode-locking pattern, it is best to operate at TEM_{00} or as low TEM modes as possible. Hence, it is necessary to use some device which will give high losses to all transverse modes except the desired one. Since the higher order modes spread further from the axis, the easiest way to obtain the single TEM mode is to use an aperture whose size is large enough to let TEM_{00} mode through, but small enough to increase substantially the losses of the higher order modes.

2. Mode-Locking of the Laser

In general, a solid state laser is an inhomogeneous [5] laser. The oscillating modes (the ones that lie in the region where the gain curve is above the loss line in Fig. 3) may vary in frequency spacing,

relative phases, and amplitude. This causes the intensity of the laser output to fluctuate randomly and greatly reduces its usefulness. In order to fix the relative phases or phase-lock the laser, a modulator is needed inside the laser cavity.

It is reasonable to assume that one resonant frequency ν_m will be nearest the peak of the laser gain profile and will therefore be the first to oscillate. If an electro-optic amplitude modulator [6] operating at a frequency f is inserted in the laser feedback interferometer, the frequency ν_m will be amplitude-modulated at a frequency f, such that the time dependent intensity output will be of the form [6]

$$\frac{I_o}{I_i} \simeq \frac{1}{2}[1 + M \sin 2\pi f t] \tag{7}$$

where I_o is the output intensity $\propto E_o^2$

I_i is the input intensity $\propto E_i^2$

M is the modulation index (i.e., the degree of modulation)

From (7)

$$E_o^2 \propto E_i^2(t)[1 + M \sin 2\pi f t] \tag{8}$$

Now

$$E_o(t) = E'\cos 2\pi \nu_m t \tag{9}$$

$$E_o(t) \propto E'[1 + M \sin 2\pi f t]^{1/2} \cos 2\pi \nu_m t \tag{10}$$

In general, $M << 1$; using Taylor's expansion (10) becomes,

$$E_o(t) = E[1 + M \cos 2\pi f t] \cos 2\pi \nu_m t \tag{11}$$

By expansion of Eq. (11), the equation of a wave with a simple sinusoidal amplitude modulation can be written in the form

$$E_o(t) = E \cos 2\pi\nu_m t + \frac{ME}{2} \cos 2\pi(\nu_m - f)t + \frac{ME}{2} \cos 2\pi(\nu_m + f)t \qquad (12)$$

If the modulating frequency f is chosen to be commensurate with the axial mode frequency spacing $f = \Delta f$ (Fig. 3), superposition of the upper (ν_m+f) and lower (ν_m-f) side bands of the amplitude modulated light beam with the adjacent resonances, couples the (ν_m+f), (ν_m-f), and ν_m axial modes with a well-defined amplitude and phase [7]. As the (ν_m+f) and (ν_m-f) oscillations pass through the modulator, they also become amplitude-modulated; their sidebands, in turn, couple the (ν_m+2f) and (ν_m-2f) axial modes to the previous three modes. This process continues until all axial modes falling within the oscillating linewidth are coupled.

In order to compute the peak power of the pulses, the phases are made equal to zero and, writing the total optical field in the simplest form,

$$E(t) = \sum_{-(N-1)/2}^{(N-1)/2} e^{2\pi i(\nu_m+nf)t} \qquad (13)$$

$$= e^{i\omega_n t} \frac{\sin(N\omega t/2)}{\sin(\omega t/2)} \qquad (14)$$

where N is the number of modes locked together; the average laser power output is proportional to $E(t)E^*(t)$:

$$P(t) \propto \frac{\sin^2(N\omega t/2)}{\sin^2(\omega t/2)} \tag{15}$$

thus the peak power is N times the average power.

The above discussion is called "active mode-locking". In our experiment a "passive mode-locking" technique is used. They have, however, the same principle, as will be seen later in Section 4.

Since the "passive modulator" which is utilized in generating picosecond pulses serves both as a Q-switch and an amplitude-modulator, it is appropriate to first discuss the Q-switching principles [8].

3. Q-Switching Principles

It has been shown in Eq. (1) that the laser reaches the threshold of oscillation when α reaches the value

$$\alpha = \gamma/L \tag{16}$$

where the quantity α is proportional to the population inversion

$$N = N_2 \frac{g_1}{g_2} - N_1$$

In order to relate Q to the loss of the resonator, a decay lifetime (photon lifetime) t_c of a cavity mode needs to be defined as follows:

$$\frac{d\mathcal{E}}{dt} = -\frac{\mathcal{E}}{t_c} \tag{17}$$

where $\mathcal{E}$ is the energy stored in the mode. We can also write the intensity loss per unit time as

$$\frac{d\mathcal{E}}{dt} = -\frac{c_o\gamma}{nL} \tag{18}$$

From (17) and (18),

$$t_c = \frac{nL}{c_o\gamma} \tag{19}$$

The quality factor is defined as [8]

$$Q = \frac{\omega\mathcal{E}}{P} = -\frac{\omega\mathcal{E}}{d\mathcal{E}/dt} \tag{20}$$

where $P = -\frac{d\mathcal{E}}{dt}$ is the rate of energy dissipation.

By comparing (19) and (20), we obtain

$$Q = \omega t_c = \frac{\omega nL}{c_o\gamma} \tag{21}$$

$$\frac{\gamma}{L} = \frac{\omega n}{c_o Q} \tag{22}$$

or

$$\alpha = \frac{\omega n}{c_o Q} \tag{23}$$

The Q-switching technique is done by keeping the Q factor of the resonator very low during pumping, which will increase the loss rate of a system (Eq. (22)) so that the population inversion can build up to a very high value without oscillation. This high inversion serves as an energy reservoir. When the inversion reaches its peak, the Q is restored suddenly to the (ordinary) high value. The gain per pass in the laser medium is now well above (ordinary) threshold (Eq. (23)). This causes the extremely rapid build-up of the oscillation and a

simultaneous exhaustion of the inversion by stimulated $2 \rightarrow$ transition. This process converts most of the energy that was stored by atoms pumped into the upper laser level into photons, which are now inside the optical resonator. All this happens in an extremely short time, resulting in very short pulsewidth (nanoseconds), high power, and intensity.

Q-switching may be accomplished by changing the reflectivity of one of the mirrors, by inserting or moving the diaphragm, by changing the path of rays between the mirrors, and also by changing the transparency of the material within the laser cavity. For the efficient production of the single large pulse, it is essential that the Q-switching process be fast compared to the photon-decaying time in the cavity, and that the time of switching from low Q to high Q be chosen so as to assume the accumulation of the greatest possible inversion of the material.

Most typical pulsewidths are 10 to 50 nsec, with the pulse peak on the order of megawatts.

4. Saturable Absorption and Passive Mode-Locking [9]

Mode-locking a laser oscillator with an active modulator requires the critical adjustment of mirror spacing and modulating frequency. In order to avoid this problem, a passive modulator which simultaneously serves as a Q-switch and as an amplitude modulator is utilized.

Saturable Absorption [10]

If a material is normally absorbing at ω due to the transition between levels $|1\rangle$ and $|2\rangle$, the rate of absorption may become so

great at high intensities that a sizable population N_2 builds up in the excited level $|2\rangle$. Since the absorption rate is proportional to the population difference (N_1-N_2), the absorption coefficient will decrease at high intensities. Thus, at optical frequencies, the material acts as a bleachable filter, i.e., it absorbs at low intensity and becomes transparent at high intensity. Such an absorber turns out to be well suited for the role of passive modulator in mode-locking lasers. However, certain properties are required:

1. That it have an absorption line at the laser wavelength;
2. That it have a linewidth equal to or greater than the laser linewidth;
3. That the dye-recovery time be shorter than the loop-time delay (the time it takes for a pulse to travel back and forth between the two reflectors) of the laser.

The simple mode-locking laser set-up is shown in Fig. 4.

Consider a pulse propagating back and forth in the laser cavity. As the pulse propagates through the absorber (assuming a two-quantum level system), the leading edge (which is the low-intensity part) of the pulse is heavily absorbed and molecules make transitions to the upper state. As a result, the absorber tends to saturate (i.e., becomes transparent only at high intensities). This process represents the opening of the passive modulator. After the pulse has propagated through the system, the atoms make transitions back to the ground state which corresponds to the shutting of the modulator. As the pulse is reflected back and forth between two mirrors, more and more of the low

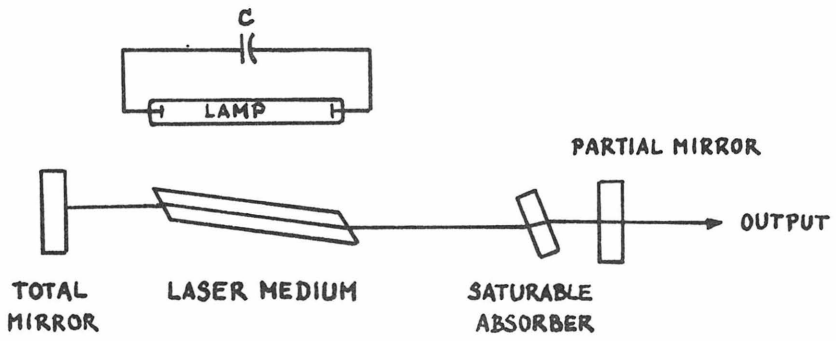

Figure 4 A Mode-Locked Laser

intensity parts of the pulse get absorbed, until the sharpness of the pulse continues to increase to the point that harmonic content of the pulse equals the overall bandwidth of the system. When this occurs, the pulse cannot become narrower. This pulse is then let out of the cavity through the partial reflector.

When viewed from the phase relationship of the modes in such a pulse, the simplified explanation of the mode-locking of the pulse can be given with the aid of the diagram in Fig. 5. When the laser action begins, several axial modes are inevitably excited in the resonator, and the beats (or couplings) between them give rise to intensity fluctuations with a characteristic time $\sim T/m$, where T is the time necessary for the light to travel through the resonator; and m is the number of the excited modes. In the region of the linear development (the ordinary absorption of the dye), natural mode selection by the amplifying medium takes place, owing to the preferred amplification of the modes near the center of the gain line. If an optical carrier frequency ν_0 (which is the mode at the center of the gain line in this case) along with two sidebands $\nu_0 \pm f$ are superimposed, an amplitude modulation of the light results at a frequency $f = \Delta f$ with some peak to peak variation M, and a peak intensity I_0 [see Figs. 5b and 5c]. When this beam is passed through a saturable absorber having the typical characteristic illustrated by Fig. 5a, and the relaxation time is much shorter than T/m, then the absorber builds up intensity fluctuations in the nonlinearity region. As a result, the most intense fluctuation parts become stronger and are compressed much more rapidly, and the peak to peak excursions of the fluctuations will be increased,

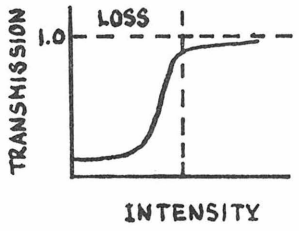
TRANSMISSION
1.0
LOSS
INTENSITY

(a)

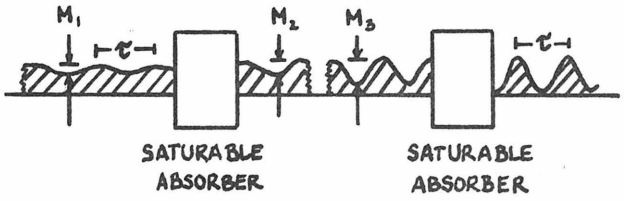
M1
τ
M2
M3
τ
SATURABLE ABSORBER
SATURABLE ABSORBER

(b)

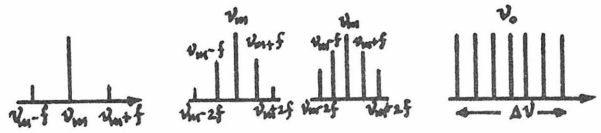

(c)

Figure 5

i.e., $M_2 > M_1$, and the time duration of the fluctuation will be shorter as a result of the nonlinear transmission characteristics of the saturable absorber. With the sharpening of the amplitude variation, additional sidebands are added to the spectrum. In the optical cavity of length $L = c/2\Delta f$, this process is repeated over and over again by reflecting the light beam back and forth between the two mirrors. The fluctuation will continue to sharpen until a discrete pulse is circulating in the cavity. The laser media provide gain to compensate for the residual saturation loss of the absorber and the mirrors. The circulation rate Δf is given by $c/2L$. The pulse will eventually acquire a steady-state width $\Delta\tau$ determined by the bandwidth of the laser media. The repetitive output pulse train emitted from the laser mirrors will have discrete spectral components defined by the Fabry-Perot resonances of the cavity extending $\pm m\Delta f$ on either side of ν_o for a bandwidth $\Delta\nu$, as illustrated in Fig. 5c. The frequencies are all multiples of Δf, and the narrower the pulse width $\Delta\tau$, the larger the bandwidth required for reproducing the repetitive pulse, i.e.,

$$\Delta\tau \simeq \frac{1}{\Delta\nu} \sim 10^{-12}\text{sec}$$

The magnitude and characteristic of pulse sharpening depends mainly on two factors:

1. The relaxation time of the saturable absorber T_b as compared to the pulse width $\Delta\tau$: The shorter the relaxation time is, the shorter and more sharpened the pulse will be. When the bleachable absorber relaxes to the initial state within the time interval

$T_b << \Delta\tau$, the absorber is predominantly bleached by the most intensive peaks. As a result, the pulse width is reduced (all other parts of the pulse being absorbed) and a significant intensity discrimination of large peaks against the background of numerous weaker peaks takes place. On the other hand, when $T_b \gtrsim \Delta\tau$ or when the inertia of the absorber becomes appreciable, the absorber does not have time to "collapse" on one trailing edge of the pulse. As a result, absorption occurs only on a leading front, and the trailing edge of the pulse remains practically undeformed, as has been shown experimentally by [9d]. For the best nonlinear absorbers that are available for ruby and Nd-glass lasers, the values of T_b are: for Kodak dye #9740 = 35 psec; for Kodak dye #9860 = 6 psec; DDI = 14 psec; cryprocyamine = 22 psec [11,12].

2. The number of passes of the pulse through the absorber in the laser cavity.

Experiment

Picosecond Pulse Generation. The Nd^{3+}:glass laser rod is used as the laser amplifying medium in our experiments. The Nd^{3+}:glass energy levels and laser lines are shown in Fig. 6. The laser operation in these transitions depends on the suppression of the favored $^4F_{3/2} \rightarrow {}^4I_{11/2}$ transition by proper choice of frequency dependent mirrors. Moreover, the 0.918 μm line cannot be observed above 77^oK. The main advantages of glass as a laser host as opposed to the crystal (YAG or $Y_3Al_5O_{(2)}$ for example) are:

1. flexibility in size and shape and excellent optical activity;
2. flexibility in refractive index, which may be varied from

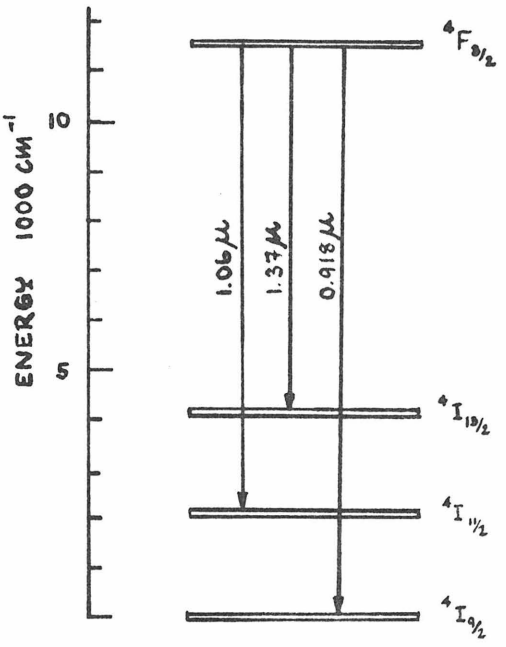

Figure 6. Levels and Groups of Nd^{3+}: Glass Laser Lines (Each Level Shown Represents a Group of Closely Spaced Levels).

approximately 1.5 to 2.0 by selection of the glass. It is possible to adjust the temperature coefficient of the index of refraction so as to produce thermally stable optical cavities, which is very critical in mode-locking the laser.

3. Glass hosts produce broader spectral lines than crystal. This is useful because it provides for absorption of a greater position of the pumping radiation. Also for the mode-locking operation, the broader spectral lines (containing more modes) lead to the shorter pulse width (initial T/m or final $\Delta\tau \simeq 1/\Delta\nu$ as discussed above).

The disadvantages are:

1. The low thermal conductivity of glass which imposes limitations on continuous operation or high repetition rate operations.

2. The broad spectral lines make it more difficult to attain threshold because a larger inversion is required to compensate for the lower peak of the lineshape.

In this laboratory a Nd^{3+}:glass rod, 8 inches long and 1/2 inch in diameter is employed. The rod is constituted of 3.1 wt.% of Nd^{3+} ions which gives 2.83×10^{20} ions/cc glass. The fluorescence decay time (1/3) is 300 microsecond. The threshold required for this laser is 1.4 joules. Both faces of the rod are polished with extreme care (a scratch on the face may cause great damage to the rod when high-powered laser pulses travel back and forth through the rod in the cavity), and cut at Brewster angle: $57^{o}16'$. The rod must be cleaned by using a dust-free microduster each time before operation. The excitation source or the laser head is a helical xenon flashlamp (by Korad Laser Systems, Union Carbide) which is connected to a 5 KV power supply (Korad, model

K-1). The laser rod is placed inside this laser head and is cooled by filtered water (chemical ion-free)--at the rate of about 2 gal/min (ITT self-pumping pump; the rate is controlled by a Variac set at 120V out for 120V in). A 99.99% R (at 1.06μ) 10M radius mirror and a 55% R (at 1.06μ) wedged mirror (both from Optical Coating Division) are used as the back and front reflectors for the laser cavity, respectively. The Q-switch dye solution is Kodak #9860 which is light- and acid-sensitive. The solvent used to dilute the dye down to the appropriate concentration for the laser cavity is acid-free dichloroethane (provided with the #9860 dye). A 40 mm diameter; 1,0 cm thick (Pyrex Opticell) is used as the dye cell. The cell is placed at the Brewster angle, $55^{o}41'$ to the laser light so as to eliminate the unwanted reflection back to the rod. At the Brewster angle, the optical path length of the cell becomes 1.229 cm (see Figs. 7 and 8).

70% T at 1.229 cm path length of the dye solution is made up using dichloroethane as solvent. The absorption is checked by Cary 14 (infrared region adapted) at only one wavelength of 1.06μ .

Result (from the first run as an example):

absorption at 1.0 cm path length = 0.125

at 1.229 cm path length = 0.125 x 1.229 = 0.1533

which is 70.30% T

The #9860 solution is very strong; in order to obtain 100 ml of the desired solution, only 1.35 ml of the dye is needed.

Figure 9 shows the result for this run from Cary 14.

Aligning the laser cavity. A He-Ne laser (at 6328Å, 1.0 mwatt, Astrophysics model 133) is used to align the cavity as shown in Fig. 10

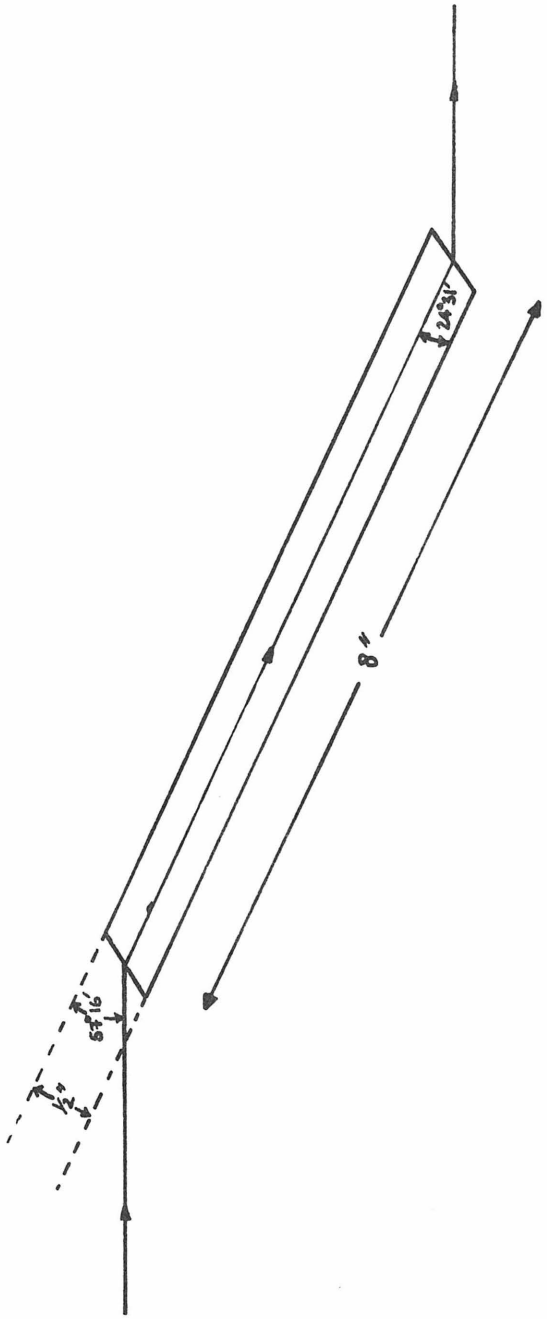

Figure 7. The Nd^{3+}:Glass Laser Rod Placed at Brewster Angle.

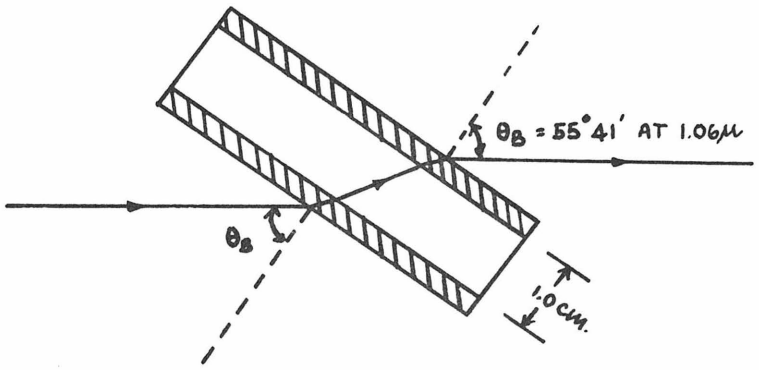

Figure 8. A Saturable Absorber Cell, Filled with Kodak Dye #9860 in Dichloroethane, at Brewster Angle (θ_B).

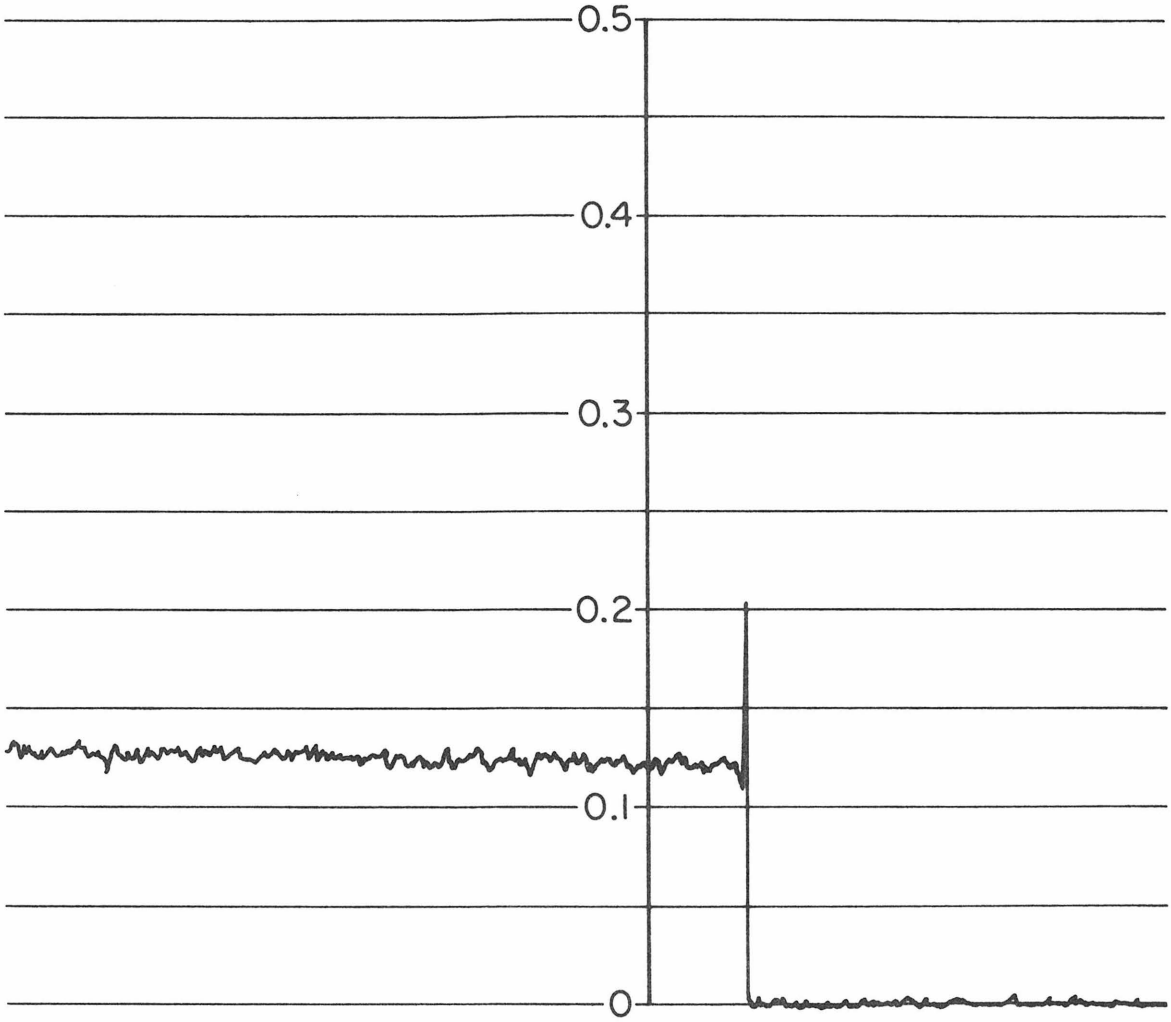

Figure 9. Absorption Spectrum of #9860 Dye Solution from Cary 14 set at 1.06μ

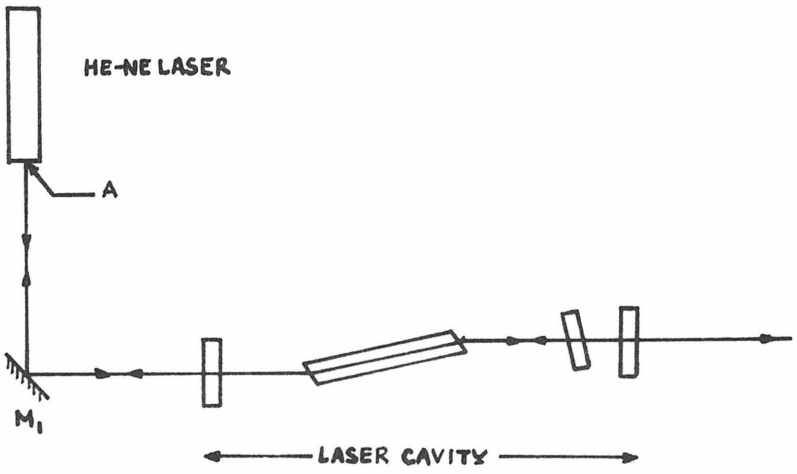

Figure 10. The Laser Cavity Alignment

It is to be noted here that all our optics are mounted on magnetic bases (from Rutland Company, Japan), which are placed on a 4' x 9' steel board on top of a wooden table. A piece of foam is inserted between the board and the table in order to absorb the vibration from the floor. The center of the laser rod is 5-3/16" above the steel board, which becomes the height of our laser beam. The alignment is such that the reflections of the He-Ne laser from the mirrors are on top of the laser beam itself at the laser output (point A in the diagram).

The He-Ne laser is bolted on one corner of the table; the laser beam is aligned by moving the laser and also mirror M_1 until the beam becomes level. One must check, also, whether the He-Ne beam is on the axis of the mode-locked beam. This is done by using a photograph as a target for 1.06μ pulse. The high-powered pulses will make a burnt spot on the photograph. Then unblock (the He-Ne beam is always blocked when the laser is fired) the He-Ne beam and see whether they are superimposed. This should be done at far field in order to increase the accuracy. If they do not superimpose, the correction can be made by moving M_1 sideways. This part is very critical, since we will be using the He-Ne beam to align all the optical systems.

The threshold of the power input depends on how well the laser cavity is aligned. It is always better to operate the laser at the threshold or very close to the threshold, in order to generate a good mode-locking pulse train or good pulse structure, for some analytical purposes. In doing so, an extra mirror may be placed at the very far end of the table, to make this alignment more sensitive. First align the reflection spot from the mirror on the He-Ne laser, split this

reflected beam by the beam splitter BS (see Fig. 11) and then align the cavity mirrors so as to get the reflected spots from them on the spot from the far-field mirror. An interference pattern will occur if the three spots are superimposed.

After the cavity alignment, we look at the threshold of the conventional mode laser first (i.e., without the dye solution). The values observed are in the range of 2.2 - 2.6 KV (power supply), which was quite low. In order to check whether it lases, we put a photograph as a target and looked for a burnt spot. Then we put the 70% T (for example, the concentration of the dye is about 70% T to 65% T) dye solution in, realigned the cavity because the dye solution at Brewster angle changed the laser direction. The threshold was 3.0 KV (the range is from 3.0 to 3.90 KV, depending on the concentration of the dye solution).

At the threshold, usually there is only one TEM mode which can sometimes be observed from the burnt spot. Operating at higher voltages, many TEM modes are produced and that may distort the pulse train.

The pulse train is observed by means of the oscilloscope, Tektronix 519 model, which has a rise time of 0.35 nsec. This is the fastest time resolution available so far. The photodetector is a pin photodiode HP 5082 (Hewlett-Packard) which is an ultrafast light detector for visible and near infrared radiation. Suitable filters (e.g., Corning 1-64) together with a ground glass are needed to attenuate the incident radiation on the diode. The pictures are taken by Polaroid camera type C-17, using 410 Polaroid film. A typical good mode-locked

pulse train is shown in Fig. 12a.

If the pulses are not well mode-locked, or the diode is overloaded, the baseline of the pulse train does not stay at the same level as shown in Fig. 12b. Also, if the dye solution cell is not placed at the Brewster angle, the picture will show more than one pulse train (the additional ones are called "satellites") due to the reflection at the cell window back to the laser rod. These trains do not arrive at the oscilloscope at the same time. The separated distance depends on the position of the dye cell inside the cavity [1a]. Or, if the laser rod is overpumped, the pulse patterns are shown in Fig. 13b.

The deviation from an ideal picture [1a] in this case is due to the nonlinear losses in the optical media--due to powerful radiation [9d]. The change in the refractive index of the laser glass matrix results in self-focusing of the radiation and spectral broadening. The influence of the nonlinear loss is suggested in the following way. Beginning from a certain level of intensity, amplification of the most intensive ultrashort pulses decreases, i.e., there occurs a limitation on the pulse power. At the same time, less intensive USP can be amplified and reach the same power level as the most intensive pulses. This should result in an increase in the number of satellite pulses at the end of the train. The wide pulses with shoulders probably contain many substructures of picosecond widths as shown in Fig. 14. Some of the very intense and powerful spikes cause the self-focusing and hence "hot spots" in the optics, and damage them.

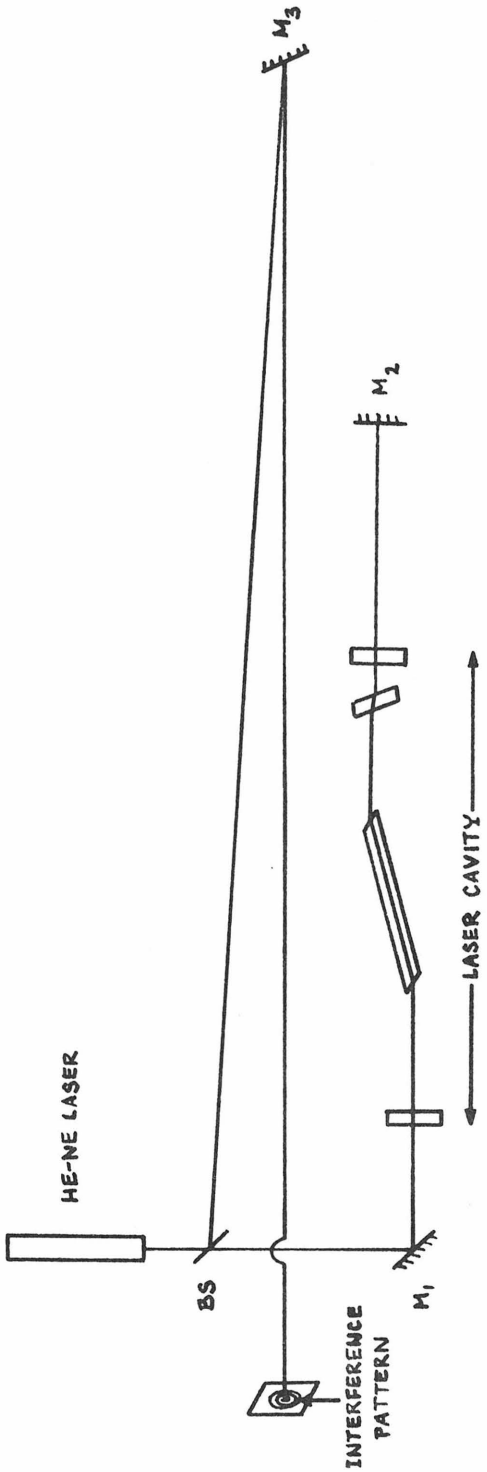

Figure 11 A "Far Field" Method of Alignment.

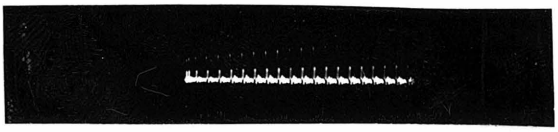

Figure 12a. A Well-Mode-Locked Pulse Train (from 519 Oscilloscope) at 20 nsec/div.

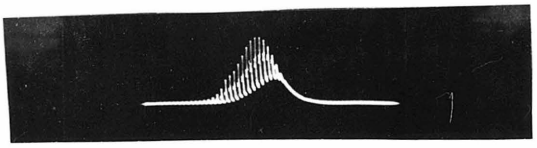

Figure 12b. A Bad Mode-Locked Pulse Train at 50 nsec/div.

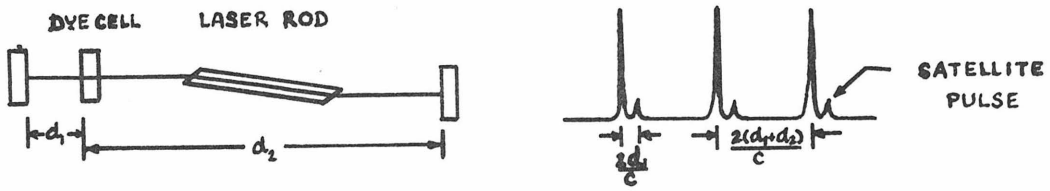

Figure 13 a. A Pulse Train with Satellites.

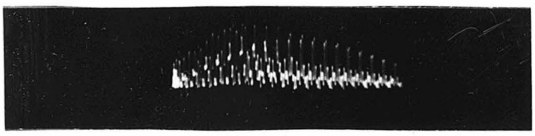

Figure 13 b. An Overpumped Mode-Locked Pulse Train.

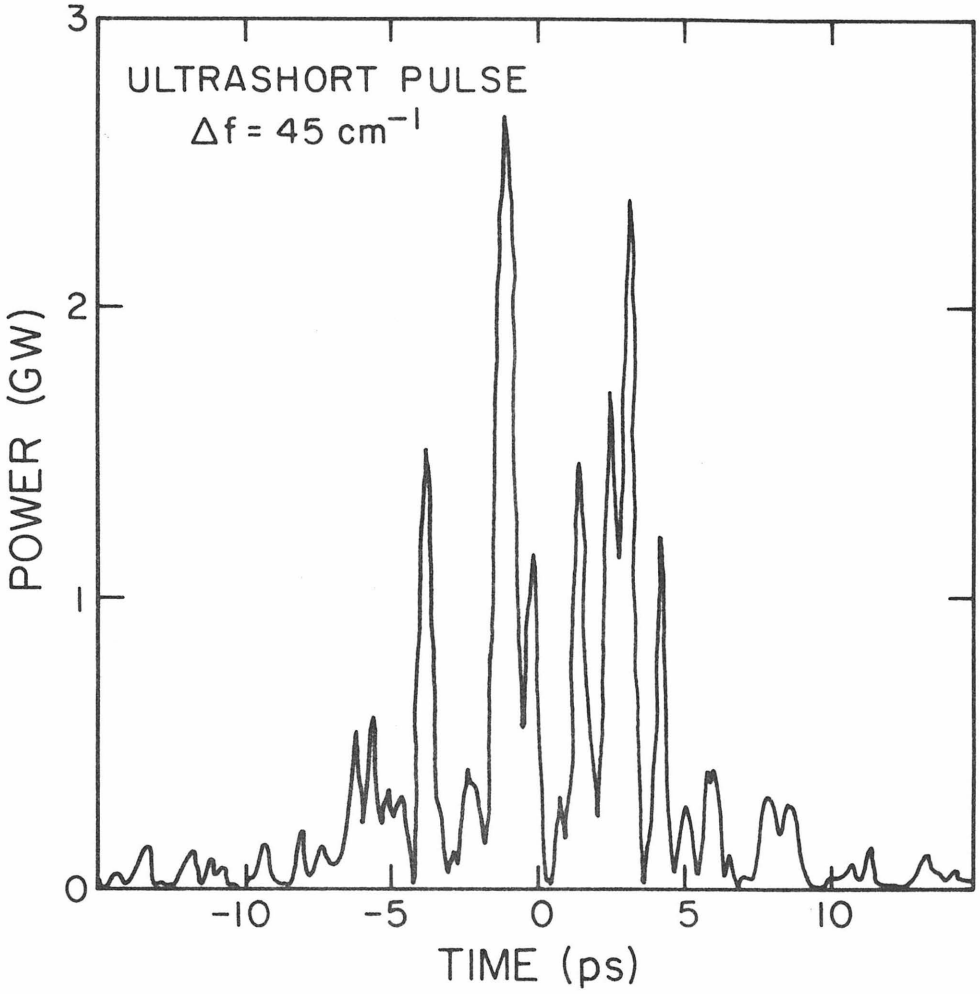

Figure 14
A Calculated Mode-Locked Nd:Glass Pulse Shape with Substructures (ref. 31)

C. Two-Photon Method as a Pulse Width Measurement

Since the direct electronic techniques are not yet capable of measuring time durations down to 10^{-12}sec, a special technique is required in order to measure the picosecond pulse widths. The first technique developed for measuring ultrashort light pulses is based on two-photon absorption [13]. Excitation of a molecule under very intense irradiation takes place by absorption of two photons, provided that the molecule has an excited energy level corresponding to $2\nu_1$ where ν_1 is the frequency of the exciting light. Such two-photon absorption takes place via a virtual state of essentially zero lifetime and can occur only when the two photons are absorbed simultaneously. If the resulting excited state fluoresces, one can monitor the extent of two-photon absorption by following the emission study. The method is done by directing a mode-locked train of pulses through a cell containing a suitable solution; the resultant trail of two-photon excited emission can be photographed and will appear as a bright streak. If the pulse train is reflected back on itself by a 100% R mirror, the instantaneous light intensity at the mirror and other points where the pulses overlap will be higher and a brighter fluorescence spot will be observed. Thus, the length of the bright spot is a measure of the length of the pulse.

For a Nd^{3+}:glass laser, rhodamine 6G (fluorescence is centered at 5500Å) has proved to be one best detector for the TPF method. Two methods have been conducted as follows:

1. The correlation of one pulse with the succeeding pulse (cross correlation). From the picture of the pulse train (Fig. 15), one can

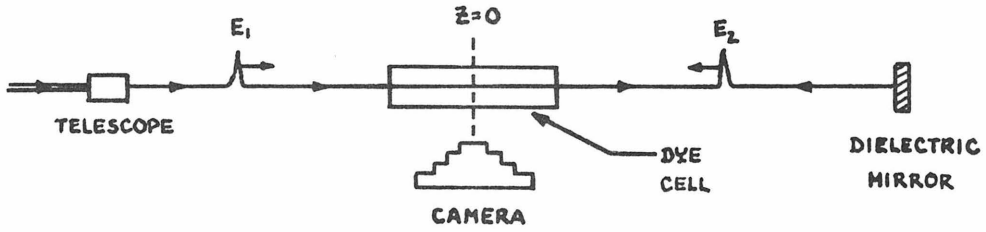

Figure 15. Cross Correlation Two Photon Method.

see that there are more than 50 pulses. These pulses are separated from the succeeding ones by twice the round trip time in the cavity. A mirror (usually a dielectric 100% R at 1.06 μ is used) is then placed at a distance of roughly the cavity length away from the cell of Rh 6G.

The telescope is put in to reduce the size of the beam, in order to give a better depth of the field of the pulse train to the camera.

The distance x must satisfy the following condition, in order to observe the TPF at the middle of the cell. Assume the cell is 5 cm long:

$$2L = \frac{5}{c_R} + \frac{2x}{c} \qquad (1)$$

where L = optical path length of the cavity

$c_R = c/n_R$, n_R is the index of refraction of Rh 6G

c = velocity of light = 3×10^{10} cm/sec

Note: The distances must be measured and calculated accurately in order to observe TPF picture.

2. The correlation of the pulse with itself (autocorrelation). This seems to be experimentally easier than the first method; the measurement is not as critical.

In this method the laser pulse is split into two equal parts by a 50% R beam splitter (at 45^{o} to the beam). Then the two pulses are reflected to meet in the Rh 6G cell (see Fig. 16).

The pictures are taken by Polaroid film type 47, speed 3000, and by transparent type 46L. The transparent pictures are read by the

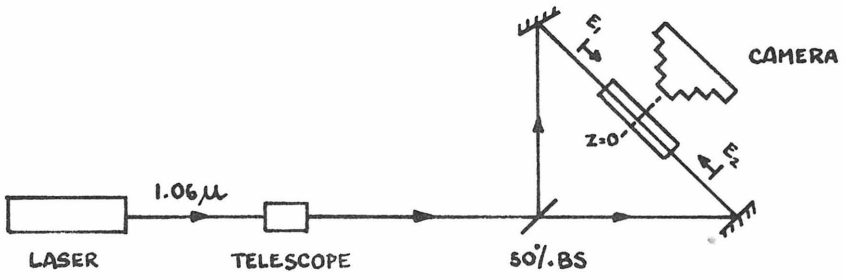

Figure 16. Autocorrelation Two Photon Method

Jarrell-Ash microdensitometer. The length of the bright spot is the width of the pulse which is read from the half-width of the curve from the densitometer. Some results are shown in Fig. 17.

The calculation is rather simple: for example, from Fig. 17:

The densitometer is run at 1 mm/min

The scale is 32 sec/1.25 cm

The half-width readings are 3.7 - 3.9 cm

3.7 cm corresponds to $\frac{3.7}{1.25} \times \frac{32}{60} = 1.58$ min, or 1.58 mm

$$\Delta\tau = \frac{d \times n_R}{c} \qquad (2)$$

n_R is equal to 1.344

$$\Delta\tau = \frac{1.58 \times 10^{-1} \times 1.344}{3 \times 10^{10}} = 7.015 \text{ psec}$$

The curve from the microdensitometer is not sharp--there are many shoulders. This is due to the glow around the bright spot. The half-width is then read from the adjusted curve, taking the highest peak in the curve. However, the results are probably within ±2 psec.

The factors involved in obtaining good TPF pictures are:

1. The two pulses are exactly superimposed.
2. The background is very dim.
3. The camera is not overexposed and is in focus.

The intensity ratio between the TPF and the background is 2.5 which is close to the theoretical value of 3 .

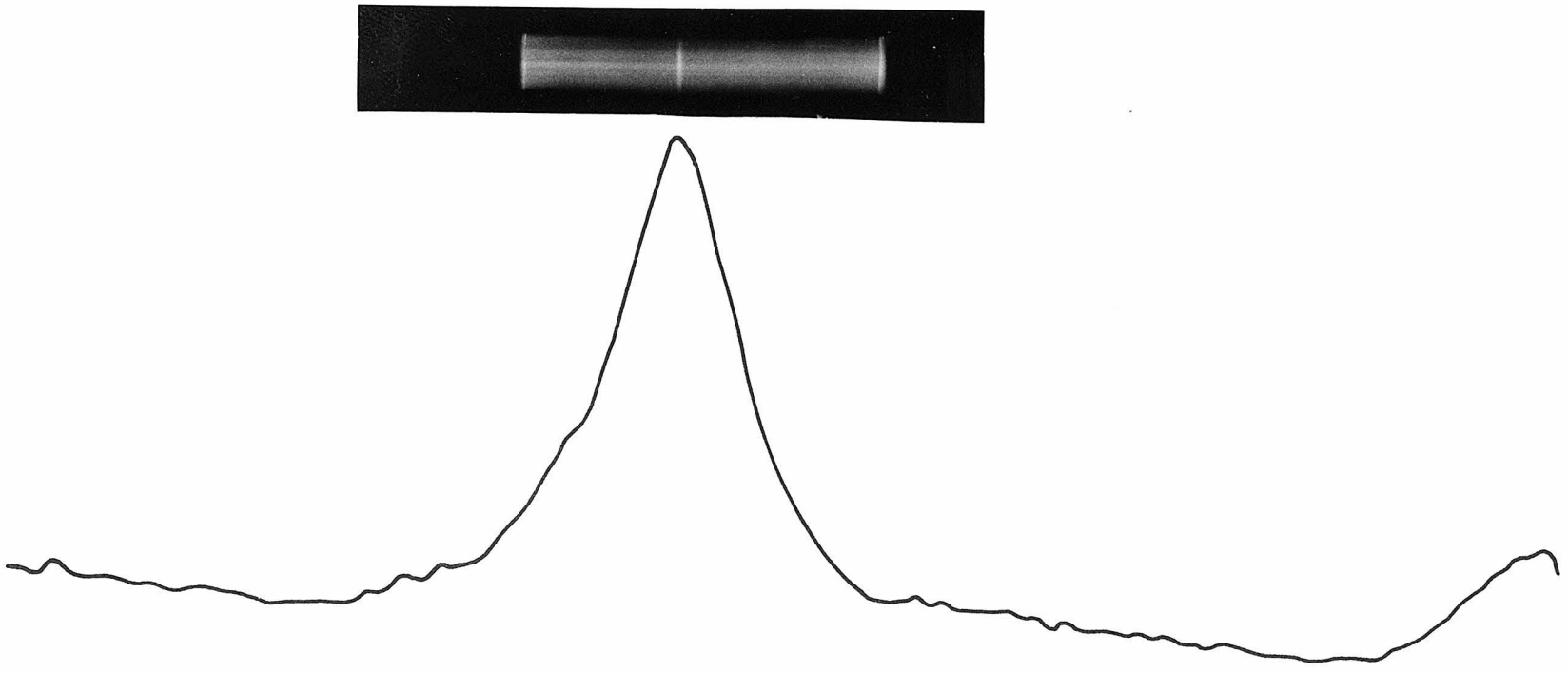

Figure 17
Two Photon Fluorescence in Rh 6G Solution and the Microdensitometer Trace.

Theory

If we consider the center of the cell to be the origin $(z = 0)$ and denote the pulses approaching the cell from the left and right as

$$E_1(t - \tfrac{z}{c}) \sin(kz-\omega t) \qquad \text{and} \qquad E_2(t + \tfrac{z}{c}) \sin(-kz-\omega t) \tag{3}$$

respectively, the intensity I_ω in the dye cell will then be given by

$$I_\omega = E_1^2(t - \tfrac{z}{c}) + 2E_1(t - \tfrac{z}{c})\, E_2(t + \tfrac{z}{c}) \cos 2kz + E_2^2(t + \tfrac{z}{c}) \tag{4}$$

If we assume that the fluorescent intensity is proportional to the intensity squared: $I_F \propto I_\omega^2$ (or $I_F \propto I_{\omega'} I_{\omega''}$ for TPF from two different frequency pulses), then

$$I_F \propto \{E_1^4(t - \tfrac{z}{c}) + E_2^4(t + \tfrac{z}{c}) + 2E_1^2(t - \tfrac{z}{c})\, E_2^2(t + \tfrac{z}{c}) + [1 + 2(\cos 2kz)^2]$$

$$+ 4[E_1^3(t - \tfrac{z}{c})\, E_2(t + \tfrac{z}{c}) + E_1(t - \tfrac{z}{c})\, E_2^3(t + \tfrac{z}{c}) \cos 2kz\} \tag{5}$$

The time-and-space averaged through the photographic process of I_F is given by

$$S(\tau) \propto \int_{-\infty}^{\infty} E_1^4(t - \tfrac{z}{c})dt + \int_{-\infty}^{\infty} E_2^4(t + \tfrac{z}{c})dt + 4 \int_{-\infty}^{\infty} E_1^2(t - \tfrac{z}{c})\, E_2^2(t + \tfrac{z}{c})dt \tag{6}$$

Letting $E_1(t) = E_2(t)$ at $z = 0$, the second harmonic pulse energy $^{2\omega}W$ is given by

$$2\omega_W = \int_{-\infty}^{\infty} E^4(t)\, dt \tag{7}$$

The normalization of $S(\tau)$ gives

$$\frac{S(\tau)}{W} \propto 1 + 2G(\tau) \tag{8}$$

where $G(\tau)$, the autocorrelation function of the pulse energy, is given by

$$G(\tau) = \frac{\int_{-\infty}^{\infty} E^2(t)\, E^2(t-\tau)dt}{\int_{-\infty}^{\infty} E^4(t)dt} = 1 \quad \text{at} \quad \tau = 0 \tag{9}$$

$$\Longrightarrow \frac{S(\tau)}{W} = 3 \qquad \text{when} \quad \tau = 0 \tag{10}$$

This intensity ratio is also the degree of mode-locking of the laser as suggested by J. R. Klauder, et al. [14]. If the intensity ratio is 3, that means it is mode-locked; if 1.5, it implies the free running laser (randomly phased modes). Our results are then interpreted to be quite well mode-locked.

In order to narrow the pulse width and increase the peak power, the following techniques may be considered:

1. Decrease the %T of the absorber dye solution.

There is no theoretical way of predicting the %T of the dye solution in order to obtain the narrowest pulse width or well mode-locked pulse train. This varies from one system to another.

2. Decrease the %R of the front mirror, to obtain higher powered pulses.

3. Decrease the path length of the dye cell. D. J. Bradley, et al. [32] reported that the shortest pulses and the most reliable mode-locking were achieved when the saturable dye was placed in contact with one of the cavity mirrors and the dye cell length was reduced to $\simeq 30\mu$.

4. Better alignment of the cavity.

D. Second Harmonic Generation (SHG)

The mode-locking laser, in spite of the fact that it produces very short pulses in picosecond time scale, seems to be of limited usage with only one wavelength in the infrared (1.06μ). However, in 1961, Franken, et al. [15] reported the second harmonic generation experiment by focusing the ruby laser beam at 6940Å on the front surface of a crystalline quartz plate. One of the emerging beams was found to have the frequency twice that of the input. Later Giordmaine [16] and Maker [17] independently reported the method of index-matching of the KDP crystal in order to obtain the best output of the SHG.

Theory

SHG is a nonlinear optical phenomenon which has been observed in some crystals, such as quartz, ADP (ammonium dihydrogen phosphate) and KDP (potassium dihydrogen phosphate), etc. A suitable material for this process must be relatively transparent to the fundamental optical frequency and the desired harmonics. In addition, lack of an inversion symmetry of such crystal is a prerequisite for the SHG crystal, in order that the second order ($P \propto E^2$) nonlinear optical

properties can be displayed.

In general, a schematic expression for the dependence of the optical polarization P as a function of applied electric field E is:

$$P = XE(1 + a_1E + a_2E^2 + \cdots) \tag{1}$$

where X is the linear optical polarizability, of order unity

a_i is the nonlinear coefficient.

The second term xa_1E^2 is of interest, since it gives rise to the SHG.

Consider the nonlinear coupling of two optical fields, the first, having its electric field of frequency ω_1 along the j-direction, is given by

$$E_j^{\omega_1}(t) = \mathrm{Re}(E_j^{\omega_1} e^{i\omega_1 t}) = \frac{1}{2}(E_j^o e^{i\omega_1 t} + \text{c.c.}) \tag{2}$$

the second field at ω_2 along the k-direction is

$$E_k^{\omega_2}(t) = \mathrm{Re}(E_k^{\omega_2} e^{i\omega_2 t}) \tag{3}$$

If the medium is nonlinear, the presence of these field components can give rise to polarization at frequency $n\omega_1 + m\omega_2$, and n and m are any integers. Taking the polarization component at $\omega_3 = \omega_1 + \omega_2$ along the i-direction

$$P^{\omega_3=\omega_1+\omega_2}(t) = d_{ijk}^{\omega_3=\omega_1+\omega_2} E_j^{\omega_1} E_k^{\omega_2} \tag{4}$$

where $d_{ijk}^{\omega_3}$ is a third rank nonlinear susceptibility tensor and has the following properties:

(1) It is nonvanishing only in noncentrosymmetric crystals.

(2) It is independent of frequency, since the material is transparent over the region which includes ω_1, ω_2, and ω_3. We can then write

$$P_i(t) = d_{ijk} E_j(t)\, E_k(t) \tag{5}$$

(3) Since no physical significance can be attached to an exchange of E_j and E_k in (5), it follows that $d_{ijk} = d_{ikj}$. We therefore can replace the subscripts k,j by a single symbol and hence reduce the full form of d tensor from $(3 \times 3 \times 3)$ to a contracted one which is (6×3)

The contracted d_{ij} tensor obeys the same symmetry restriction as the piezoelectric tensor, and in the crystals of a given point group symmetry it has the same form. For KDP, the symmetry is $\bar{4}2m$, and the tensor is

$$d_{ij} = \begin{vmatrix} 0 & 0 & 0 & d_{14} & 0 & 0 \\ 0 & 0 & 0 & 0 & d_{14} & 0 \\ 0 & 0 & 0 & 0 & 0 & d_{30} \end{vmatrix} \tag{6}$$

where the full equation of P is

$$\begin{vmatrix} P_x \\ P_y \\ P_z \end{vmatrix} = \begin{vmatrix} d_{11} & d_{12} & d_{13} & d_{14} & d_{15} & d_{16} \\ d_{21} & d_{22} & d_{23} & d_{24} & d_{25} & d_{26} \\ d_{31} & d_{32} & d_{33} & d_{34} & d_{35} & d_{36} \end{vmatrix} \begin{vmatrix} E_x^2 \\ E_y^2 \\ E_z^2 \\ 2E_zE_y \\ 2E_zE_x \\ 2E_xE_y \end{vmatrix} \tag{7}$$

and the components of the nonlinear polarization are

$$P_x = 2d_{14} E_z E_y$$

$$P_y = 2d_{14} E_z E_x$$

$$P_z = 2d_{36} E_x E_y \tag{8}$$

In order to obtain an expression for one power of the second harmonic, Maxwell equations are the starting point:

$$\nabla \times \vec{H} = \vec{i} + \frac{\partial \vec{D}}{\partial t} = i + \frac{\partial}{\partial t} (\varepsilon_o \vec{E} + \vec{P})$$

$$\nabla \times \vec{E} = - \frac{\partial}{\partial t} (\mu_o \vec{H}) \tag{9}$$

where $$\vec{P} = \varepsilon_o x_L \vec{E} + \vec{P}_{NL} \tag{10}$$

and $$(P_{NL})_i = d_{ijk} E_j E_k \tag{11}$$

The derivations are given in Ref. [18], and the power output of the second harmonic in cgs units is

$$\frac{P(2\omega)}{\text{area}} = \frac{\pi}{2cn_3} \sin^2\theta \, \omega_3^2 \, d_{ijk}^2 \, E_{1i}^2 \, E_{1k}^2 \, L^2 \, \frac{\sin^2(\Delta k \frac{L}{2})}{(\frac{\Delta kL}{2})^2} \tag{12}$$

where $\omega_3 = 2\omega_1$, $\omega_1 = \omega_2 = \omega$ is the fundamental frequency

ω_3 is the second harmonic frequency

n_3 = index refractive of second harmonic in crystal

θ = the angle between the j direction of the second harmonic and the direction of propagation

L = length of the crystal

and

$$k = k_3^{(j)} - k_1^{(i)} - k_1^{(k)} \tag{13}$$

Index-Matching Technique. From (12), it is clear that in order to get appreciable SHG, the condition $\Delta k = 0$ must be satisfied, and if the i and k components of ω_1 propagate with the same phase velocity, then

$$k_3^{2\omega} = 2k_1^{\omega} \tag{14}$$

or, using $k^{\omega} = \omega n^{\omega}(\theta)/c$, we obtain

$$n^{2\omega}(\theta) = n^{\omega}(\theta) \tag{15}$$

where we recognize that in a uniaxial crystal (i.e., the crystal in which the highest degree of rotational symmetry applies to no more than a single axis), the index of refraction n for a given frequency depends on the angle θ between the direction of propagation and and z (optic) axis. KDP is a negative uniaxial crystal so that $n_e^{\omega} < n_o^{\omega}$ (where n_e^{ω} is the index of refraction along the extraordinary ray, and n_o^{ω} is that along the ordinary ray, for a birefringent crystal). Index matching can be obtained if the fundamental beam is an ordinary ray, while the second harmonic is an extraordinary beam, both beams propagating in a direction making an angle θ_m with one z-axis, so that

$$n_e^{2\omega}(\theta_m) = n_o^{\omega}$$

(Note that, once we choose an appropriate optical axis, n_o (ordinary ray), but not n_e (extraordinary ray) is independent of the propagation direction. This subject can be seen in detail in Ref. [18],

Chapter 18). A plot is shown in Fig. 18.

Experimentally, the crystal face has to be adjusted both horizontally and vertically with respect to the incident fundamental beam until the maximum second harmonic is obtained (i.e., the incident beam is now in the propagation direction, making θ_m angle with the optic axis). Once this condition is satisfied, both the fundamental and second harmonic beams emerge from the KDP crystal (in our case) at the same time and in the same direction, but with cross polarization.

Experiment

The experiment is shown in Fig. 19; a fraction of the incident 1.06μ , which was our monitoring beam, was split off by the beam splitter BS_1 and fed into a fast photodiode filter with appropriate output. The 0.53μ was also sent into the fast photodiode with 1.06μ out-off and neutral density filters. Both photodiodes were connected to a dual beam oscilloscope, Tektronix model 555. Since the fastest time scale on this oscilloscope is 100 nsec/div, no fine resolution of the pulse trains was observed. Only envelopes of the pulse trains could be recorded. The ratios were taken from the maximum points of both pulse train profiles.

The 1 inch-long KDP is placed in a doubler holder filled with oil. This whole piece is then placed in an adjustable holder (vertically and horizontally). The best positions of KDP were obtained from the maximum ratio of the output intensity of 0.53μ to that of the incident 1.06μ.

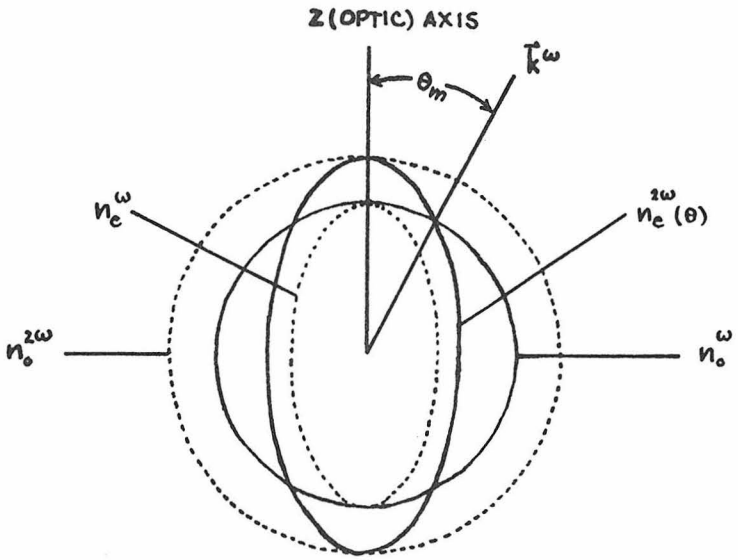

Figure 18. Normal (Index) Surfaces for the Ordinary and Extraordinary Rays in a Negative Uniaxial Crystal (from ref. 18).

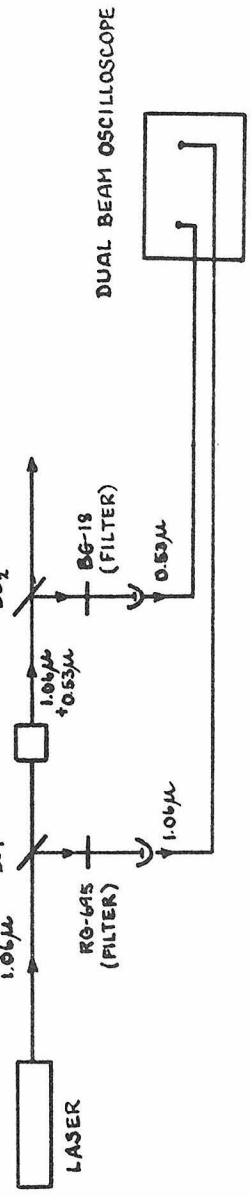

Figure 19. The Second Harmonic Phase Matching of KDP Crystal Experiment.

The ratios are shown in the table and the plots on Figs. 20 and 21 from various vertical and horizontal settings, respectively.

vertical settings (horizontal position is at 2.50)		horizontal settings (vertical position is at 2.18)	
setting	ratio	setting	ratio
2.25	4.43	2.90	10.62
2.20	8.89	2.80	13.78
2.19	10.478	2.70	12.00
2.18	21.818	2.60	10.91
2.16	15.33	2.55	10.00
2.15	13.53	2.52	11.26
2.10	5.45	2.51	9.54
2.05	2.361	2.50	17.00
1.95	0.60	2.49	16.15
1.85	0.336	2.45	15.00
1.75	0.200	2.30	9.00
1.65	0.15	2.20	9.14

The best position of the doubler for index-matching is

vertical reading: 2.18
horizontal reading: 2.50

From the plot, one can see that the vertical setting is much more critical than the horizontal. Hence, one must be very careful at this point. If the doubler is not index-matched:

1. The 1.06μ and 0.53μ do not leave the doubler at the same time ($n_1^o \neq n_2^e(\theta)$).

2. The 1.06μ and 0.53μ do not travel the same direction. This is very critical at the far field when the superposition of the beams

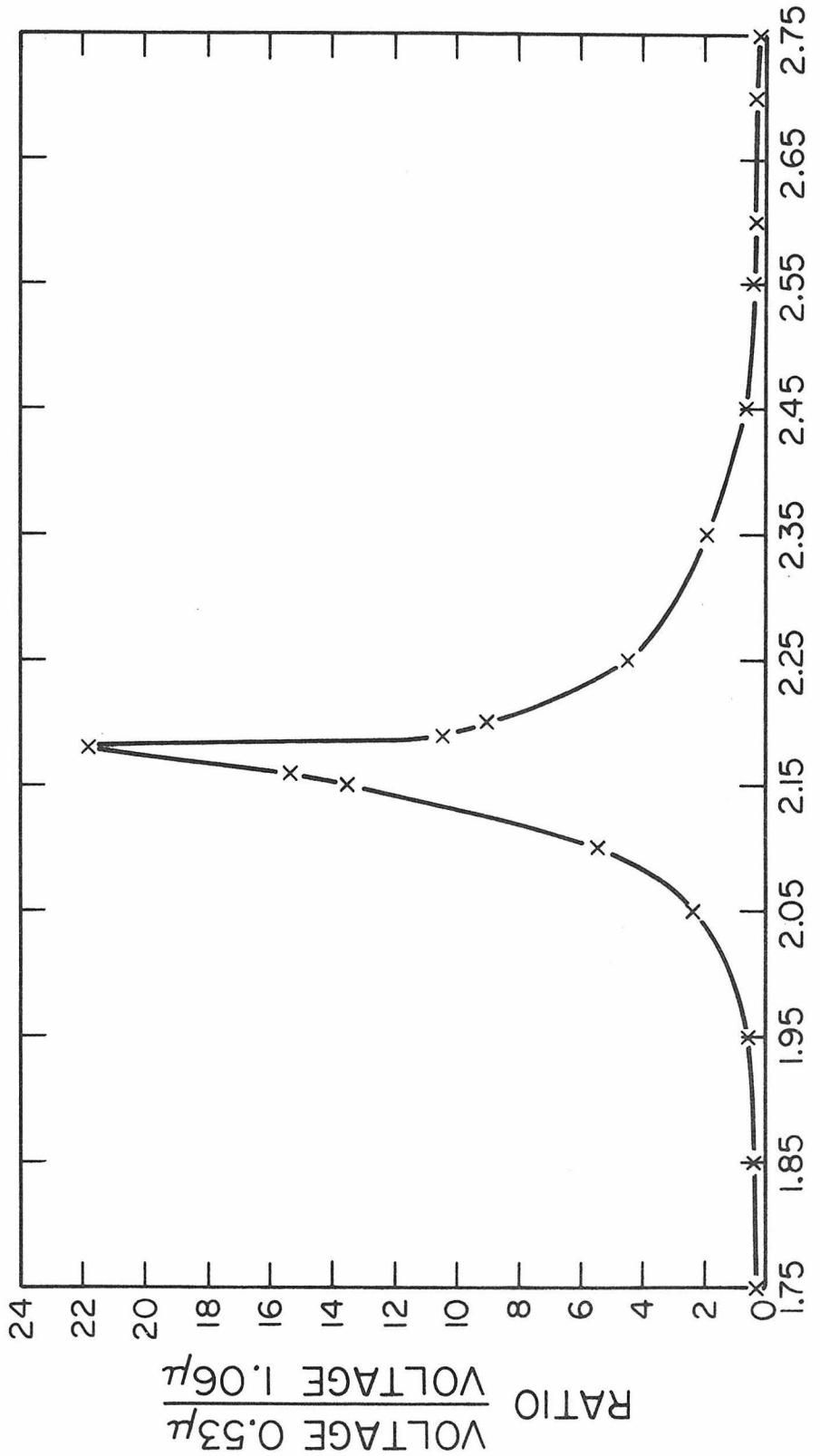

Figure 20. Results From the Phase Matching Experiment.

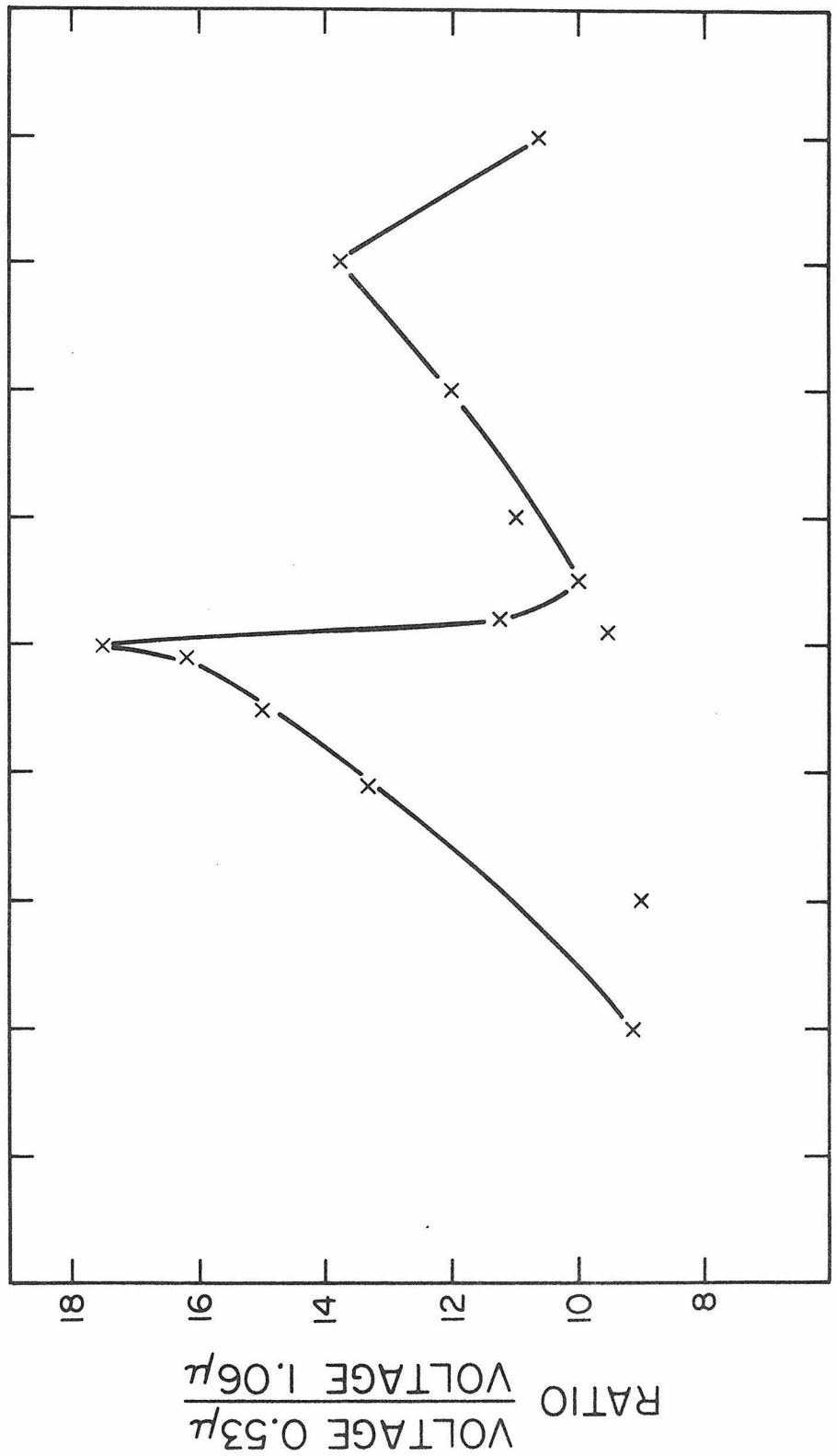

Figure 21. Results From the Phase Matching Experiment.

is required in analytical work.

The 1.06μ polarization is vertical, whereas that of 0.53μ is horizontal. The conversion factor is 5-10%.

E. Two-Photon Method of Two Different Optical Frequencies

TPF from Picosecond Pulses of Two Different Optical Frequencies. We use the same technique for the measurement. However, the method in setting up the experiment was quite different, following Rentzepis and Duguay's, as shown in Fig. 22.

We made use of the difference in the indices of refraction of the two frequencies, assuming that the doubler was index-matched, i.e., 1.06μ and 0.53μ left the doubler at the same time. After passing through a 10 cm cell of bromobenzene, 1.06μ pulse led 0.53μ by 27 psec (calculated from the table of observed dispersions as reported by Topp and Rentzepis [18]. The pulses then entered a 5.0 cm cell of BBOT in methyl cyclohexane with a dielectric mirror placed at the end of the cell. This mirror is 100% R at 1.06μ which was aligned to reflect the leading 1.06μ beam back into the cell, exactly along the same direction, in order to meet the 0.53μ beam and create the TPF in the solution. The picture was taken using Polaroid film speed 3000. A filter (Corning 7-59) was placed before the camera to eliminate the scattering of 0.53μ light. In order to attenuate the intensity of 0.53μ when entering the cell from causing too bright background (2 photons of 0.53μ absorption in BBOT solution), a Corning 1-64 filter was used. The 1.06μ and 0.53μ pulse trains were checked by Tektronix 519 scope. The pictures are shown in Fig. 23.

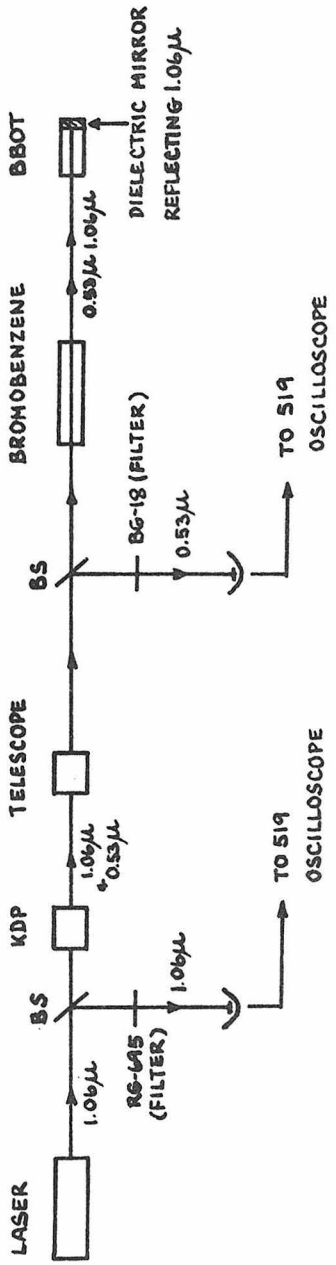

Figure 22. 1.06μ and 0.53μ Two Photon Experiment.

Figure 23a. 1.06μ Pulse Train (from 519 Oscilloscope) at 50 nsec/div.

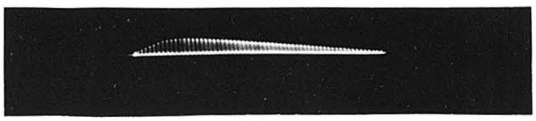

Figure 23b. 0.53μ Pulse Train (from 519 Oscilloscope) at 50 nsec/div.

The pulse widths were read by the microdensitometer and yielded the pulse duration in the range of 4-8 psec ($\pm$ 2 psec in each reading); see Fig. 24, for example.

We had a lot of trouble with this experiment, and it was learned that:

1. If the vertical setting of the doubler is off, the two pulses do not travel in the same direction, i.e., they are not superimposed. Hence, the TPF are not observed.

2. If not enough intensity of 0.53μ pulse enters the BBOT cell, the TPF will be too weak to be observed.

3. Weak 0.53μ light is always due to weak 1.06μ, which means the dye solution is degraded and a new fresh solution must be made.

One should check the burnt spots periodically, to get an idea of how high the power and the structure of pulse are (from the sound and the shape of the burnt spot).

4. If the alignment of the dielectric mirror is off, then 1.06μ and 0.53μ are not superimposed.

5. After the first four points have been corrected and still no TPF is observed, then check whether the reflection from the dielectric mirror goes right back into the laser cavity or not. If it does, this will ruin the outgoing mode-locking beam and no output is to be expected. The reflection must be pushed off a little.

This last point is actually very important in all experiments having to do with reflecting the beam by mirror or by other optical pieces. It may not ruin only the pulse train but also may damage the

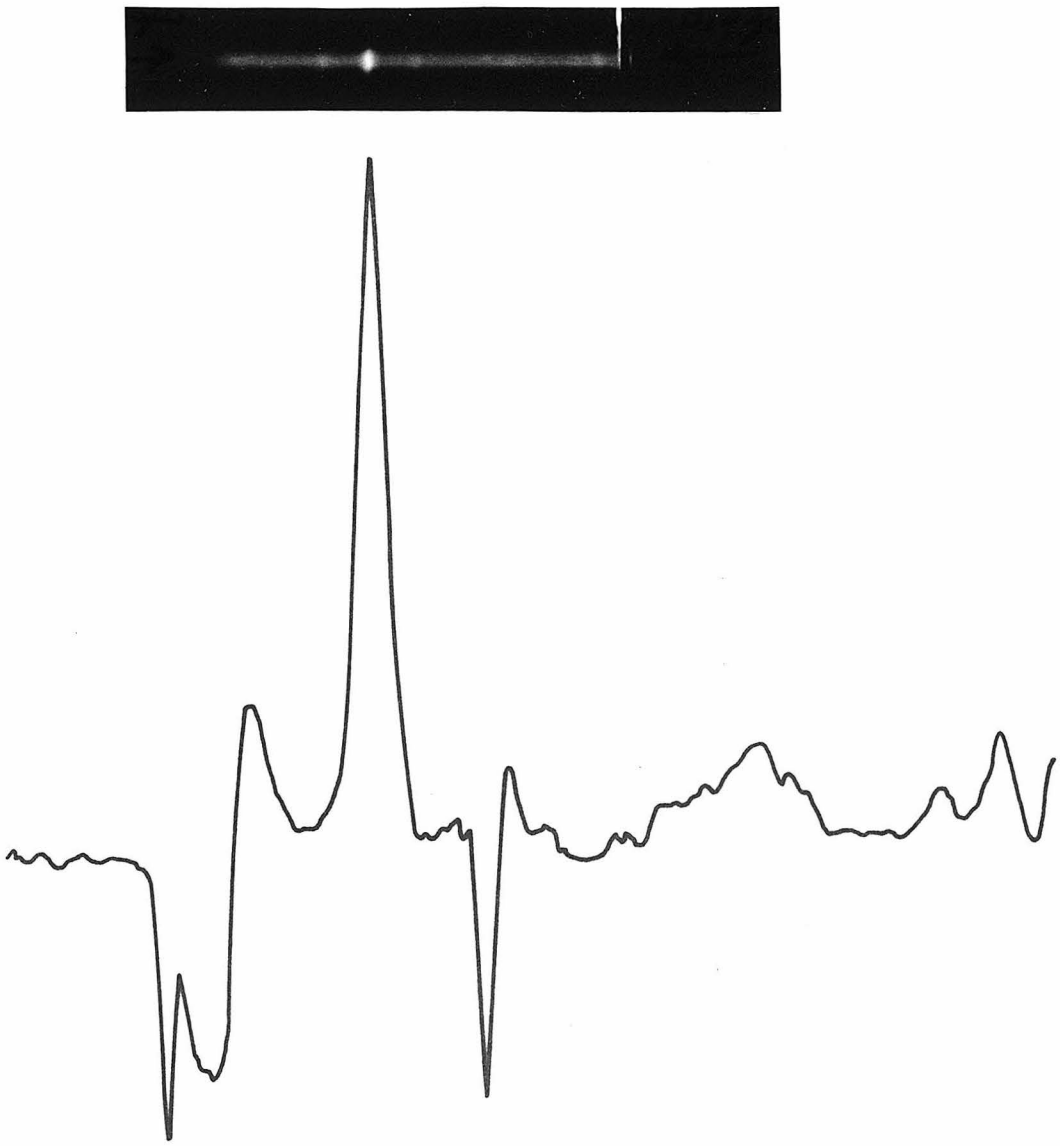

Figure 24. 1.06 μ and 0.53 μ Two Photon Fluorescence in BBOT Solution, and the Microdensitometer Trace (5 mm/min.)

laser rod. Care must be taken not to let the reflection go right back into the rod.

F. Synchronization of Two Optical Paths

Most of the picosecond spectroscopy experiments that have been applied to chemistry are involved in the studies of time dependent reactions of various molecules. In general, two light beams are used as the exciting and the probing pulses. The time delay between the two beams has to be known in picosecond time scale. There are two methods that have been of use in many experiments:

1. The CS_2 optical shutter method [23]. The fact that powerful optical pulses can be used in lieu of electrical pulses to induce a birefringence in liquid traditionally used in Kerr cells, is employed in this technique. The experimental diagram is shown in Fig. 25. The 1.06μ pulses are used to induce the Kerr effect in CS_2 liquid in cell C. Such an effect in CS_2 is due to a field induced reorientation which has the relaxation of about 2 psec. The CS_2 cell is placed between cross polarizers which are in the 0.53μ light path. The 0.53μ passes through the first polarizer and the CS_2 cell. If there is no Kerr effect in the cell, the light will be blocked by the crossed polarizers and not observed in the picture (camera placed behind the polarizer). However, if the 1.06μ and 0.53μ light paths are synchronized (by means of an optical delayer), the 1.06μ pulses will arrive at CS_2, inducing the Kerr effect which will rotate the polarization of 0.53μ beam by 90^o. The rotated beam can then pass through the crossed polarizers.

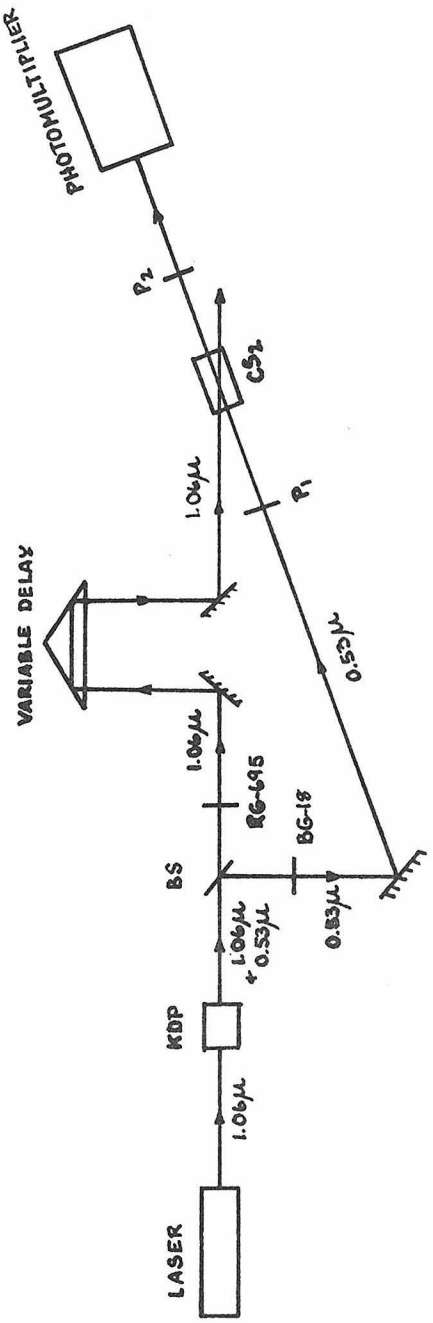

Figure 25. Synchronization By CS_2 Optical Shutter Method (P_1 and P_2 are Cross Polarizers).

2. The two-photon method. The experimental setup is shown in Fig. 26. The 1.06μ path can be adjusted using a variable delay which consists of a prism placed on a micrometer which has a very fine scale on the order of 10^{-2} millimeters. The variable delay is such that the 1.06μ pulses will lead the 0.53μ into the BBOT (2,5 bis[5-terbutyl-benzoxazolyl-(2)]thiophene) solution. After being reflected by the mirror (99.9% at 1.06μ), the 1.06μ will meet 0.53μ (if the variable delay is placed at the right position) and the two-photon fluorescence spot can be observed by means of a camera. Knowing the distance of the bright spot from the mirror, one can calculate the position of the variable delay that will synchronize the two light paths.

Experiment

Assuming 1.06μ pulses are ahead of 0.53μ by a distance y, the TPF-mirror distance is x, and a variable delay is set at position 3.00 (see Fig. 27).

The time 1.06μ travels in the cell: (BBOT in dichloroethane)

$$(48.6 \text{ min} + x) \times \frac{1.412}{c} + (1.8 \text{ mm}) \times \frac{1.465}{c}$$

The time 0.53μ travels:

$$y + (48.6 \text{ min} - x) \times \frac{1.447}{c} + (1.8 \text{ mm}) \times \frac{1.476}{c}$$

where $n_{0.53\mu}$ in dichloroethane = 1.447 (interpolation from the values given in the International Critical Table, Vol. VII (from Ref. [22])

$n_{1.06\mu}$ in dichloroethane = 1.412

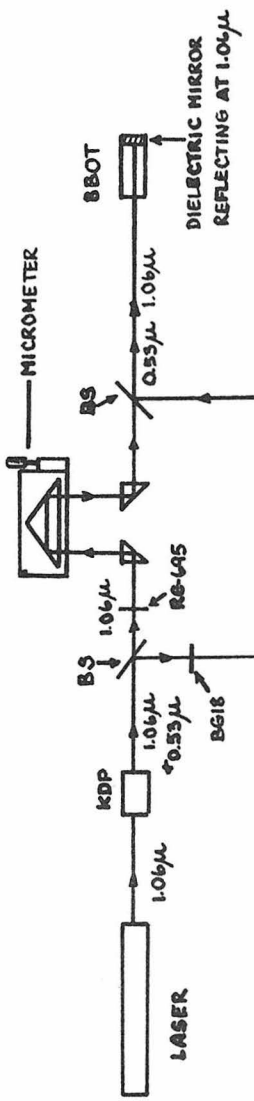

Figure 26. Synchronization by Two Photon Method.
[B.S Transmits Maximum at 1.06μ, Reflects Maximum at 0.53μ, When Placed at 45° to the Incident Beam, M Reflects Maximum at 0.53μ, When Placed at 45°]

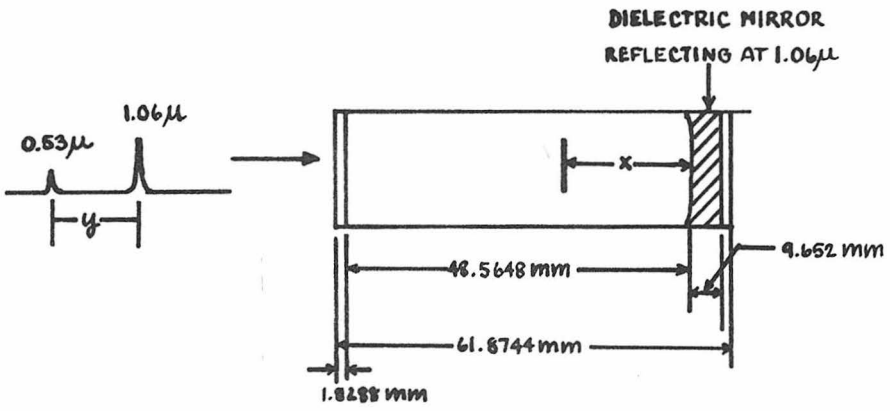

Figure 27 BBOT Cell

$n_{0.53\mu}$ in pyrex = 1.476

$n_{1.06\mu}$ in pyrex = 1.465

Now the time taken by both light beams until they meet at x must be the same, so

$$(48.6 + x) \times 1.412 + (1.8) \times 1.465 = y + 48.6 - x) \times 1.447 + (1.8) \times 1.476$$

and y can be calculated once x is known. Then we know that the variable delay has to be set at the position $(3.00 - \frac{y}{2})$.

A result from one variable delay position is not sufficient, however. This is due to the fact that the 99.9% at 1.06μ reflector also reflects some 0.53μ . The two-photon spot observed can then be from the reflected 0.53μ meeting the 1.06μ in the cell. A simple check can be done as follows:

1. Move the variable delay ahead, i.e., shorten the 1.06μ path source. If 1.06μ is leading by y' , $y' > y$ and x should move away to the mirror. On the other hand, if 0.53μ is leading, then x will move closer to the mirror.

2. Move the variable backward, the opposite effect should be observed.

For example, some results are shown in Table I.

Once the proper variable delay setting is obtained, a time-dependent experiment can be operated.

TABLE I

Variable delay position (moving backward down the row)	x (cm)	proper setting
3.00	1.25	19.91
8.00	0.96	20.76
13.00	0.60	20.60
18.00	0.30	21.40

The proper setting (average) = 20.70 min

G. Experiment on Radiationless Transitions of Azulene

Azulene exhibits anomalous fluorescence in that the emission originates not from the lowest excited singlet ($S_1 \rightarrow S_0$), but from the second excited singlet ($S_2 \rightarrow S_0$). Furthermore, the first excited singlet state lies substantially lower in energy at $\sim$ 14400 cm^{-1} (S_2 lies at $\sim$28000 cm^{-1}) than in other chemically similar systems. The energy diagram is shown in Fig. 28. Rentzepis [19,20] reported the experiments on measuring the radiationless transition--vibration relaxation in the first electronically excited state, and the emission from the singlet and triplet state of azulene [20].

From the diagram, the radiation from 0.53 laser pulse (ν_2 = 18863 cm^{-1}) photolyses azulene, raising to approximately the fifth vibrational level of the first excited singlet. The subsequent arrival of the laser fundamental, ν_1 = 9431 cm^{-1} which acts as the interrogating

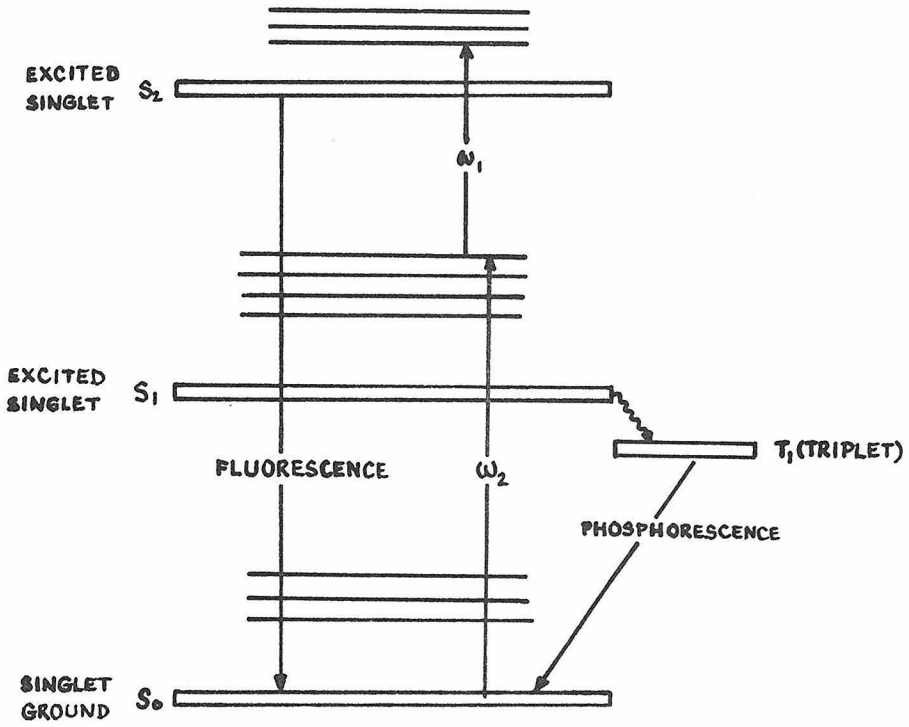

Figure 28. Energy-Level Diagram for Azulene
($\omega_1 = 1.06\mu$, $\omega_2 = 0.53\mu$) (ref. 2d)

or probe beam will raise azulene molecules up to S_2 singlet state, provided they are still in the vibrationally excited state when the 1.06μ pulse arrives. The fluorescence produced as a function of the delay between the arrival of two pulses provides a direct measure of the lifetime of the vibrational level. This can be done using the TPF technique.

In our experiment we looked for the absorption of 1.06μ (a probe pulse) as a function of time delay. The experimental set-up is shown in Fig. 29. Right after KDP, a special dichrometer beam splitter (transmitting maximum at 1.06μ , reflecting maximum at 0.53μ) was placed to separate 1.06μ and 0.53μ beams into two different paths, with appropriate filters to purify the wavelengths in each path. The two beams were rejoined again at BS_2 (also a dichrometer BS) and travelled coaxially into the sample cell. A small amount of the light (∿4%) was deflected out by a glass plate (BS_3) and fed into the fast diode with two RG715 filters as a 0.53μ cut off. This 1.06μ signal was a monitoring beam for the experiment and will be referred to as "b". The rest of the light, after passing through the sample cell, was also fed into the same photodiode as "b", which was connected to a 519 Tektronix oscilloscope. By adjusting the path length of "a" (the interacting 1.06μ pulses) such that "a" would arrive about 2-3 nanoseconds after "b", a double pulse train picture can be obtained as shown in Fig. 30. The decrease in the ratio a/b as a function of time delay (by moving the variable delay backward so as to delay 1.06μ from 0.53μ) would yield the decay curve for the 5th vibrational excited state of S_1 state of azulene.

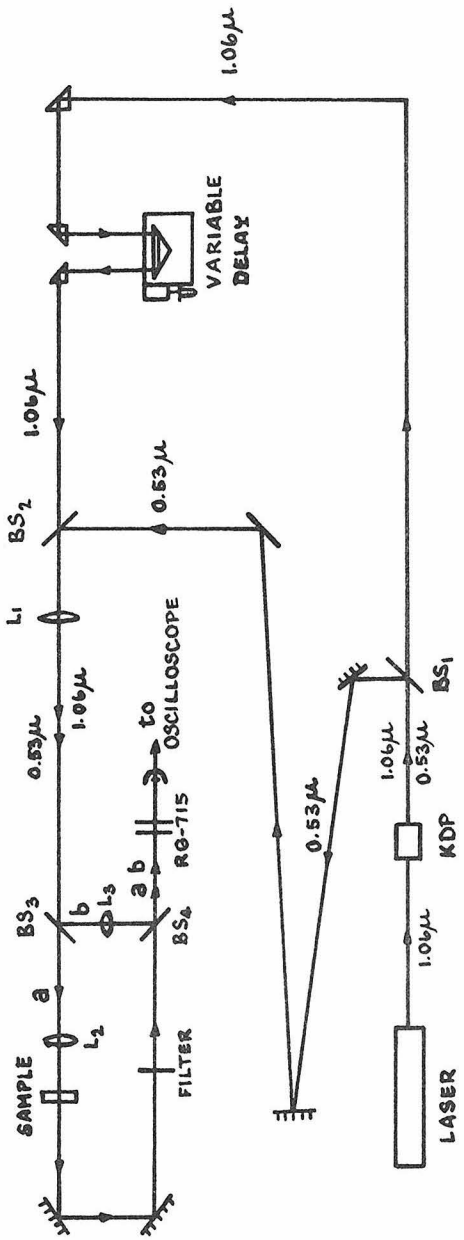

Figure 29. Azulene Experiment.
(L_1L_2 and L_1L_3 are Telescopes)

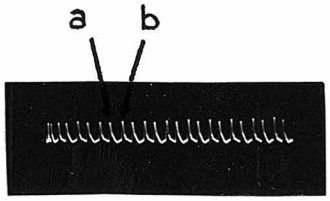

Figure 30. b-a Pulse Train from Azulene Experiment (519 Oscilloscope set at 20nsec/div.)

The experiment turned out to be much more difficult than expected, and many problems were gradually realized and corrected, as follows:

1. The He-Ne laser beam and the mode-locked beams did not always travel exactly in the same direction. The problem was due to the fact that all systems had been aligned by means of the He-Ne beam.

The correction was made by adjusting mirror M_1 (diagram in Fig. 10).

2. The 1.06μ and 0.53μ pulses were not superimposed. It was checked by the burnt spots of the two reduced beams at the far field. This problem was caused by the index-mismatching of the KDP crystal, resulting in 0.53μ not travelling coaxially with 1.06μ. This accounted for difficulties in doing the experiment (bad TPF, no effect from the azulene experiment, etc.)

The correction was done by adjusting the doubler (vertically) until the two beams were superimposed (the other optical pieces had been well aligned).

3. The 1.06μ (interrogating) beam was of higher intensity than the 0.53μ (photolysis) beam. The effect was then not marked enough to be observed. Stronger absorbing filters were needed to attenuate the 1.06μ beam.

4. The 1.06μ beam was of the same or slightly larger size than that of the 0.53μ beam. Corrections were needed to be made (e.g., reduction of the 1.06μ beam by lenses) so that the 1.06μ pulse would "see" only the molecules excited by 0.53μ pulse.

5. The 0.53μ could be too intense and caused two-photon absorption in azulene.

6. It is important to realize that the high accuracy in the measurement of distances is required for this type of experiment. One psec in air corresponds to 1 mm. Hence, we are working with the accuracy in the range of 1 or 2 mm. Besides, doing the experiment at the far field makes the measurements become extremely critical.

A result was finally obtained. The decay curve is shown in Fig. 31 where A refers to the ratio of a/b normalized to the maximum absorption of 1.06μ . The maximum absorption was observed when the variable delay was set at 14.00. From the curve (1/e) point was at variable position 15.90, corresponding to the time

$$(15.90 - 14.00)\ \text{cm} \times 2 \times 3.3\ \frac{\text{psec}}{\text{cm}} = 12.5\ \text{psec}$$

The maximum absorption was only 16% and each point on the curve was the average of four readings. This result, however, did not agree too well with Rentzepis' work, which was reported to be 8 psec.

H. Generation of Continuum from 1.06μ Laser Pulses

A very important technique, which has become an important tool in many picosecond spectroscopy experiments, is the generation of continuum from 1.06μ or 0.53μ pulses in BK-7 glass [24], water and heavy water [25], toluene, benzene, CCl_4 , liquid N_2, and the laser amplifier

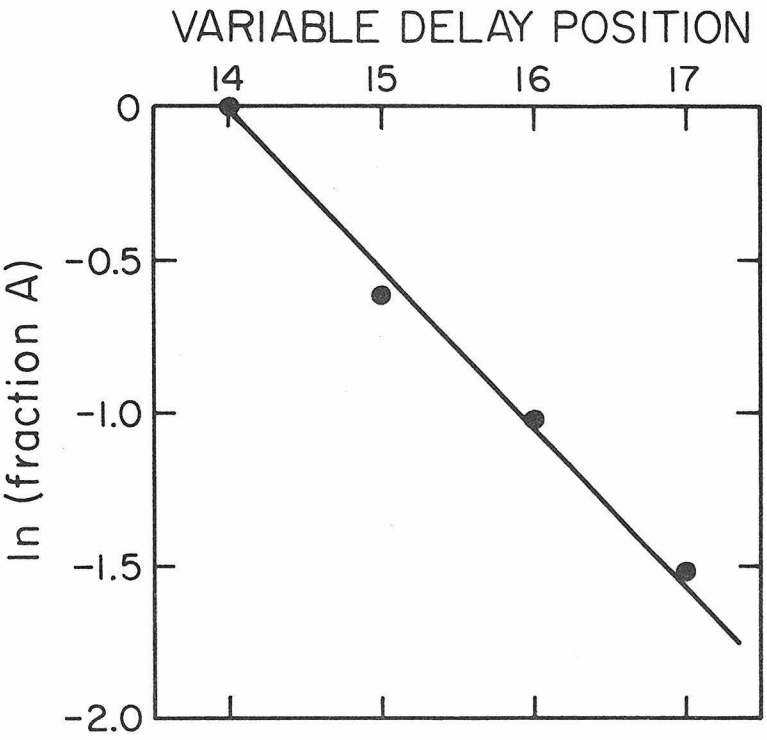

Figure 31. Results from Azulene Experiment

itself [26]. The 1.06μ pulses generate the continuum from 1.06μ to 4000Å, whereas 0.53μ generates the whole visible region 4000-7000Å. Two mechanisms have been proposed for this nonlinear phenomenon.

1. Broadening of stimulated Raman emission [25,27]. First the stimulated Stokes-Raman (SSR) and the stimulated anti-Stokes-Raman (SASR) emissions are built up by the pumping laser. In addition the Stokes and anti-Stokes waves are coupled individually to the field of the pumping light, causing the gain as well as a broadening from both SR and ASR [28]. Simultaneously, this coupling leads to broadening of the original pump light. Some of the excited molecular vibrational levels are not populated at room temperature and have to be excited through the process of SSR emission, the SASR wave should be retarded relative to the SSR. This has proved to be the case by Varma and Rentzepis [27]. The retardation time is 6 psec.

2. Broadening due to phase modulation effect of SSR and SASR and the pumping laser [29]. From the structure of the frequency spectrum, the pattern can be explained by phase modulation through the intensity-dependent refractive index ($n = n_o + n_2(E^2)$, where $n_2(E^2)$ is the stationary value of the intensity-dependent refractive index), which is the result of the inhomogeneous phase velocity within a pulse. The change in phase velocity leads to the reduction in frequencies in the peak front and an increase in frequency in the tail of the pulse.

Experiment

In our laboratory, BX-7, toluene, H_2O, and D_2O were tried as the continuum generating liquids. D_2O turned out to be the best. The

set-up was quite simple as shown in Fig. 32. The 1.06μ light was focused into a 10 cm cell of D_2O. The emerging light was collected and recollimated by a couple of convex lenses. After attenuating the 1.06μ intensity (down to ∿2%), the light was sent into a spectrograph (2M CIT, with the resolution of 8Å/mm) and the spectra were obtained on the Kodak IN and IM (hypersensitized) photographic plates as shown in Fig. 33. We observed the continuum from 0.06μ → 0.4μ . It is very important that a spike filter for 1.06μ was placed before the D_2O cell, in order to prevent the flashlamp light and continuum that could have arisen from the laser rod itself, from getting into the spectrograph. The duration of the continuum was shown by Varma and Rentzepis [27] to be on the order of picoseconds.

The continuum emitted by D_2O with excitation by a train of 0.53μ pulses were also observed in our laboratory. The anti-Stokes and Stokes sides were collected separately due to the lack of an appropriate filter. The 0.75M Jarrell-Ash 5 x 7" spectrograph was used and the spectra were recorded on a Polaroid film, type 57 as shown in Fig. 34.

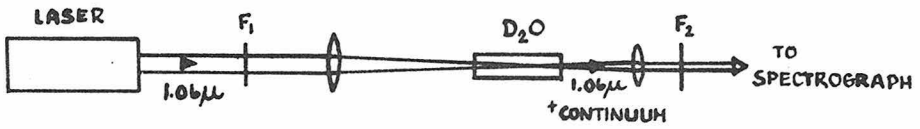

Figure 32. Continuum Generation from 1.06μ Picosecond Pulses (F_1 is a Spike Filter at 1.06μ ; F_2 is a 1.06μ "Cut Off" Filter).

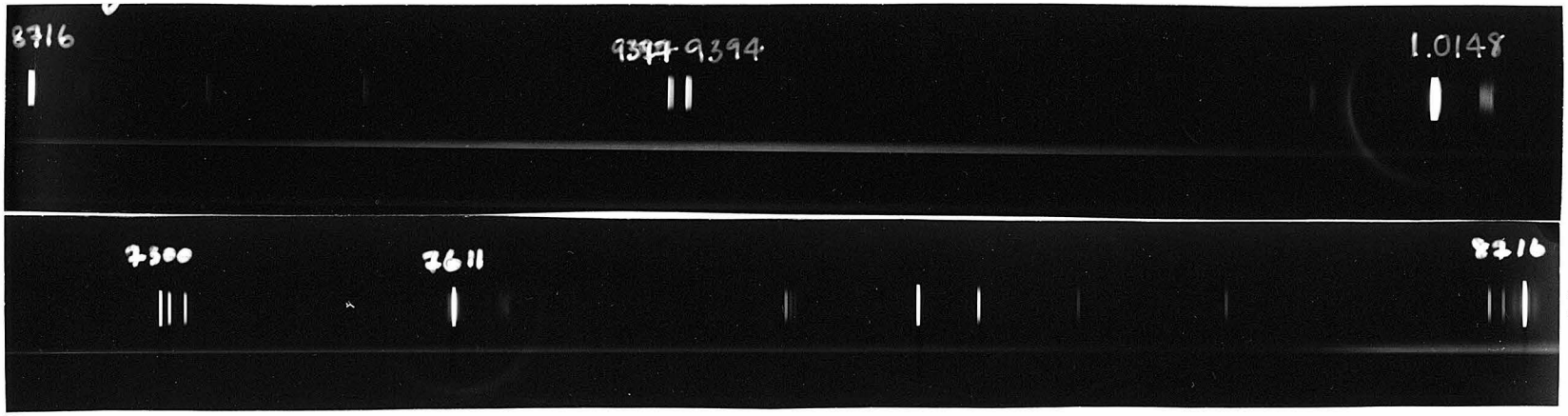

Figure 33. Sections of Continuum from 1.06μ Picosecond Pulses, with Hg Spectral Lines (Recorded on Kodak I-N and I-M Photographic Plates).

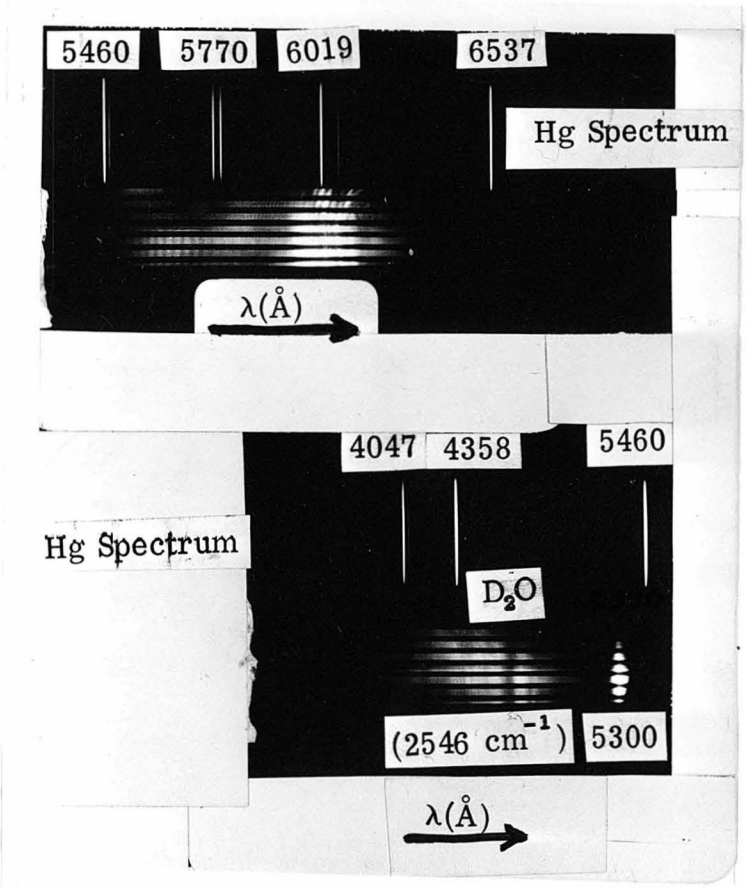

Figure 34. Continuum from 0.53μ through an Echelon (recorded on Polaroid Film Type 57)

References

1. See, for example, A. Yariv, Introduction to Optical Electronics (Holt, Rinehart, and Winston, Inc., 1971), Chapter 4.

2. The review articles on this subject are:
   a. A. J. DeMaria, et al., Science 156, 1557 (1967)
   b. A. J. DeMaria, et al., Proc. of the IEEE 57, 2 (1969)
   c. P. W. Smith, Proc. of the IEEE 58, 1342 (1970)
   d. P. M. Rentzepis and C. J. Mitschele, Anal. Chem. 42, 20 (1970)
   e. A. J. DeMaria, Progress in Optics, Vol. IX, Wolf ed., (North Holland, 1971), page 33.

3. H. Kogelnik and T. Li, Appl. Opt. 5, 1550 (1966)

4. H. Kogelnik and W. Rigrod, Proc. IRE 50, 220 (1962)

5. "Inhomogeneous" here refers to the broadening of the linewidth of the system. This is due to the fact that the individual atoms are distinguishable, each having a slightly different transition frequency ν_0, and different linewidths; the total of these together constituting the inhomogeneous linewidth of the system.

6. See for details, Section 9.3 of Ref. 1.

7. M. DiDomenico, Jr., J. Appl. Phys. 35, 2870 (1964); A. Yariv, ibid 36, 388 (1965).

8. The quality factor Q is a measure of the property of optical resonators in building up large field intensities with moderate power inputs, and is defined by the relation

$$Q = \omega \times \frac{\text{field energy stored by resonator}}{\text{power dissipated by resonator}}$$

$$Q = \frac{\omega\varepsilon E^2 V}{4P}$$

where ω is the frequency of field inside the resonator P is the power input, E is the peak field, V is the resonator volume and ε is the dielectric constant.

9. The references on this topic are:

   a. A. J. DeMaria, et al., Proc. of the IEEE 57, 2 (1969)
   b. A. J. DeMaria, et al., Science 156, 1557 (1967)
   c. V. S. Letokhov, Soviet Phys. JETP 28, 562 (1969)
   d. P. G. Kryukov and V. S. Letokhov, IEEE J. Quant. Elect. QE-8, 766 (1972)

10. Bloembergen, Am. J. Phys. 35, 989 (1969)

11. J. W. Shelton and J. A. Armstrong, IEEE J. Quant. Elect. QE-3, 696 (1967)

12. M. A. Duguay and J. W. Hausen, Opt. Comm. 1, 254 (1969)

13. J. A. Giordmaine, et al., Appl. Phys. Lett. 11, 216 (1967)

14. J. R. Klauder, Appl. Phys. Lett. 13, 174 (1968)

15. P. A. Franken, et al., Phys. Rev. Lett. 7, 118 (1961)

16. J. A. Giordmaine, Phys. Rev. Lett. 8, 19 (1962)

17. P. D. Maker, et al., Phys. Rev. Lett. 8, 21 (1962)

18. A. Yariv, Quantum Electronics (John Wiley and Sons, Inc., 1967), pp. 348-355.

19. P. M. Rentzepis, Chem. Phys. Lett. 2, 117 (1968)

20. P. M. Rentzepis, Chem. Phys. Lett. 3, 717 (1969)

21. M. R. Topp, et al., J. Appl. Phys. 42, 3415 (1971)

22. M. R. Topp, P. M. Rentzepis, J. Chem. Phys. 56, 1566 (1972)

23. M. A. Duguay and J. W. Hansen, Appl. Phys. Lett. 15, 192 (1969)

24. R. R. Alfano and S. L. Shapiro, Phys. Rev. Lett. 24, 584 (1970)

25. W. Werneke, et al., Opt. Comm. 4, 413 (1972)

26. N. N. Il'ichev, et al., Zhetf Piz. Red. 15, No. 4, 191-194.

27. C.A.G.O. Varma and P. M. Rentzepis, J. Chem. Phys. 58, 5237 (1973)

28. M. J. Colles, et al., Ch. Phys. Lett. 4, 621 (1970)

29. For example:

a. R. J. Joenk and R. Landauer, Phys. Lett. 24A, 228 (1967)

b. F. Shimizu, Phys. Rev. Lett. 19, 1097 (1967)

c. S. A. Akhmanov, et al., Sov. Phys. USP 93, 609 (1968)

d. K. Shimoda, Z. Physik 234, 293 (1970)

30. See, for example:

a. P. M. Rentzepis and M. R. Topp, Ann. N. Y. Acad. of Sci. 33, 284 (1971)

b. P. M. Rentzepis, Adv. in Ch. Phys. 23, 189 (1973), with references therein.

31. M. A. Duguay, et al., IEEE J. Quant. Elect. QE-6, 725 (1970).

32. D. J. Bradley, et al., Opt. Comm. 2, 41 (1970).

PART II Applications of Picosecond Laser in Chemistry: Vibrational Relaxation Times in Liquid Alkanes and Alkenes

A. Introduction

With the advent of ultrashort and high power laser pulses, chemistry on the picosecond time-scale can be studied. P. M. Rentzepis and co-workers have contributed a great deal in the area of Picosecond Spectroscopy, both instrumentation and chemical studies. Fast decay times (electronic, fluorescence, intersystem crossing, vibrational, reorientational) and energy transfers in many chemical systems have been studied by various groups [1]. For wider applications, techniques in generating various wavelengths other than 1.06μ and 0.53μ are necessary. Some of them are

1. Optical Third Harmonic Generation in Organic Liquids [2]. The wavelengths between 0.373μ to 0.232μ have been observed in liquids such as BBOT, etc., from the high power fundamental beam (1.06μ).

2. Fourth Harmonic Generation. By passing 0.53μ into the phase-matched KDP crystal, 0.265μ light can be generated.

3. Stimulated Raman Scattering. The Stokes lines in many liquids have been observed with high yield [3]. By employing 0.53μ, many wavelengths in the red can be chosen from various liquids or gases (2900 cm^{-1} shift from ethanol, acetone, etc.; 4000 cm^{-1} shift from H_2 gas; 2300 cm^{-1} shift from N_2-gas). From these Raman-shifted wavelengths, second harmonic generation technique will give the desired light in the ultraviolet region.

4. Continuum Generation in Liquids. As discussed in Part I H, the continuum between 0.4-0.7μ from 0.53μ or 0.4-1.06μ from 1.06μ can be easily obtained from D_2O liquid.

5. Mode-locked Dye Lasers. The mode-locking of organic dye laser can be achieved by pumping the laser with the second harmonic pulse train from a Nd laser or a Ruby laser, depending on the dyes employed. The wavelengths between 0.56-0.59 from the mixture of Rh 6G and RhB using a Nd laser have been reported by [4].

However, with the available 1.06μ and 0.53μ lights, direct observations of vibrational decay times in the ground state can be studied in many appropriate chemical systems (i.e., the compounds with the excited electronic levels lying in the ultraviolet region or higher).

B. Historical Review

In 1966, F. DeMartini and J. Ducuing [5] reported the first direct observation of vibrational lifetime in Hydrogen gas using a Q-switched Ruby laser. Gaseous H_2 was first excited by Q-switched laser pulse (the duration of which was 20 nsec) which produced the excess population in the first vibrational excited state by stimulated Raman scattering. The sample was then probed with an ordinary ruby laser (a train of spikes lasting about 500 μsec), the power of which was below the threshold for stimulated scattering. The time evolution of spontaneous anti-Stokes scattering from the probing laser yielded the vibrational lifetime of hydrogen to be about 60 μsec.

The vibrational lifetime of an optical phonon on a picosecond

timescale was first reported by R. R. Alfano [6]. The lifetime of 1086 cm^{-1} optical phonon in calcite was measured directly to be 12.5 ± 5 picosecond, using two picosecond laser beams operating at a wavelength of 0.53μ and 1.06μ . The stimulated Raman was produced by 1.06μ pulses, whereas spontaneous anti-Stokes scattering came from 0.53μ pulses.

As for liquids, direct measurement of the molecular dephasing time was accomplished by D. von der Linde, et al. [7]. In their work, molecular vibrations were coherently excited by a first short light pulse (1.06μ) and the rise and decay of the vibrational amplitude was measured with a second light pulse (0.53μ) properly delayed with respect to the first one. Both light pulses were of high enough intensity to produce stimulated Raman scattering. The stimulated anti-Stokes signal from the 0.53μ pulse was collected at 0° scattering angle. The authors pointed out the fact that when the laser pulse width was much longer than the dephasing time, the anti-Stokes curve as a function of time gave direct information on the shape of the probe pulse [8]. This was found to be in the case of ethyl alcohol (Raman shift at 2928 cm^{-1}), the decay time was the pulsewidth. As for CCl_4, the dephasing time was obtained directly to be 4.0 ± 0.5 psec. (Raman line at 459 cm^{-1}).

From the same laboratory, vibrational lifetimes were also obtained for the CH_3 valence bond vibration in 1,1,1 trichloroethane and ethyl alcohol [9]. The results were 5 ± 1 psec and 20 ± 5 psec respectively. The incoherent or spontaneous anti-Stokes from the

probing 0.53μ pulse was collected at 90° scattering angle (discussed below in the theory section).

In order to establish the molecular-vibration decay route in a liquid, R. R. Alfano and S. L. Shapiro [10] did the study on methyl vibrations in alcohol. By measuring the decay curves and intensities of spontaneous anti-Stokes scattering at 2928 cm^{-1} and 1464 cm^{-1} vibration, together with the delay between the 2928 cm^{-1} and 1464 cm^{-1} signals, the authors were led to believe that the decay route of methyl stretching vibration was due to a splitting into daughter vibrations at half the frequency. Recently, A. Laubereau, et al [11], interpreted from the Raman study of CH_3CCl_3, the mechanism of vibrational relaxation as intermolecular (a trimolecular interaction). They concluded this fact from the dependence of the vibrational lifetime on the concentration in the binary liquid mixture of CH_3CCl_3 and CCl_4. The vibration-vibration energy transfer mechanism was also confirmed; the near energy resonance occurs in CH_3CCl_3 when the methyl stretching vibration (2939 cm^{-1}) decays to 1450 cm^{-1} bending modes. In the solution of CH_3CCl_3 and CD_3OD, however, the 2939 cm^{-1} was found to decay into 2227 cm^{-1} of CD_3 stretching vibration and 713 cm^{-1} of C-Cl vibration.

C. Theory

Before going further to describe the experiment, it is useful to discuss some aspects of the dephasing times, the stimulated Raman scattering, and the vibrational lifetimes.

1. Dephasing times. Consider a number of molecules, vibrating in the vibrational excited state, after interacting with non-absorbing

light. These molecules will start out vibrating in phase with each other. In a very short time (picoseconds) after, the vibration will dephase, due to two possible mechanisms:

a. Irreversible Dephasing. This is due mainly to the collision among molecules. Each collisional event will "wipe out" the phase memory of the molecules and hence the in-phase vibration cannot be restored.

b. Reversible Dephasing. The molecules can vibrate out of phase from each other by slight molecular movement (rotation) or due to the different environment for each molecule. The loss of phase memory by this mechanism, can, however, be restored by certain non-linear optical methods (such as phonon echo [12]).

Generally, in liquids, the irreversible mechanism seems more likely due to the rapid interaction among the molecules. In gas and solids, the second mechanism seems more probable, as has been studied by I. D. Abella, et al. [12].

The dephasing time can be observed by means of stimulated or coherent Raman scattering.

2. Vibrational Lifetime. This corresponds directly to the depopulation of the vibrational excited state, and can be obtained from the spontaneous or incoherent Raman scattering. The mechanisms of the vibrational decays have been studied as described in the previous section [10, 11].

3. Stimulated Raman Scattering [13]. The stimulated Raman scattering has the following properties which make it different from

the ordinary Raman effect:

a. It occurs only above a certain intensity threshold of the exciting beam.

b. The scattered intensity increases non-linearly as the input intensity becomes very large, yielding the conversion in the order of 10-20%.

c. The scattered beam has directionality properties which are similar to that of the exciting beam.

d. The frequencies of higher order Stimulated Stokes lines are exact multiples of ω (the fundamental frequency shift) away from the laser frequency: $\omega_\ell - 2\omega$, $\omega_\ell - 3\omega$, etc. The Stokes intensity is high enough to take over the role of the laser beam and stimulate in turn radiation at the second Stokes frequency $\omega_\ell - 2\omega$. In comparison, the higher Stokes lines from spontaneous radiation are always very weak and not equally spaced, since these transitions are due to the slightly anharmonic molecular vibrations.

In order to understand the non-linear increase of the scattered light, it is appropriate to describe the Raman effect using quantum mechanics.

For a molecular vibration to be Raman active, there must be a change in the induced dipole moment resulting in polarizability change of the molecule. This can be written as

$$\mu_i = \alpha E \qquad (1)$$

where μ_i - induced dipole moment of molecule i

α - the polarizability which is a tensor of 2nd rank

E - the electric field strength of the incident beam.

For a vibrating molecule, α changes as a function of a normal coordinate of vibration X. The series expansion of $\alpha(X)$ can then be written:

$$\alpha(X) = \alpha_o + \left(\frac{\partial \alpha}{\partial X}\right)_o X + \ldots \tag{2}$$

We can write the perturbation Hamiltonian that corresponds to the Raman effect as

$$H'_{\text{Raman}} = - \left(\frac{\partial \alpha}{\partial X}\right)_o \cdot XE^2 \tag{3}$$

Using creation and annihilation operators, we have

$$E \alpha (\omega_\ell)^{\frac{1}{2}} [a_\ell^\dagger - a_\ell] + (\omega_s)^{\frac{1}{2}} [a_s^\dagger - a_s] \tag{4}$$

and

$$X \alpha (a_\nu^\dagger + a_\nu) \tag{5}$$

where ω_ℓ, ω_s - frequencies of the incident laser and stokes respectively

$a^\dagger, a$ - are photon creation and annihilation operators

$a_\nu^\dagger, a_\nu$ - are harmonic oscillator creation and annihilation operators

The rate of Stokes photon emission is therefore proportional to

$$W_{emiss} \quad \alpha |\underset{final}{\langle n_\ell - 1,\ n_s + 1, 1|}\ a_\ell a_s^\dagger a_\nu^\dagger |\underset{initial}{n_\ell, n_s, 0\rangle} = n_\ell (n_s + 1) \quad (6)$$

Or we can write

$$\frac{dn_s}{dt} = An_\ell (n_s + 1) \quad (7)$$

where n_ℓ, n_s are the occupation numbers of the incident laser mode (ω_ℓ) and the Stokes mode (ω_s) respectively.

A is an expression depending upon the scattering medium. From Eq. (7)

$$\frac{dn_s}{dt} = An_\ell n_s + An_\ell \quad (8)$$

$$n_s = (n_s)_o \, \ell^{An_\ell t} + An_\ell t \quad (9)$$

In general, for an ordinary Raman scattering, the intensity of the incident beam is small and $An_\ell t << 1$, so

$$n_s = An_\ell t \quad (10)$$

The Stokes intensity varies linearly with the incident light.

If n_ℓ is large enough such that $An_\ell t > 1$, then

$$n_s \simeq (n_s)_o \, \ell^{An_\ell t} \quad (11)$$

and the Stokes intensity grows exponentially with that of the incident laser.

From another point of view, electromagnetic treatment of Raman scattering will show us the directionality property of the Stimulated Raman scattering. We can start by considering the potential energy

of a molecule with polarizability α in an electric field $\vec{E}(\vec{r}_1 t)$:

$$W = -\frac{1}{2}\alpha(x)|\vec{E}(\vec{r},t)|^2 \tag{12}$$

If we again write

$$\alpha(x) = \alpha_o + \alpha_1 x \quad \text{(in the lowest order approximation)} \tag{13}$$

Hence, the force driving such vibrations will be

$$\frac{\partial W}{\partial x} = -\frac{1}{2}\alpha_1 E^2 \tag{14}$$

A sinusoidal varying force, F cos ωt, will give the following differential equation for the vibrational coordinate:

$$m\ddot{x} + R\dot{x} + \omega^2 x = F\cos\omega t \tag{15}$$

where R is a phenomenological damping coefficient

ω is the resonance frequency

F is the effective driving force.

This force includes the interaction between the induced dipole moment of the adjacent molecules. If the polarizabilities of the two molecules are α_1 and α_2, then their interaction energy is approximately $\left(2\alpha,\alpha_2/d^3\right)E^2$ where d is the intermolecular distance. The corresponding force driving the vibration of molecule 2 is $\left(2\alpha_1/d^3\right)\left(\frac{\partial\alpha_2}{\partial x}\right)E^2$. Since both forces have the same dependence on E^2, they will combine into an effective force $F = fE^2$.

The electric field $\vec{E}$ for the system is now composed of the shifted (Stokes) and the unshifted (the incident laser) lights, the total $\vec{E}$ is then

$$\vec{E} = \vec{E}_\ell \cos(\omega_\ell t - \vec{k}_\ell \vec{r}) + \vec{E}_s \cos(\omega_s t - \vec{k}_s \cdot \vec{r} + \phi_s) \tag{16}$$

where the subscript ℓ refers to the incident laser beam and the subscript s refers to the Stokes field. $\vec{k}$ is the propagation vector of the light wave.

The resonant condition is when $\omega_\ell - \omega_s = \omega$.

Solving for x in Eq. 15 leads to

$$x = \frac{f\vec{E}_\ell \cdot \vec{E}_s}{R(\omega_\ell - \omega_s)} \sin\left[(\omega_\ell - \omega_s^*)t - (\vec{k}_\ell - \vec{k}_s)\cdot\vec{r} - \phi_s\right] \tag{17}$$

Here, we can see that the phase of the molecular vibration is $(\vec{k}_\ell - \vec{k}_s)\cdot\vec{r}$ which reflects that the molecular vibration is driven by the product of the electric fields with the frequency ω_ℓ and ω_s.

From Eqs. (1) and (2)

$$\mu = \frac{\partial \alpha}{\partial x} \cdot x\vec{E} \tag{18}$$

and the rate of energy exchange between the dipole moment and the component of the field of frequency ω_s is given by

$$P_s = - \langle (d\vec{\mu}/dt) \cdot \vec{E}_s \rangle \tag{19}$$

We have so far left out the anti-Stokes part of the electric field. In order that the anti-Stokes radiation be amplified the total field is considered in the form

$$\vec{E} = \vec{E}_\ell \cos(\omega_\ell t - \vec{k}_\ell \vec{r}) + \vec{E}_s \cos[(\omega_\ell - \omega)t - \vec{k}_s \cdot \vec{r} + \phi_s]$$

$$+ \vec{E}_{AS} \cos[(\omega_\ell + \omega)t - \vec{k}_{AS} \cdot \vec{r} + \phi_{AS}] \qquad (20)$$

Using Eqs. (15), (17), (18), (19), we obtain,

$$P_{AS} = \frac{f}{4R} \frac{d\alpha}{dx} \frac{\omega_\ell + \omega}{\omega} \left\{ -(\vec{E}_\ell \cdot \vec{E}_{AS})^2 - (\vec{E}_\ell \cdot \vec{E}_{AS})(\vec{E}_\ell \cdot \vec{E}_s) \cos \right.$$

$$\left. [(2\vec{k}_\ell - \vec{k}_s - \vec{k}_{AS}) \cdot \vec{r} + \phi_s + \phi_{AS}] \right\} \qquad (21)$$

If $E_s > E_{AS}$ (which is the case), E_{AS} will be amplified if

$$2\vec{k}_\ell - \vec{k}_s - \vec{k}_{AS} = 0 \qquad (22)$$

and $\cos(\phi_s + \phi_{AS}) < 0$, the maximum will be at

$$\phi_s + \phi_{AS} = \pi \qquad (23)$$

Equation (22) is the phase matching requirement. It turns out that from Eq. (22), the anti-Stokes radiation is emitted in the form of a conical shell with a half-apex angle β defined by [14]

$$\beta = \left\{ \frac{1}{n_\ell} \frac{\omega_s}{\omega_{AS}} [n_{AS} - n_s + \frac{\omega_o - \omega_s}{\omega_\ell} (n_{AS} + n_s - 2n_\ell)] \right\}^{\frac{1}{2}} \qquad (24)$$

where all the n's are indices of refraction of the medium. This angle turns out to be very small, in the order of a few degree.

As for the Stokes propagation directions, it was found to be along the laser axis [15]. This can be explained qualitatively as follows: first, the process is initiated by that portion of the spontaneous Stokes radiation which passes through the focal volume and is amplified

there by a Raman gain. Since the focal volume resembles a long thin cylinder, the gain will peak at nearly forward angles, thus making the stimulated Stokes emission predominatly along the axis.

At this point, it is of interest to compare this directionality properties of the stimulated Raman to that of the spontaneous Raman. From Placzek's Theory of Raman intensities, the final form can be written as

$$I = \frac{2^4\pi^3}{45\cdot 3^2\cdot C^4} \quad \frac{hI_\ell N(\nu_\ell - \nu)^4}{\mu\nu(1 - e^{-h\nu/kT})} \quad [45(\bar{\alpha}'_a)^2 + 7(\gamma'_a)^2] \tag{25}$$

where C is the velocity of light

N is the total number of molecules in the exciting beam

I_ℓ is the laser intensity

μ is the reduced mass of the oscillator

ν and ν_ℓ is the transition frequency and the laser frequency respectively

$\bar{\alpha}_a$ is the mean value of the isotropic part of the polarizability tensor, defined as

$$\bar{\alpha} = \frac{1}{3}[\alpha'_{xx} + \alpha'_{yy} + \alpha'_{zz}] \tag{26}$$

$$\alpha' = \partial\alpha/\partial Q$$

γ^2 is the mean value of the anisotropic part of the tensor:

$$\gamma^2 = \frac{1}{2}[(\alpha_{xx}-\alpha_{yy})^2 + (\alpha_{yy}-\alpha_{zz})^2 + (\alpha_{zz}-\alpha_{xx})^2 + 6(\alpha^2_{xy} + \alpha^2_{yz} + \alpha^2_{zx})] \tag{27}$$

$$\gamma' = \partial\gamma/\partial Q$$

From Eqs. (25), (26), and (27), it can be seen that I is the absolute intensity radiated in all directions by the sample.

From these facts, one can distinguish experimentally the dephasing time from the vibrational lifetime. Since the former is characterized by the stimulated Raman, the coherent anti-Stokes signals can be collected "head-on". The spontaneous or incoherent anti-Stokes signals are then collected at 90° scattering angle.

4. Radiation Transfer Equations. In order to obtain the expression for the anti-Stokes signal as a function of time, we have to apply the electromagnetic treatment to the problem, in a slightly different manner from the previous one.

We start out writing the Hamiltonian in the form [3c]

$$H = H_o - \frac{1}{2}\frac{\partial\alpha}{\partial Q} Q' E^2 \qquad (28)$$

where Q' is the operator representing the oscillator displacement

Q is the coordinate

H_o represents the total Hamiltonian of the molecule in the absence of the field

E is the applied electric field

If we consider a two-level Raman system, we define

$$\Delta = n_o - n \qquad (29)$$

where n_o and n are the amplitudes of the ground state, and the vibrational excited state respectively.

Let N be the molecular density, then $N\Delta$ represents the population difference density between the ground and excited states.

We will call $Q_{av} = \langle Q' \rangle$ the expectation value of the displacement operator Q'.

Again, we write down the mechanical forced vibration equation similar to Eq. (15),

$$\frac{\partial^2 Q_{av}}{\partial t^2} + \Gamma \frac{\partial Q_{av}}{\partial t} + \omega^2 Q_{av} = \frac{1}{2m} \frac{\partial \alpha}{\partial Q} E^2 \Delta \tag{30}$$

where Γ is the phenomenological damping constant and is equated to $\Delta\omega$ which is the halfwidth of the resonance curve.

The non-linear polarization can be written as

$$P_{NL} = N \frac{\partial \alpha}{\partial Q} \cdot Q_{av} E \tag{31}$$

The equation of motion of Δ is then

$$\frac{\partial \Delta}{\partial t} = - \frac{1}{\hbar\omega} \left(\frac{\partial \alpha}{\partial Q} \right) E^2 \frac{\partial Q_{av}}{\partial t} + \Gamma'(1 - \Delta) \tag{32}$$

where Γ' which is another damping constant corresponding to $1/T_1$, in the Bloch equations, is the inverse lifetime of the excited vibrational state. In comparison, Γ then corresponds to $1/T_2$ in the Bloch equations.

Finally we need one of the Maxwell's equations

$$\frac{\partial^2 E}{\partial z^2} - \frac{1}{C^2}\frac{\partial^2 D}{\partial t^2} = \frac{4\pi}{C^2}\frac{\partial^2 P_{NL}}{\partial t^2} \tag{33}$$

where z is the propagation direction.

We will assume the form of the total electric field as in Eq. (16) but without a phase constant:

$$E = E_s \cos(\omega_s t - k_s z) + E_\ell \cos(\omega_\ell t + k_\ell z) \tag{34}$$

The expectation value Q_{av} of the molecular displacement will then have also a sinusoidal form:

$$Q_{av} = Q \sin(\omega t + kz + \phi) \tag{35}$$

and

$$\omega = \omega_\ell - \omega_s \tag{36}$$

Assuming Q, E_ℓ, E_s, and Δ to be slowly varying functions of z and t, if we substitute Eqs. (34) - (36) into (30) - (33), we obtain,

$$\frac{\partial Q}{\partial t} + \frac{1}{2}\frac{Q}{T_1} = \frac{1}{4m\omega}\frac{\partial \alpha}{\partial Q} E_\ell E_s (1-n) \tag{37}$$

$$\frac{\partial \Delta}{\partial t} = \frac{1}{2h} E_\ell E_s Q + \Gamma'(1 - \Delta) \tag{38a}$$

$$\Longrightarrow \quad \frac{\partial n}{\partial t} + \frac{n}{T_2} = -\frac{1}{2h} E_\ell E_s Q \tag{38b}$$

$$\frac{\partial E_s}{\partial z} + \frac{1}{v_s}\frac{\partial E_s}{\partial t} + \frac{1}{2}\gamma_s E_s = \frac{\pi N \omega_s^2}{C^2 k_s}\left(\frac{\partial \alpha}{\partial Q}\right) E_\ell Q \qquad (39)$$

where v_s is the phase velocity of the Stokes wave

γ_s represents the finite attenuation constant for the Stokes wave

Here, we assume $n_o \cong \text{const} \cong 1$ so

$$\frac{\partial \Delta}{\partial t} \cong \frac{\partial}{\partial t}(1 - n) \cong -\frac{\partial n}{\partial t}$$

From Eq. (37), T_1 is the dephasing time which governs the decay of the coherent vibrational field Q. Also from Eq.(38b), T_2 represents the vibrational lifetime of the changing n.

What we have neglected so far is the anti-Stokes field equation which is of interest here. In the experiment, the stimulated anti-Stokes field depends on the changing coherent vibrational field, the electric field of the probe laser, and also the directionality of the k's. Using the similar form as Eq. (20) and the derivations of E_s, we can write

$$\frac{\partial E_{AS}}{\partial t}(x,t') = \frac{2\pi i \omega^2_{AS}}{e^2 k_{AS}} N \frac{\partial \alpha}{\partial Q} e^{ix\Delta k} (t' + t_D) E_{\ell 2}(t') \qquad (40)$$

where

$$\omega_{AS} = \omega_{\ell 2} + \omega$$

$$k_{AS} = k_{\ell 2} + k$$

$\Delta k = k_{\ell 2} + k - k_{AS}$

$E_{\ell 2}$ is the probe laser electric field

t_D is the delay time between the exciting (E_ℓ) and the probe ($E_{\ell 2}$) beams

The coherent anti-Stoke signals is

$$s(t_D)_{coh} = \int |E_{AS}|^2_{coh}\, dt$$

$$= \left(\frac{2\pi\omega^2_{AS}}{c^2 k_{AS}}\right)^2 N^2 \left(\frac{\partial\alpha}{\partial Q}\right)^2 \left(\frac{\sin \frac{1}{2}\ell\Delta k}{\frac{1}{2}\ell\Delta k}\right)^2 \ell^2$$

$$x \int {}^2(t' + t_D)\, |E_{\ell 2}(t')|^2\, dt \qquad (41)$$

In Eq. (41), we have a phase-matching condition Δk.

On the other hand, the incoherent anti-Stokes can be derived from Eq. (38). The signal depends on the changing ω (with time) of the vibrational excited state and the probe laser electric field; the beam cross-section and the solid angle have to be considered as in spontaneous Raman scattering process. Thus, we can write

$$s(t_D)_{inc} = \frac{3\omega^2_{SA} N^2 A\Omega}{8\pi c^3 \rho} \left(\frac{\partial\alpha}{\partial Q}\right)^2 \int dzdt\, n(z,t)\, |E_{\ell 2}(t-t_D,z)|^2 \qquad (42)$$

where A is the beam cross-section

Ω is the solid angle of acceptance

and ρ is the density.

It is to be noticed that there is no phase-matching requirement here and $s(t_D)_{inc}$ can be collected at any scattering angle.

D. Experiment

Alkanes were picked to be studied for an experimental reason: they have the most intense Raman line at the 2900 cm^{-1} shift (C-H stretching mode) which is quite far enough from the incident laser. The second harmonic laser beam (0.53μ) which is used as the probe pulse, is so intensed that it gets scattered over hundreds of wavenumbers in the spectrometer. The farther and more intense the Raman shift is, the less difficult it will be in attenuating the 0.53μ intensity and observing the anti-Stoke signal. Very good "cut off" or interference filters together with a spectrometer (which can be left off if one has good enough interference filters) are required in the experiments. Furthermore, many alkanes are liquids which make it easy to work with and are more promising that the dephasing and vibrational lifetimes will be in the order of picoseconds or even subpicoseconds.

1. Materials. Decane, Tridecane, Pentadecane, 1-hepene, 1-decene, were bought from the Aldrich Company, 99 +% grade. Heptane was of spectroquality from Matheson, Coleman, and Bell Company; isodecane and 1, 6 heptadiene were made by Chemical Sample Company, also 99% grade. Finally, $CD_3\text{-}(CH_2)_2\text{-}CD_3$ gas was obtained from Merck-Sharpe and Dohm. All these compounds were used without further purification.

2. Dephasing Times of Heptane, Decade, Tridecane, and Pentadecane.

The experimental set-up is shown in Fig. (35). The fundamental 1.06μ pulses was used as the exciting pulses, 0.53μ pulses as probing pulses. They were both focused by a 25 cm lens and sent coaxially into the cell. The anti-Stokes signals were collected at 0° scattering angle. Beyond the cell, Corning 4-98 filter was used to attenuate 1.06μ pulses, Baird-Atomic interference filter together with a Dietrich "cut off" at 5000 Å filter were used to minimize the 0.53μ intensity and maximize the anti-Stoke signal. Since the cone angle of the anti-Stoke radiation was a few degrees off the axis, the beam was not focused directly into the middle of the spectrometer slit, but a little off sideway, in order to attenuate the 0.53μ intensity even more. The spectrometer used was a 1.8 M. Ebert set at 4594 Å (2900 cm^{-1} Raman shift). The detector was an Amperex 56 TVP photomultiplier connected to a Tektronix 585 oscilloscope. A small part (~4%) of the original light was deflected out of the normal path by a glass plate into a fast Hewlett-Packard photo diode [16] biased with +45 Voltage (DC). The reference signal was fed into a 1 microsecond delay line before being sent to the oscilloscope. A half wave plate was placed in the 1.06μ path to reorient the polarization of 1.06μ beam by 90° (and hence was the same as that of 0.53μ light).

The synchronization of the two light paths was done at position A in the figure, using BBOT and two-photon method as described in Part I. The purpose of the synchronization was to help us set the variable delay as close as possible to the correct position (which had to be checked experimentally by observing the anti-Stokes signal).

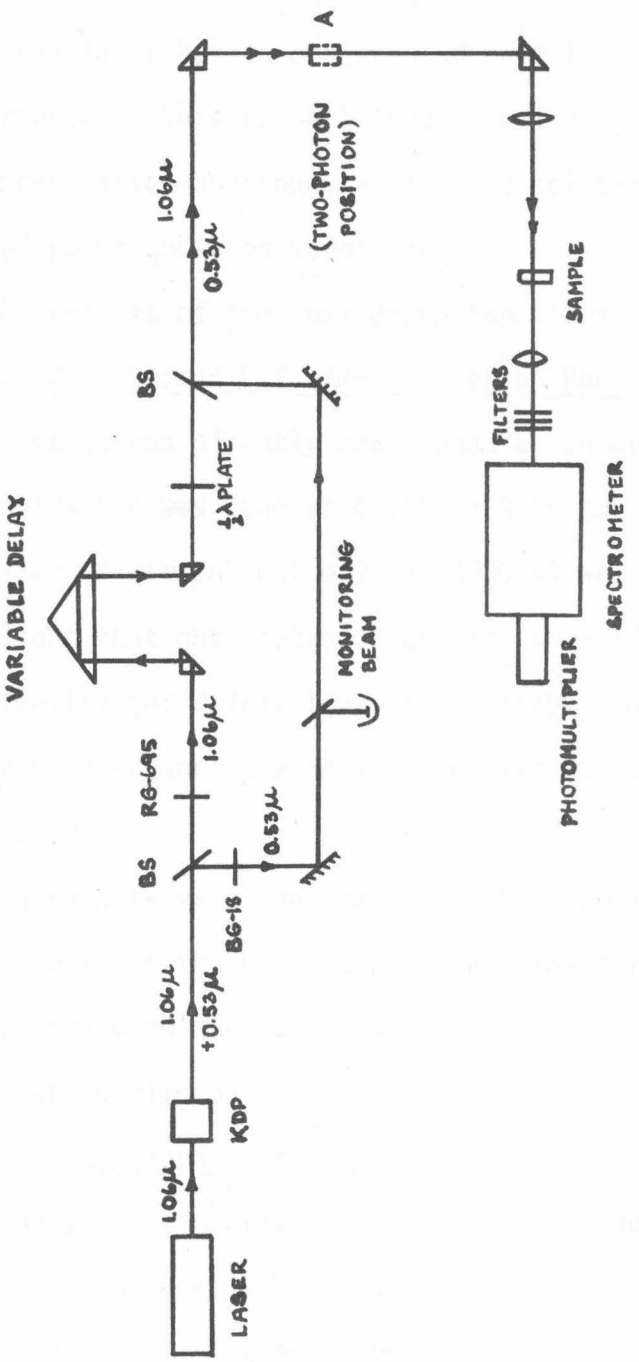

Figure 35. Dephasing Time Experiment.

Since the threshold was required in generating Stimulated Raman light, the laser had to be operated such that high enough power pulses were produced. This was achieved by using higher O.D. for the saturable dye concentration and changing the dye solution frequently enough that the high power could be maintained.

The results of the four dephasing times are shown in Fig. (36).

3. Vibrational Lifetime Studies at Room Temperature. The experimental set-up was slightly rearranged as shown in Fig. (37). The synchronization was done at position B in the figure. This time only one filter (Dietrich "cut off" at 5000 Å) was used to attenuate some 0.53μ light that got scattered off the side of the sample cell. When the intensity got fairly low, an amplifier (EG + G Model AN 101) was used to help enhance the anti-Stokes signal before feeding it into the oscilloscope.

The results were the same when the experiment was performed both with and without the half wave plate. These results confirm that the times we measured are due to the vibrational relaxation time and not the reorientation time of the molecules [17].

4. Vibrational Lifetimes Studies at Low Temperature. Some preliminary low temperature studies were conducted in a quartz dewar with optical windows. The desired temperature in the dewar was obtained by regulating one flow of dry nitrogen through a copper coil immersed in liquid nitrogen. The temperature of all the samples was monitored by a thermocouple placed inside the sample cell. The diagram is shown in Fig. (38).

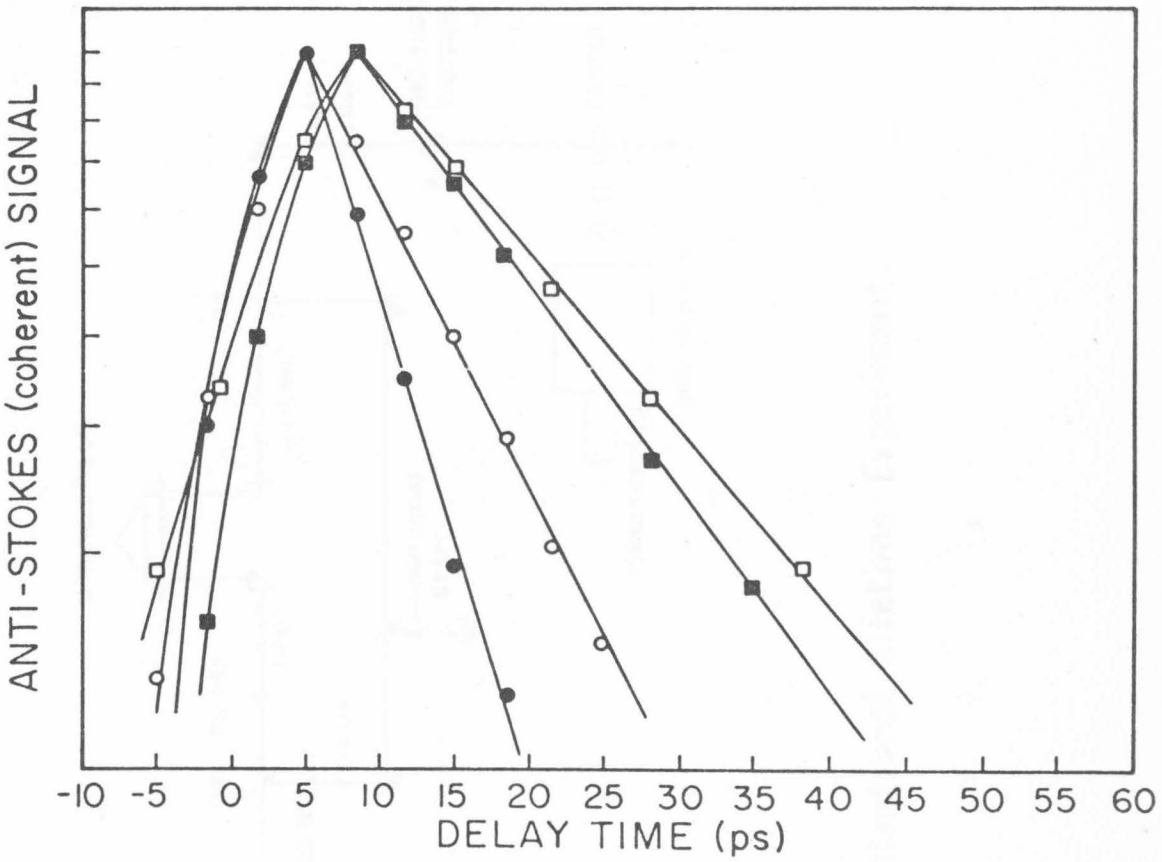

Figure 36. Dephasing Times in n-Alkanes (Temp. = 20°C): ● - Heptane, o - Decane, ■ - Tridecane, □ Pentadecane.

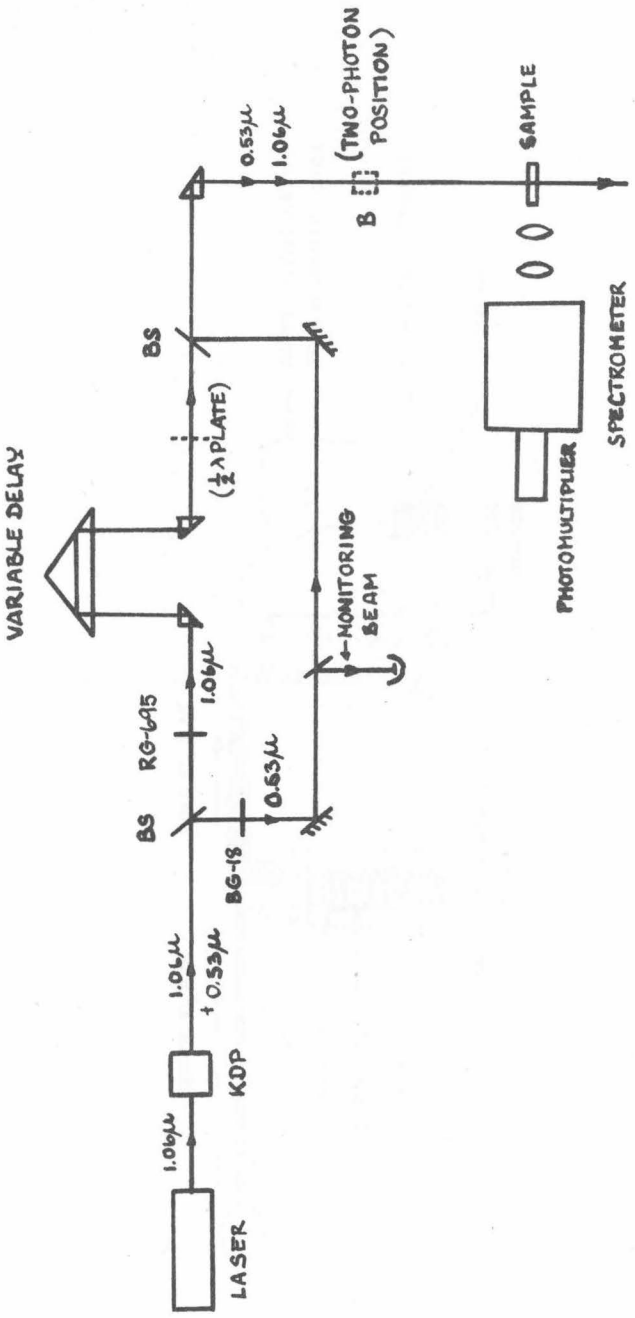

Figure 37. Vibrational Lifetime Experiment.

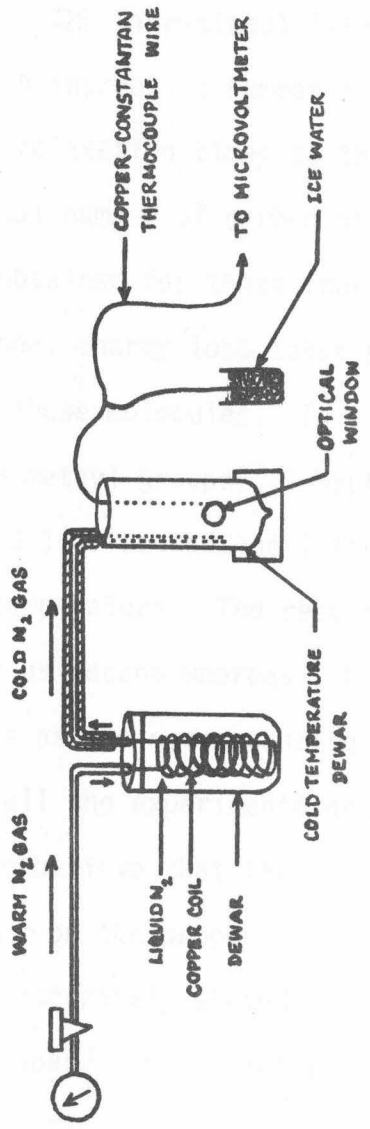

Figure 38. Cold Temperature Set-Up.

E. Results and Discussions

First, heptane, decane, tridecane, and pentadecane were studied at room temperature. The vibrational lifetime results showed the increasing lifetimes with increasing number of carbons in the molecule. When we normalize the relaxation times to the ratio of the number of CH_3 groups to the total number of carbon atoms in the chain, a reasonable correlation is obtained for these four alkanes. This seems to show that the vibrational energy loss takes place primarily through the methyl groups in these molecules. In order to check the hypothesis, isodecane (with 3-methyl groups), 1-heptene and 1-decene (with 1 methyl group), and 1, 6 heptadiene (with no methyl group) were studied at room temperature. The results show that isodecane relax about 2/3 as fast as decane whereas 1-heptene and 1-decene do at about twice as slow rate as the corresponding n-alkanes. The results and normalization of all the experiments are shown in Table I. These results lead us to believe that the C-H stretching relaxation time depends in the main on the proportion of the methyl groups in the molecule, or more accurately stated, on the proportion of time the vibrational excitation spends on the methyl groups.

The relaxation time of 1, 6 heptadiene, which is also listed in Table I, is considerably longer, further confirming the above notion. Because the Raman spectra of these types of molecules have three distinct maxima (instead of a broad band in n-alkanes) in the 2900-3000 cm^{-1} region (the CH stretching from the $-HC=CH_2$ groups peak at about 3000 cm^{-1}, whereas the CH from a single bond carbon peaks about 2900 cm^{-1}) [18], a

TABLE I

Compound	Temp. °C	a. Lifetime	b. Ratio methyl carbons to total carbons	Normalized Lifetime (a x b)
n-Heptane	20	11.0	2:7	3.14
	-25	14.0	---	----
	-70	16.0	---	---
Isodecane	20	10.8	3:10	3.24
n-Decane	20	16.0	2:10	3.20
	-25	21.0	----	----
N-Tridecane	20	21.0	2:13	3.23
n-Pentadecane	20	24.5	2:15	3.27
1-Heptene	20	21.0	1:7	3.00
1-Decene	20	33.5	1:10	3.35
1,6-Heptadiene	20	60.0	----	----

check was made to see if the measured relaxation time depended on detecting frequency. The relaxation data were found to be insensitive to the position of the 1.8 M spectrometer setting within a range of wavelengths corresponding to the Raman shifts of 2900 cm^{-1} to 3100 cm^{-1}.

In order to obtain some preliminary measurement in the C-H stretching relaxation time of the methylene groups, CD_3-CH_2-CH_2-CD_3 which is a gas at room temperature was studied. A special small cell had to be made for this purpose. The cell was connected to the gas bulb with a break-off seal. Before letting the gas into the cell, it was cleaned by flushing N_2 gas through several times (shown in Fig. (39)). The N_2 gas and water vapor was then pumped out until the pressure in the cell read $\sim 10^{-6}$ Torr. The cell was then sealed off from the vacuum line and placed in a small dewar. The study was conducted at -42°C (in order to fill the cell up with the liquid from the amount of gas we had). The relaxation time was ~72 psec.

The relaxation data are plotted in Figs. (40)-(42). It is to be emphasized that these are only raw data and the lines through the data points in these figures are purely for visualization. It was, however, possible to reproduce the data in different experiments over a period of months. This indicates that despite one inherent error in doing picosecond studies with an entire pulse train, the method has apparently proved to be fairly reliable. In order to obtain more accurate relaxation times, a single pulse apparatus is needed.

Although the pathway for decay of the C-H stretching vibration has not been investigated (due to the limitation of the apparatus), the

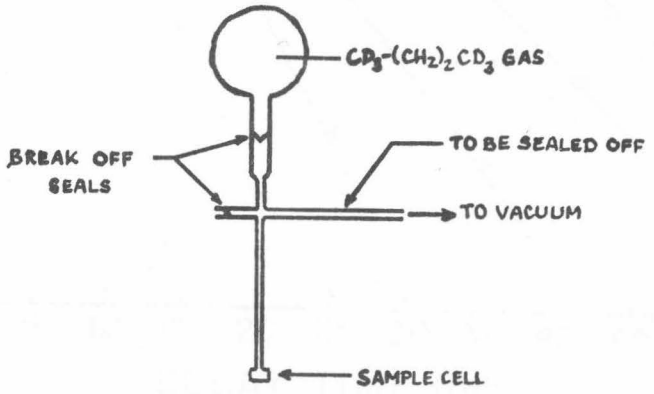

Figure 39. A CD_3-$(CH_2)_2$-CD_3 Cell.

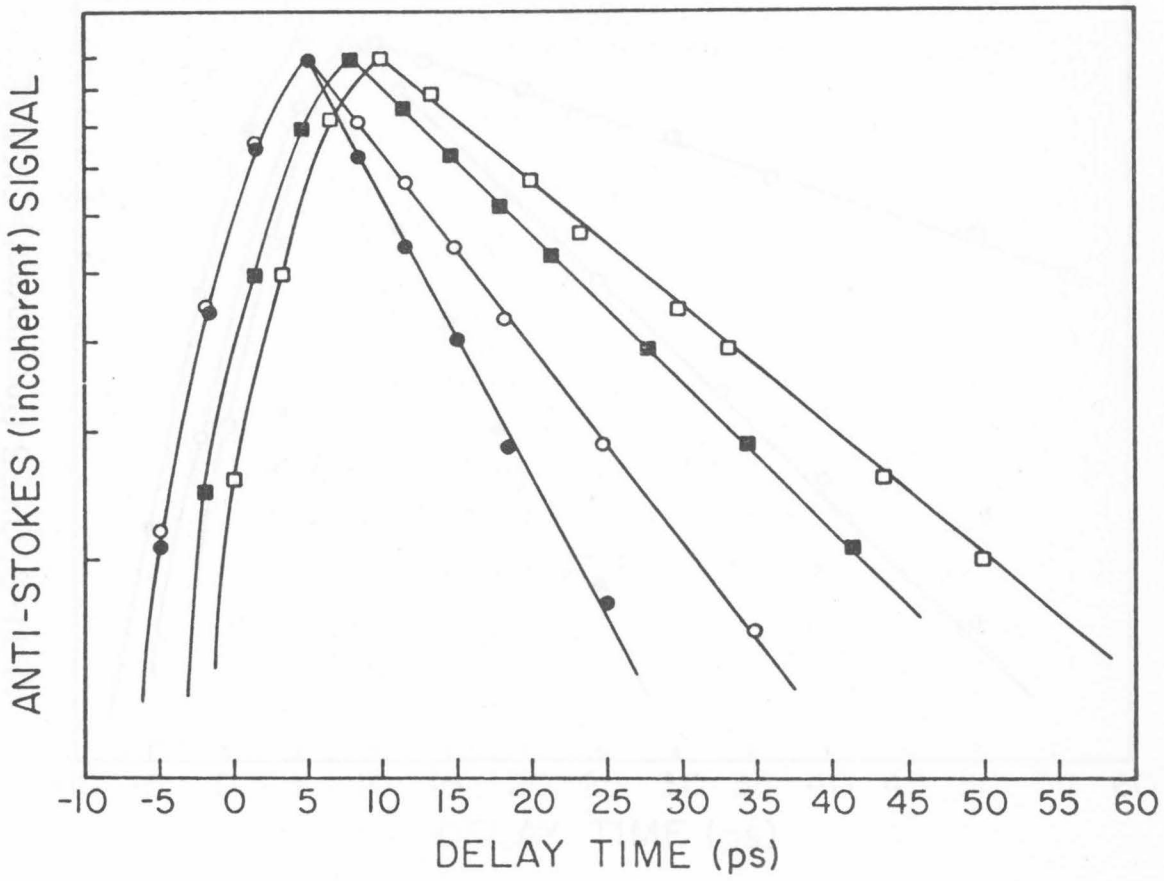

Figure 40. Vibrational Lifetimes of n-Alkanes (Temp.=20°C): ●-Heptane, o-Decane, ■-Tridecane, □ Pentadecane.

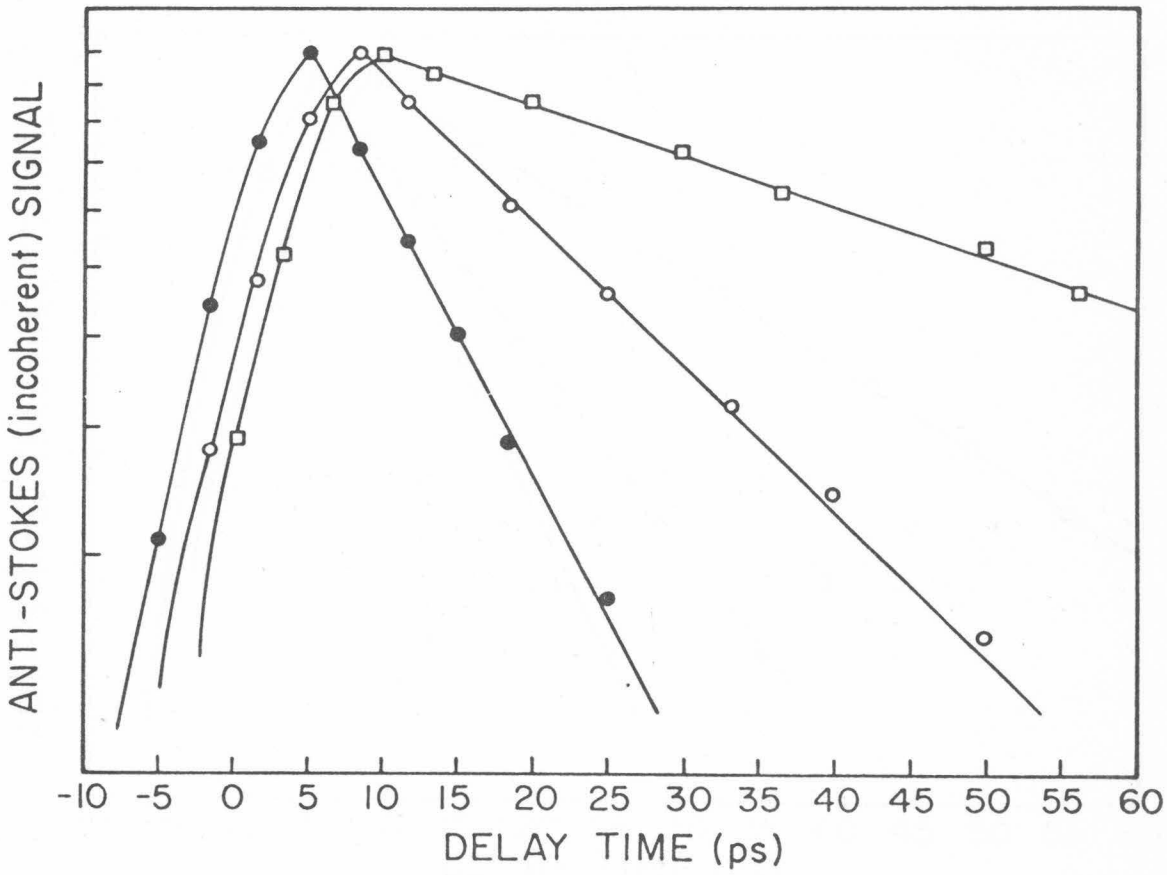

Figure 41. Vibrational Lifetimes of C_7 Hydrocarbons (Temp. = 20°C): ●-n-Heptane, o-1-Heptene, □-1,6 Heptadiene.

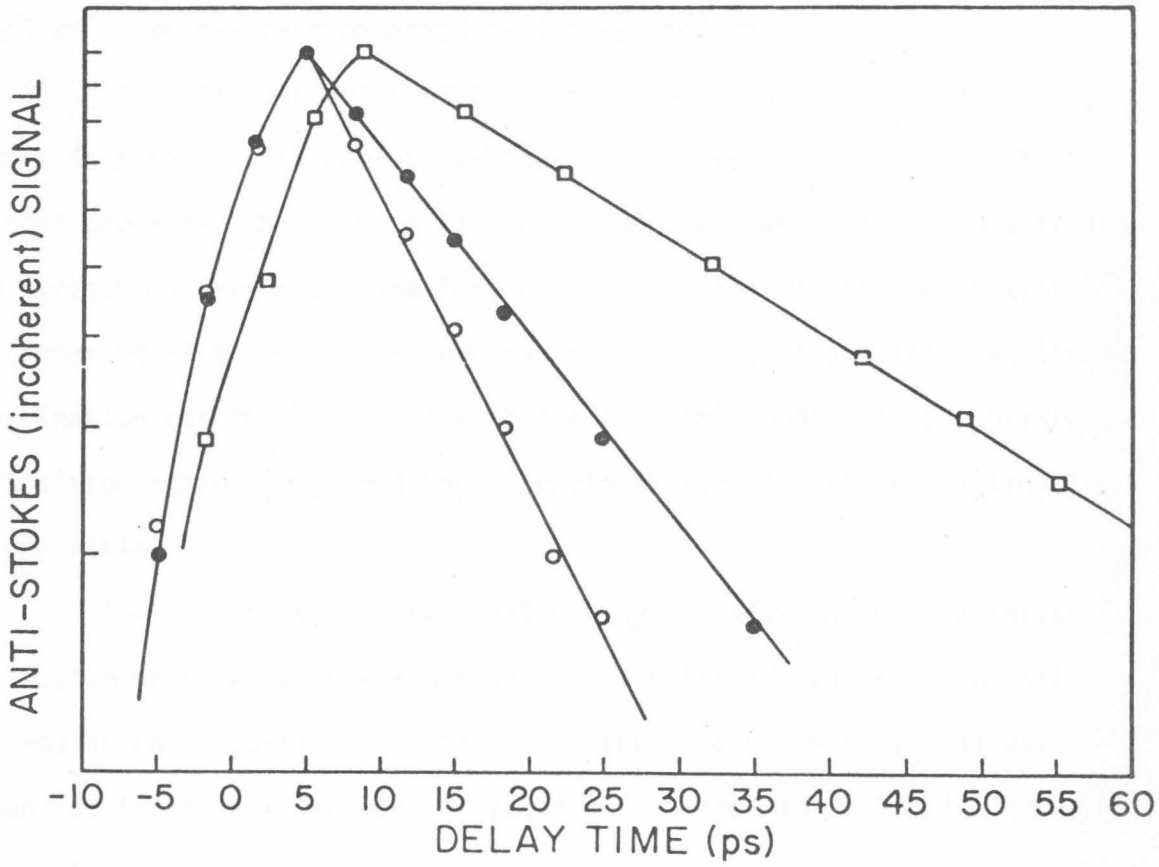

Figure 42. Vibrational Lifetimes of C_{10} Hydrocarbons (Temp. = 20°C) : o - Isodecane, ● - n-Decane, □ - 1-Decene.

vibrational excitation most likely decays by way of two CH_3 bending at 1450 cm^{-1}, as has been observed by Alfano and Shapiro [10] and Laubereau et al. [11]. The mechanism of this splitting into two lower frequency modes is probably the well-known Fermi-resonance effect. Since the second order of the CH_3-bend is around 2900 cm^{-1} which lies close to the CH stretching frequency, the Fermi-resonance will mix the two states together, giving the linear combinations of the states. This new linear combination can then interact with the 1450 cm^{-1} mode with a non-zero transition moment [20], and the vibrational-vibrational energy transfer is possible.

The vibrational-vibrational energy transfer can go via intramolecular or intermolecular mechanism. The latter can be bi- or trimolecular collisional interaction. In the case of CH_3-CCl_3, it was reported to be trimolecular interaction from the binary liquid mixture study [11].

Temperature Effect

The temperature dependence has not been studied over a wide enough range to suggest its exact origin. It seems,however, that the vibrational relaxation does not occur via purely intramolecular mechanism. The intermolecular collision also plays a role in de-exciting the vibrational energy. As has been discussed by many authors [21] the vibrational relaxation time by collision depends inversely on collision frequency and collision efficiency per collision, which in turn are both temperature dependent. At lower temperature, molecules have smaller speed which will lower the collision rate. Futhermore, the

energy per molecule becomes low and low energy collisions are very ineffective. Hence, the participation in the relaxation mechanism of intermolecular collisions would give rise to a temperature effect similar to the one observed.

It is interesting to note that proton spin-lattice relaxation (T_1 decay time) in long chain hydrocarbons seems also to take place most effectively from $-CH_3$ groups, both at room temperature [22] and at low temperature [23, 24] Furthermore, K. van Putte [25] has found that T_1 increases with the chain length in paraffinic chains.

Further experiments with a single pulse apparatus can be conducted in order to understand the mechanisms of this problem. A dilution experiment (for example, 1% of heptane in deurated heptane solution) may shed some light on the vibrational transfer mechanisms (whether it is intra- or inter- molecular). The 1450 cm^{-1} bending mode relaxation time and intensities can be obtained and compared to those of the 2900 cm^{-1} stretching mode in order to identify the decay route. Furthermore, if precise enough data were available, it might be possible to extract out the $-CH_2-$ relaxation times from the n-alkane results by taking the total rate to be the sum of $-CH_3$ and $-CH_2-$ rates normalized to the proportion of each such group in the molecule. The present data are too crude for this.

Vibrational relaxation times can become a very important tool in the understanding of molecular interactions in liquid. Many

systematic studies can be done (for example, benzene and its derivatives) in order to understand more the effect of the substituents on the molecular interactions and vibrational energy transfer mechanisms. Dephasing times, together with the photon echo technique, may promote the mechanism of dechasing phenomenon in different liquids, crystalline liquids, and solids. These experiments are extremely difficult, but with the development of the engineering art in the picosecond laser field, they may become possible.

References

1. P. M. Rentzepis, Adv. in Chem. Phys. 23, p. 189 (1973), and references therein.
2. M. R. Topp, et al., Opt. Comm. 3, 264 (1971).
3. M. J. Colles, Opt. Comm. 1, 169 (1969).
4. W. H. Glenn, et al. Appl. Phys. Lett. 12, 54 (1964).
5. F. DeMartini and J. Ducuing, Phys. Rev. Lett. 17, 117 (1966).
6. R. R. Alfano, Bull. Am. Phys. Soc. 15, 1324 (1970).
7. D. von der Linde, A. Laubereau, and W. Kaiser, Phys. Rev. Lett. 26, 954 (1971).
8. D. von der Linde and A. Laubereau, Opt. Comms. 3, 279 (1971).
9. A. Laubereau, D. von der Linde, and W. Kaiser, Phys. Rev. Lett. 27, 802 (1971).
10. R. R. Alfano and S. L. Shapiro, Phys. Rev. Lett. 29, 1655 (1972).
11. A. Laubereau, L. Kirschner, and W. Kaiser, Opt. Comm. 9, 182 (1973).
12. I. D. Abella, N. A. Kurnit, and S. R. Hartmann, Phys. Rev. 141, 139 (1966).
13. See,for example
    a. A. Yariv, Quantum Electronics (John Wiley and Sons, Inc., 1967), Chapter 23.
    b. E. Garmire, F. Pandaresse, and C. H. Townes, Phys. Rev. Lett. 11, 160 (1963).
    c. M. Maier, W. Kaiser, and J. A. Giordmaine, Phys. Rev. 177 580 (1969).
    d. N. Bloembergen, Am. J. of Phys. 35, 989 (1967).

14. See Ref. [9a] p. 398 and p. 405.

15. R. W. Minck, R. W. Turbune, and C. C. Wang, Proc. IEEE 54, 1357 (1966).

16. The diode is made from PIN diode type HP 5042, followed the instruction given by G. H. McCall in Rev. Sci. Inst. 43, 865 (1972).

17. T. J. Chuang and K. B. Eisenthal, Chem. Phys. Lett. 11, 368 (1971).

18. American Petroleum Research Project 44, Serial Number 345 (1968).

19. See for example

    a. D. von der Linde, O. Bernecker, and A. Laubereau, Opt. Comm. 2, 215 (1970).

    b. D. von der Linde, IEEE J. Q. E. Vol. QE8, 328 (1972).

20. K. F. Herzfeld, J. Chem. Phys. 47, 743 (1967).

21. See, for example

    a. K. F. Herzfeld and T. A. Litovitz, "Absorption and Dispersion of Ultrasonic Waves (Academic Press Inc., New York, 1959).

    b. K. F. Herzfeld, J. Chem. Phys. 36, 3305 (1961).

    c. G. M. Burnette and A. M. North, ed. "Transfer and Storage of Energy by Molecules" vol. 2 : Vibrational Energy (Wiley-Interscience, 1969), with references therein.

22. a. S. I. Chan, G. W. Feigenson, C. H. A. Seiter, Nature (London) 231, 110 (1971).

    b. G. W. Feigenson and S. I. Chan, J.A.C.S. 96, 1312 (1974).

23. D. W. McCall and D. C. Douglass, Polymer 4, 443 (1963).

24. J. E. Anderson and W. P. Slichter, J. Phys. Chem. 69, 3099 (1965).

25. K. van Putte, Trans. Faraday Soc. 523 (1970); and J. Mag. Res. 2, 216 (1970).

Proposition 1

REPOPULATION TIME OF THYMINE AND URACIL

Hauswirth and Daniels [1] reported the fluorescence, intersystem crossing, and calculated internal conversion rates of thymine and uracil. The fluorescence and intersystem crossing rates, $\sim 10^8$ and 10^9, respectively, are quite slow in comparison to that of the internal conversion, which is about $10^{12} sec^{-1}$. Also, the quantum yield and chemical change are very low ($\phi_{fl} \simeq 10^{-4}$ and $\phi_{chem} = 10^{-3}$). It was thus believed that most of the energy undergoes internal conversion. It is proposed here to study the internal conversion rate by measuring the rate of repopulation of the ground state from the first excited state.

The experimental set-up can be derived from Rentzepis' work on azulene [2]. In addition, a pulse-selector [3] which selects only one pulse out of the whole pulse train is needed for a more accurate result. Two KDP crystals are employed in order to obtain a fourth harmonic generation at 2650Å which will be used to excite the thymine and uracil to the first electronic excited state. As shown in the experimental diagram in Figure 1, a "cut-off" filter (F) is needed to filter out the unwanted 0.53μ and 1.06μ lights. The 0.265μ pulse will then be sent into the sample cell. In order to measure the repopulation time, a dielectric mirror which reflects ~75% at 0.265μ is placed on a translating micrometer which can move back and forth between the cell and the photodiode P_2. About 25% of the emerging light from the cell will to into the diode as a reference signal, whereas 75% of the light gets reflected back into the cell to be absorbed by the ground state

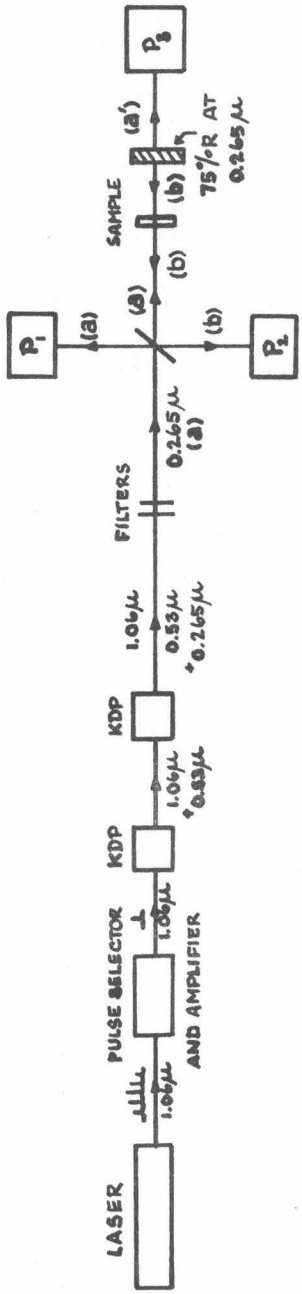

Figure 1. A Proposed Repopulation Time Experiment.

molecules. If we start out by placing the mirror right after the cell, the reflected or interrogating light will "see" molecules mostly in the excited state, and hence will go through unattenuated. This interrogating light will be reflected by a beam-splitter (BS) into a diode P_3 . As we move the dielectric mirror backward a known distance, the reflected light will see more and more ground state molecules, and will be again absorbed by the solution. Hence, the change in the intensity at P_3 as the function of time between the exciting and interrogating pulses will yield the repopulation rate of the molecules. The experiment is monitored by deflecting a small amount of 0.265μ light into diode P_1 .

References

1. W. Hauswirth and M. Daniels, Chem. Phys. Lett. 10, 140 (1971).
2. P. M. Rentzepis, Chem. Phys. Lett. 3, 717 (1969).
3. D. von der Linde, IEEE J. Quant. Elect. QE-8, 328 (1972).

Proposition 2

INVESTIGATION OF THYMINE EXCIMER FORMATION IN AQUEOUS SOLUTION BY A PICOSECOND LASER

By means of fluorescence study, excimer formations have been found in solutions of nucleic acids (for example, adenine-adenine)*, (adenine-thymine)* except (thymine-thymine)* [1,2]. However, thymine dimer (TT) has been reported with very high quantum yield. The precursor of dimerization was thought by the authors [1,2] to be the short-lived thymine excimer (TT)*. This is due to the argument that excimers may form without manifesting themselves by their fluorescence emission if another de-excitation occurs faster [1]. The fact that the fluorescence yield of thymine is very small leads one to estimate the excited state lifetime of thymine to be in the order of 10^{-11}sec. One of the possibilities of the fluorescence quenching mechanism is the dimerization itself [2]. This may occur first with excimer formation (very fast process) and then the excimer going onto the dimer.

It is proposed that thymine excimer fluorescence and lifetime be investigated by a mode-locked Nd-glass laser.

Thymine in aqueous solution (both at room and low temperature) is first excited with a single picosecond 0.265μ pulse. The fluorescence can then be observed with a spectrograph or spectrometer by means of a CS_2 light gate [3]. The proposed experimental set-up is shown in Figure 1.

In the experiment the two optical paths (1.06 path and 0.265μ path) are synchronized by means of one CS_2 optical shutter (lifetime ∿

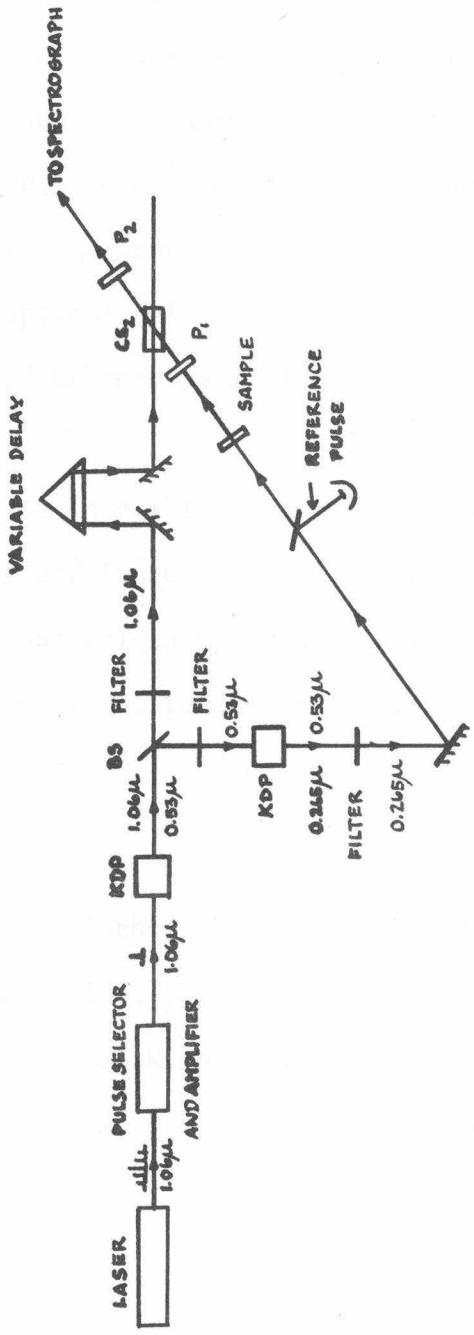

Figure 1. A Proposed Thymine Excimer Experiment.

2 psec). Then a sample cell can be put in place. The excimer fluorescence (excited by 0.265μ pulse) can then be searched with the help of a spectrograph setting around 0.3μ-0.5μ (the fluorescence spectrum of thymine is between 0.295μ-0.45μ, peaks at 0.33μ [4], but the excimer fluorescence is usually 5000-6000 cm^{-1} red shifted). Once the fluorescence is observed, the excimer formation time and lifetime can also be studied in the same manner (by delaying 1.06μ from the synchronized setting of the optical delay). The fluorescence intensity on the photographic plate can be read by a microdensitometer as a function of time delay.

It will be interesting to compare the lifetime of thymine excimers in liquid and frozen states. In the latter case, a low temperature dewar with optical quartz windows is required. This experiment should bring a new light to the mechanism of thymine dimerization.

References

1. J. Eisinger, Photochem. Photobiol. 2, 597 (1968).
2. A. A. Lamola, ibid., 7, 619 (1968).
3. M. A. Duguay and J. W. Hansen, Appl. Phys. Lett. 15, 192 (1969).
4. W. Hauswirth and M. Daniels, Photochem. Photobiol. 13, 157 (1971).

Proposition 3

INVESTIGATION OF HYDRATED e^-_{aq} IN SOME HETEROCYCLIC COMPOUNDS IN AQUEOUS SOLUTIONS

H. Joschek and L. I. Grosswiener [1] reported the studies on hydrated e^-_{aq} ejected from aromatic compounds upon flash photolysis. However, there was an absence of e^-_{aq} detection in certain compounds; namely pyridine, pyrimidine, benzoxazole, benzimidazole, benzothiazole, and purine. Since the authors were working with nanosecond flash photolysis, it is perceived that the e^-_{aq} is formed but the lifetime is too short to be detected on such a time scale. The amount and lifetimes of e^-_{aq} formed in other aromatic compounds indicated that the structures and substituents of the ring compounds played important roles in the scavenging reactivity of e^-_{aq}. It is thus of interest to investigate the e^-_{aq} formation in the mentioned compounds on a picosecond time scale, since it may yield some information on the scavenging reactivity, and toward a better understanding of mechanistic pathways of some photochemical reactions.

The absorption spectra [2] of the compounds in Figure 1 peak around 0.265μ which is the fourth harmonic of the Nd:glass laser. The experimental set-up is shown in Figure 2. The sample is excited by the 0.265μ single pulse, then probed with a continuum (0.4μ-1.06μ) produced by focusing 1.06μ in liquid D_2O. Since e^-_{aq} absorbs around 0.65μ, the formation times and lifetimes of e^-_{aq} can be obtained from the change in absorption at 0.65μ as a function of delay time between

PYRIDINE

PYRIMIDINE

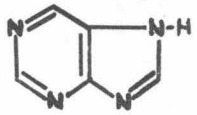

PURINE

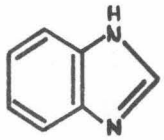

BENZIMIDAZOLE

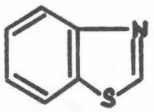

BENZOTHIAZOLE

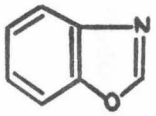

BENZOXAZOLE

Figure 1

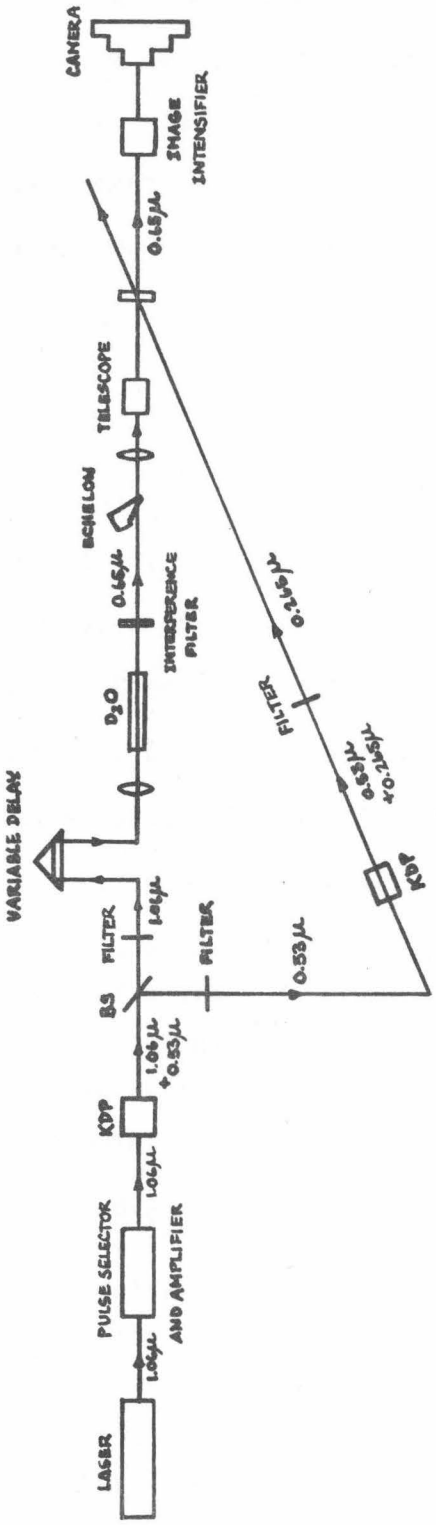

Figure 2. A Proposed Experiment on $\bar{e}_{aq}$.

the exciting and probing pulses. In the figure, F_4 is an interference filter peak at 0.65 , and E is the echelon [3]. The 0.65 pulse, after emerging from the cell, is detected by an image intensifier together with a camera. The synchronization with CS_2 shutter and the control of the experiment (i.e., monitoring the signals) can be done in the same manner as in Propositions 1 and 2.

References

1. H. Joscheck and I. L. Grosswiener, J.A.C.S. 88, 3261 (1966).

2. a. F. Halverson, J. Chem. Phys. 19, 711 (1951).

   b. S. F. Mason, J. Chem. Soc. (1954) 2071.

   c. W. A. Boggust, J. Chem. Soc. (1949) 355.

   d. E. A. Steck, et al., J.A.C.S. 70, 3406 (1948).

   e. R. Passerini, J. Chem. Soc. (1954) 2256.

3. M. R. Topp, et al., J. Appl. Phys. 42, 3415 (1971). A glass echelon consists of a stack of glass slides, equally spaced. The light pulse is spread uniformly over the face of the echelon by by means of a thin diffusing plate, experiencing varying retardations, the interpoint delay being given by

$$t = (\frac{d}{c})[(n^2 - \sin^2\theta)^{1/2} - \cos\theta]$$

   where n is the refractive index of the glass, θ the angle of incidence and d the thickness per slide.
   In this way, the pulse is split up into many parts by the number of glass slides; one part gets to the sample after another with the time separation t given above.

Proposition 4

ELECTRONIC RAMAN SPECTRA: RAMAN TRANSITION OF TRIVALENT URANIUM IN CaF_2 CRYSTAL

Electronic Raman spectra have been reported for trivalent rare earth ions in crystals [1-3], and also for the normal spinels: Ag_2MoO_4, $GcGeO_4$, and $ZnAl_2O_4$ [4]. The theory and selection rules have been worked out [5].

Electronic Raman effect is a very useful approach to the study of low-lying electronic levels where absorption and fluorescence spectra are weak or forbidden, since the Raman transitions are allowed between states of the same parity.

In this paper I would like to propose the electronic Raman study on U^{3+} doped CaF_2 crystal, for the following reasons:

1. U^{3+} doped in CaF_2 is a laser material.

2. The low lying electronic levels have been known by the method of absorption and emission spectra at liquid N_2 and liquid helium temperature [6-11]. However, the lowest energy levels assigned vary from one paper to another; as for example, G. D. Boyd reported the highest Stark levels of $^4I_{9/2}$ (ground state) to be 609 cm^{-1} [7], R. Meredith reported 464.8 cm^{-1} [10], J. P. Wittke, 515 cm^{-1} [9], V. F. Egorova observed 542 cm^{-1} for crystal type I and 655 cm^{-1} for crystal type II [11]. The electronic Raman spectra will provide another way of investigating these low energy levels.

3. The U^{3+} site in CaF_2 has been reported to be in tetragonal [10,12] and trigonal [13] crystal fields. By looking at the spectral

shift and the symmetry properties of the scattering or polarizability tensor elements, the symmetry of the U^{3+} site may be confirmed. (The results strongly depend on the orientation of the crystal to the incident laser beam.)

4. U^{3+}, being the analog of Nd^{3+} (Actinide-lanthanide analog), seems to give confidence that good results are to be expected. Electronic Raman transitions have been observed from Nd^{3+} in ytterium gallium garnet [3b].

5. The sample, U^{3+} doped in CaF_2 crystal, can be easily obtained.

Theory

The intensity of any Raman transition is given by the scattering tensor [14]

$$(\alpha_{\lambda\mu})_{kn} = \frac{1}{h} \sum \frac{(M_\lambda)_{nr}(M_\mu)_{rk}}{\nu_{rk} - \nu - i\gamma_r} + \frac{1}{h} \sum \frac{(M_\mu)_{nr}(M_\lambda)_{rk}}{\nu_{rn} + \nu + i\gamma_r} \qquad (1)$$

where $(M_\lambda)_{nr}$ is the matrix element of the electric dipole vector and the summation goes over all excited states in the system. k and n are initial and final states for Raman states, respectively. ν is the frequency of the incident light beam. γ_ν is the damping constant of state r .

O. S. Mortensen and J. A. Koningstein worked out the scattering tensors for electric Raman transitions in their papers [5a,5c] as follows.

The total wavefunction can be written by means of the zeroth order Born-Oppenheimer approximation

$$\Psi \simeq \psi(r,Q)\ \phi(Q) \tag{2}$$

where r and Q denote the electronic and nuclear coordinate, respectively.

The first order in the nuclear displacement, $\psi(r,Q)$, can be expanded as

$$\psi(r,Q) = \psi_k(r,Q=0) + \sum_Q \sum_t \frac{\langle\psi_t \left(\frac{\partial \mathcal{H}}{\partial Q}\right)_{Q=0} |\psi_k\rangle}{E_k - E_t} \tag{3}$$

where $\mathcal{H}$ is the electronic Hamiltonian that depends parametrically on Q and the zero point for the normal coordinates fixed at the equilibrium position of the nuclei.

Substitute (3) in (1), leading to the sum of scattering tensor

$$(\alpha_{\lambda\mu})_{ku;nw} = (\alpha_{\lambda\mu})^{\text{static}}_{ku;nw} + (\alpha_{\lambda\mu})^{\text{dynamic}}_{ku;nw}$$

where

$$(\alpha_{\lambda\mu})^{\text{static}}_{ku;nw} = \frac{1}{h} \sum_{r,\nu} \frac{(M_\lambda)_{nr}(M_\mu)_{rk}}{\nu_{r\nu;k\mu} - \nu - i\gamma_r} \langle\phi_\omega|\phi_\nu\rangle\langle\phi_\nu|\phi_u\rangle + \text{c.t.}$$

$$= \frac{1}{h} \langle\phi_\omega|\phi_u\rangle \sum_r \left\{\frac{(M_\lambda)_{nr}(M_\mu)_{rk}}{\bar{\nu}_{rk} - \nu} + \frac{(M_\mu)_{nr}(M_\lambda)_{rk}}{\bar{\nu}_{rn} + \nu}\right\} + \text{c.t.}$$

and

$$(\alpha_{\lambda\mu})^{\text{dynamic}}_{ku;n\omega} = \frac{1}{h} \sum_{r,\nu} \times$$

$$\times \frac{(M_\lambda)_{nr}\langle\phi_\omega|\phi_\nu\rangle \{ \sum^{t,Q} \langle\phi_\nu| Q |\phi_\mu\rangle [M_\mu)_{\nu t} h^{Q}_{tk} + (M_\mu)_{tk} h^{*Q}_{tr}]\}}{\nu_{r\nu;k\mu} - \nu - i\gamma_r} + \text{c.t.}$$

$$= \frac{1}{h} \sum_{Q} \langle\phi_\omega| Q |\phi_\mu\rangle \sum_{r} \frac{(M_\lambda)_{nr}\{(M_\mu)_{rt} h^{Q}_{tk} + (M_\mu)_{tk} h^{*Q}_{tr}\}}{\overline{\nu}_{rk} - \nu} + \text{c.t.} \quad (5)$$

where

$$h^{Q}_{tk} = \langle\psi_t| \left(\frac{\partial \boldsymbol{\alpha}}{\partial Q}\right)_{Q=0} |\psi_k\rangle \qquad (E_k - E_t)$$

The steps in (4) and (5) are carried out by the use of the closure theorem in the space made up of the vibrational wave functions.

If the static part of the scattering tensor is dominant, the transition will be independent of vibronic coupling and leads to the pure electronic effect. On the other hand, the dynamic part leads to the vibronic effect. The major factor that determines the scattering tensor is the frequency of the region of the exciting radiation. If the transitions in the region are comparatively weak, then $h^{Q}_{tk} \ll 1$ and the static term predominates. If one or more first order transition in the region of the frequency of the incident beam is relatively strong, then the dynamic part predominates. For experimental reasons, the chosen and appropriate frequencies of incident radiation are those outside any strongly absorbing frequency range of the scattering system. So the vibronic effect can be neglected.

The main difference between the electronic and vibrational Raman effects is that in electronic effect the antisymmetric part (static in this case), $\alpha_{\lambda\mu} \neq \alpha_{\mu\lambda}$, often dominates over the symmetric part, and vice versa in the vibrational case. Thus, in the electronic effect, the polarizability of the system need not be expanded in terms of a particular normal coordinate (equation (3)).

Selection Rules. These are the same in electronic effect as i-vibrational effect, i.e., the transition is allowed if the product of the irreducible representation of the ground and terminal excited states of a species occurs in which one or more, or a combination of components of the scattering tensor, belongs.

The selection rules for D_{4h} and D_{3d}^{5f} are given on page 133.

The electronic Raman transitions originate mainly from the crystal field splitting of $(4,5f)^n$ levels. The $(4f)^{n-1}(5d)$ levels and the charge transfer states are of too high energy [15].

Energy Levels of U^{3+} in CaF_2 Crystal. Trivalent uranium has an electronic configuration consisting of closed shell and three electrons in the unfilled (5f) shell - $(5f)^3$. By Hund's rule, the lowest term of an f^3 configuration is ^4I, with $J = 9/2$ state lying lowest since the uranium multiplet is regular. The number of Stark splittings depends on the symmetry of the site of U^{3+} in CaF_2. Each splitting level is doubly degenerate (Kramer's doublet).

The absorption and emission (fluorescence) spectra with fairly high resolution at low temperature have been reported by R. E. Meredith [10]. He interpreted the spectra as arising from ions in the tetragonal sites. In such a case the ground $^4I_{9/2}$ level splits

SELECTION RULES FOR D_4, C_{2v}, D_{2d}, D_{4h} SYMMETRY

$(\Gamma_1,\Gamma_1), (\Gamma_2,\Gamma_2), (\Gamma_3,\Gamma_3), (\Gamma_4,\Gamma_4)$	zz, xx, yy
$(\Gamma_1,\Gamma_2), (\Gamma_3,\Gamma_4)$	S_z
$(\Gamma_1,\Gamma_3), (\Gamma_2,\Gamma_4)$	$xx-yy$
$(\Gamma_1,\Gamma_4), (\Gamma_2,\Gamma_3)$	$xy-yx$
$(\Gamma_1,\Gamma_5), (\Gamma_2,\Gamma_5), (\Gamma_3,\Gamma_5), (\Gamma_4,\Gamma_5)$	(S_x,S_y) $(zx+xz, yz+zy)$
(Γ_5,Γ_5)	S_z, zz, $xx-yy$, $xy+yx$
$(\Gamma_6^*,\Gamma_6^*), (\Gamma_7^*,\Gamma_7^*)$	S_z, zz, $xx+yy$, (S_x,S_y), $(zx+xz, yz+zy)$
(Γ_6^*,Γ_7^*)	$xx-yy$, $xy+yx$, (S_x,S_y), $(zx+xz, yz+zy)$

$\Gamma_1 \rightarrow A_1$, $\Gamma_2 \rightarrow A_2$, $\Gamma_3 \rightarrow B_1$, $\Gamma_4 \rightarrow B_2$, $\Gamma_5 \rightarrow E$

$\Gamma_6 \rightarrow E_{1/2}$ $\Gamma_7 \rightarrow E_{3/2}$

WHERE $S_x = yz-zy$, $S_y = zx-xz$, $S_z = xy-yx$

SELECTION RULES FOR C_{3v}, D_3, D_{3d} SYMMETRY

$(\Gamma_1,\Gamma_1), (\Gamma_2,\Gamma_2)$	zz, $xx+yy$
(Γ_1,Γ_2)	S_z
$(\Gamma_1,\Gamma_3), (\Gamma_2,\Gamma_3)$	$(S_x,S_y), (zx+xz, yz+zy), (xx-yy, xy+yx)$
(Γ_3,Γ_3)	ALL POLARIZATIONS ALLOWED
(Γ_4^*,Γ_4^*)	ALL POLARIZATIONS ALLOWED
$(\Gamma_4^*,\Gamma_{5,6}^*)$	$(S_x,S_z), (zx+xz, yz+zy), (xx-yy, xy+yx)$
$(\Gamma_{5,6}^*,\Gamma_{5,6}^*)$	S_z, zz, $xx+yy$

$\Gamma \rightarrow A_1$, $\Gamma \rightarrow A_2$, $\Gamma \rightarrow E$

$\Gamma_4 \rightarrow E_{1/2}$, $\Gamma \rightarrow E_{3/2}$

into 5 doublets and the $^4I_{11/2}$ levels split into 6 doublets implying that six absorption transitions should be observed in the near infrared. The diagram of the energy levels is shown on page 135.

However, J. P. Wittke [9] reported only 3 doublets in the $^4I_{9/2}$ levels and 4 doublets in $^4I_{11/2}$. The diagram is shown on page 135. The author had to use the cubic crystal field to interpret the data despite the fact that the distortion in the symmetry occurs when U^{3+} substitutes Ca^{2+} in the crystal.

V. F. Egora looked at the absorption spectrum and the stimulated emission spectrum of $U^{3+}:CaF_2$ crystal and observed two different results, depending on whether U^{3+} is in crystal type I or type II or hybrid (mixture of both) (see page 135).

A. Yariv reported the observation of trigonal S_6 system for $U^{3+}:CaF_2$ about 111 direction and five Kramer doublets were expected for $^4I_{11/2}$ level.

Experimental Set-up. Either a He-Ne laser or an argon laser is appropriate for the exciting source. The laser beam is focused on a single crystal which is mounted on top of a cold finger of a low temperature research dewar. A Jarrell-Ash monochromator is used. Some appropriate filters may also be needed to cut unwanted lights or emissions (for example, Rayleigh scattering). A high sensitivity diode is used as the detector for the laser from the monochromator which is then fed into the digital voltmeter and the sample signal displayed on the recorder.

It is better to work at low temperature since the electronic levels at room temperature are diffused and broad. Hence, the Raman

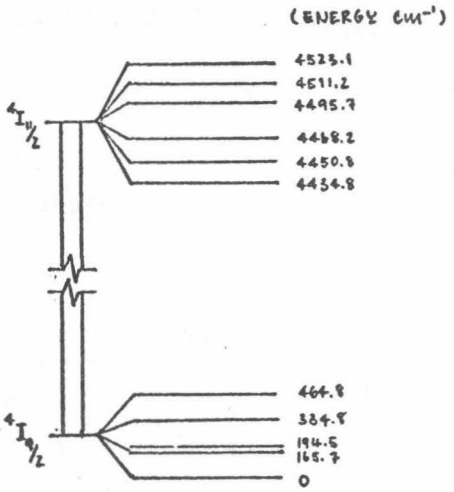

Splitting of the $^4I_{11/2}$ and $^4I_{9/2}$ levels as deduced from absorption and emission spectra (Meredith and Jenney)[10]

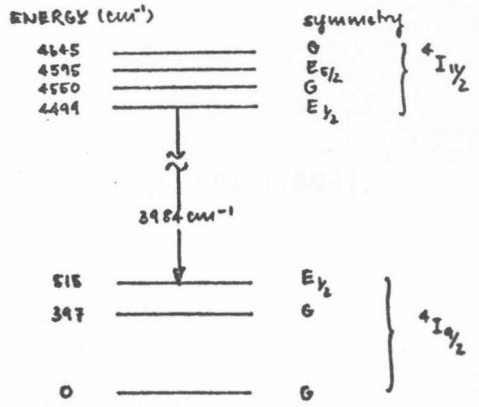

Partial energy-level diagram of isolated U^{3+} ions in CaF_2.
(Wittke, et. al.)[9]

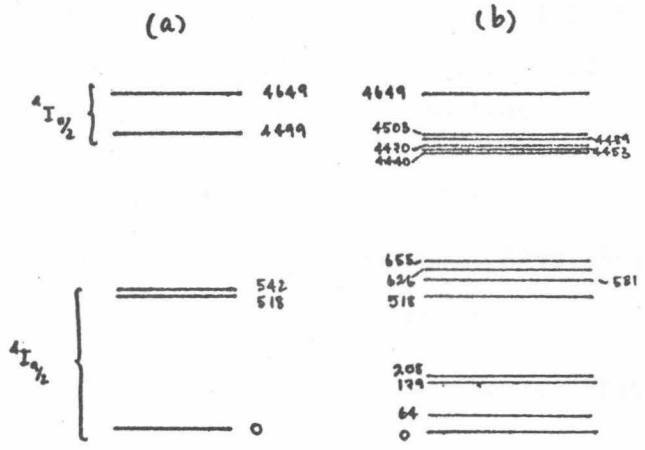

Level scheme of U^{3+} in CaF_2.
a - crystal type I b - crystal type 2
(V.F. Egorova, et. al.)[11]

spectra may not be observed.

Two sets of Raman lines are expected, one from $^4I_{9/2}$ level, the other from $^4I_{11/2}$ level. However, the phonon band from the crystal will also be observed.

References

1. J. T. Hougon and S. Singh; Phys. Rev. Lett. 10, 406 (1963).
2. J.J.H. Chau, J.C.P. 44, 1708 (1966).
3. a. J. A. Koningstein, J. Opt. Soc. Am. 56, 1402 (1966).
   b. J. A. Koningstein, J.C.P. 46, 2811 (1967).
   c. J. A. Koningstein, Appl. Spect. 22, 438 (1968).
4. J. A. Koningstein, et al., J.C.P. 56, 354 (1972).
5. a. O. S. Mortensen, J. A. Koningstein, J.C.P. 48, 3971 (1968).
   b. O. S. Mortensen, J. A. Koningstein, Chem. Phys. Lett. 1, 409 (1967).
   c. J. A. Koningstein, Phys. Rev. 174, 477 (1968); 169, 74 (1968).
   d. G. C. Tobisz, Chem. Phys. Lett. 12, 203 (1971).
   e. J. A. Koningstein and O. S. Mortensen, J. Opt. Soc. Am. 58, 1208 (1968).
   f. A. Kiel and S.P.S. Porto, J. Mol. Spect. 32, 458 (1969).
6. P. P. Sorokin and M. J. Stevenson, Phys. Rev. Lett. 5, 557 (1960).
7. G. D. Boyd, et al., ibid 8, 269 (1962).
8. L. N. Galkin and P. P. Feofilov, Soviet Phys. Doklady 2, 255 (1958); Opt. Spectrometry 7, 492 (1959).
9. J. P. Wittke, et al., Proc. IRE 51, 56 (1963).
10. R. Meredith and J. A. Menney, J.C.P. 39, 3127 (1962).
11. V. F. Egorova, et al., Opt. Spectrometry 20, 491 (1966).
12. B. Bleaney, et al., Proc. Phys. Soc. 69B, 858 (1956).
13. S.P.S. Porto and A. Yariv, J. Appl. Phys. 33, 1620 (1962).

14. G. Placzek, in Handbuch der Radiologie, Bd. VI, Teil II (Leipzig, 1934), page 205.

15. H. M. Crosswhite, et al., M.C.P. 43, 2047 (1965).

Proposition 5

ORGANIC PHOTOCHEMISTRY: STUDIES ON MECHANISMS OF PHOTODECONJUGATION OF CYCLOALKYLIDENE ESTERS

The study on ring size and conformational effects on photodeconjugation of cycloalkylidene esters [1] has shown that

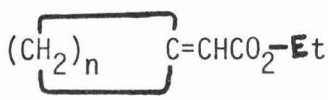

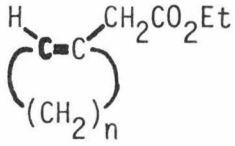

n = 6	⟶	n = 5	slow
n = 5	⟶	n = 4	smooth
n = 4	⟶	n = 3	slow
n = 3	⇢	n = 2	

The mechanism was studied by putting one methyl group in the five and six membered ring systems. In the five-membered ring, the reaction underwent, as expected from the stability of the free radicals that were formed in the intermediate state,

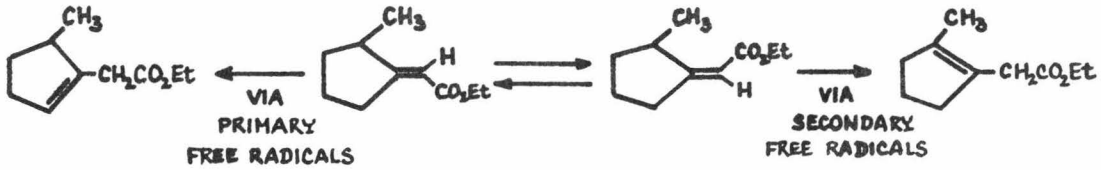

However, for the six-membered ring system, the reaction underwent in the opposite direction. In fact, there was only one product formed (or enough to be detected by conventional methods):

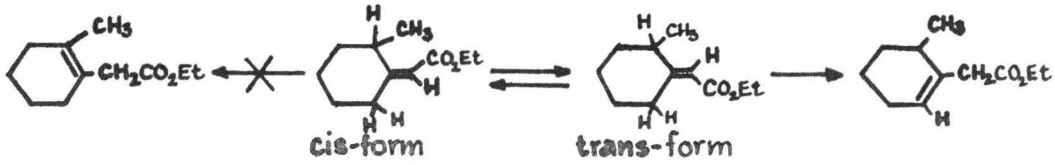

The cis-trans forms of this compound have been identified by H. Hauth, et al.[2]

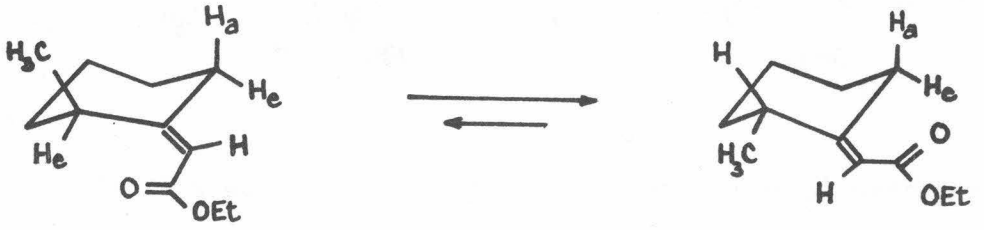

cis-

trans
(favored form)

As for the cis-form, the available H for abstraction seems to be the equatorial one, whereas in the trans-form, there are both the axial and equatorial ones. This seems to lead to the interpretation of the selectivity in terms of chemical demand for this reaction, which dictates the removal of the hydrogen which has its σ bond parallel to the π-orbital of conjugated system (i.e., the axial hydrogen).

These results also implicate a concerted sigmatropic 1,5 hydrogen shift--an antarafacial process, of hydrogen to oxygen atom [3], and the transition of π-π^* excited state [4].

However, in order to have a better understanding of the mechanisms of this reaction (of the six-membered ring), the following tests are proposed:

1. Studies on the conformationally rigid systems, by putting one more methyl group to the monosubstituted ring system. The more favored form should be

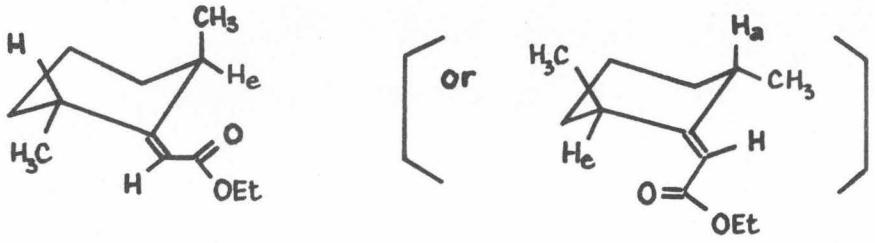

In this way, we can identify whether the axial hydrogen is the stereochemical requirement for the electronically excited molecule, since there are only equatorial hydrogens available.

2. In order to identify the type of transition, the dependence of the rate of product formation on the wavelength variation should be determined [5]. If the dependence does occur, that implies it is a π-π^* transition. Consequently, this will lead to the interpretation that it is not the equatorial hydrogen that is abstracted.

3. The flash photolysis technique to identify whether it is a singlet or triplet excited species that is involved in the mechanism.

The irradiations may be conducted in about 1% solution in hexane, using a Hanovia lamp and vycor filter (as done in Ref. [1]). Different filters are required in the wavelength variation experiment. Products are identified by the NMR technique, and reaction progress by vapor phase chromatography.

References

1. M. J. Jorgenson and S. Patumtevapibal, Tetrahedron Lett. 489-492 (1970).

2. H. Harth, et al., Helv. Chim. Acta. 48, 1087 (1965).

3. R. Hoffman and R. B. Woodward, Acc. Chem. Res. 1, 17 (1968), and references therein.

4. N. J. Turro and D. S. Weiss, J.A.C.S. 90, 2185 (1968).

5. K. Ogura and T. Matsuura, Tetrahedron 26, 449 (1970).